SEARCH FOR MASSIVE NARROW MESONS IN $\bar{p}d$ INTERACTIONS AT 15 GeV/c

By HARTMUT PREISSNER

A thesis submitted to
The Graduate School of Rutgers University
in partial fulfillment of the requirements
for the degree of
Doctor of Philosophy

Written under the direction of
Professor Richard J. Plano of the Department of Physics
and approved by

_____

_____

_____

_____

New Brunswick, New Jersey
October, 1975

ABSTRACT

Search for Massive Narrow Mesons
in $\bar{p}d$ Interactions at 15 GeV/c

by Hartmut Preissner

Thesis director: Professor Richard J. Plano

63300 photographs taken at BNL during an exposure of the 80" deuterium - filled bubble chamber to a beam of antiprotons are used to study the neutron interactions $\bar{p}d \longrightarrow p_s X^-$ at an incident momentum of 15 GeV/c. The mass recoiling against the spectator proton p_s has a range from ~5 to 6 GeV/c^2 and is determined by the beam momentum and the kinematic quantities of the spectator. A special technique for reconstructing the angle of the spectator track by constraining the curvature according to the momentum from its range provides an average accuracy of ~15 MeV/c^2 for the mass. The beam momentum was monitored by measuring non-interacting beam tracks using PEPR in an automatic mode. With a resolution of 22 ± 3 MeV/c^2 and a sensitivity of 10 to 20 μb per standard deviation of significance no resonance is found in the total sample of events nor in any of the topological channels. On each event the track forming the largest angle with the beam has been measured for a better determination of the vertex if the angle with the beam was greater than 20° in each view. An analysis of the hypothetical reaction $\bar{p}d \longrightarrow p_s \pi X$ for these events shows no narrow structure exceeding a significance of 3 standard deviations in either the doubly charged (exotic) or the neutral missing mass distribution.

ACKNOWLEDGEMENTS

I wish to thank Professor Richard J. Plano for the freedom granted to me in the pursuit of this experiment which, combined with his advice and encouragement in seemingly unresolvable difficulties, created a pleasant atmosphere for work.

I am indebted to all people who helped with the run for this experiment. My thanks to the crew at the AGS, especially to Horst Foelsche for discussions and his efforts to achieve a stable momentum for the antiproton beam. For his experienced help in coordinating the run I would like to thank Byerly Brucker.

I appreciate the effort of the measurers for scanning this film, which by any standard, is not an easy one to scan.

Each member of the group within the past 5 years has been involved in discussions about this experiment. I would like to thank especially my (former) fellow graduate students Tom Handler (his program MCKART was very valuable for making the histograms in this thesis) and Tung Ching Ou for many detailed discussions and his useful suggestions especially during my work (fight) with PEPR.

My special thanks to Raymond Badiak and Annamary McCann for the operation, maintenance and improvement of the computer and data encoding system. One of their most recent efforts made this thesis the first one in this department that has been typed by a computer.

TABLE OF CONTENTS

LIST OF FIGURES

LIST OF TABLES

1. INTRODUCTION

High mass meson spectroscopy has experienced varying interest in the last 10 years. The results from the CERN missing mass spectrometer[1] in 1966 initiated experimental activity for meson searches in the mass region up to ~3 GeV/c^2 as well as many theoretical attempts to explain the data. The Regge model described the high mass resonances as members of some rotational band of well established particles. A few years later it became apparent that most experimental studies on meson resonances did not reproduce the results of the CERN experiment. $\bar{p}p$ total cross section data[2] showed broad bumps in the T- and U- region; beyond this region the cross section appeared to approach smoothly and fairly rapidly the Pomeranchuk limit. Most high statistics experiments failed to see narrow high mass mesons in exclusive reaction channels and many of them even provided evidence against the existence of previously claimed resonances. The "killing" of dubious resonances was accompanied by attempts from theorists to explain the broad bumps in the total cross section data as threshold effects. When by the end of 1972 the first data were obtained from the accelerator at Fermilab attention and activity in particle physics were concentrated on interactions at very high energies. The recent discovery

of the J/Ψ meson[3] revived the interest in heavy meson spectroscopy with the aspect of charm.

This experiment was started in 1970 and was influenced in its design and goals by the Regge theory. It is a search for mesons with a mass close to 5.5 GeV/c^2, aiming for a resolution that is able to separate narrow Reggeons. The spacing between the resonances on a straight trajectory with a slope of 1 $(GeV/c^2)^{-1}$ in this mass region is 90 MeV/c^2, requiring a resolution of approximately 20 MeV/c^2.

Exposures of the BNL 80-in. deuterium - filled bubble chamber to an RF- separated beam of antiprotons are used to study the reaction

$$\bar{p}d \longrightarrow p_s X^- \qquad (1\text{-}1)$$

where p_s is a spectator proton,
X^- is the particle or the system of particles recoiling against the spectator,

at an incident momentum of 15 GeV/c. The total film of ~225000 pictures was obtained in two runs. The results from the data of the first run in June 1970 are summarized in chapter 6. In the other chapters only the data of the second run in Feb.1973 are discussed; most analysis procedures, however, apply to the data of the first run as well. One half of the 125000 useful photographs of run #2 were scanned for events with a spectator proton. If the proton is a real spectator, not participating in

the strong interaction of the antiproton, then reaction (1-1) is equivalent to the reaction

$$\bar{p}n \longrightarrow X^- \qquad (1\text{-}2)$$

in the approximation of a zero binding energy for the deuteron. The neutron target is not at rest in the laboratory frame; the Fermi motion in the deuteron varies the center-of-mass energy of the $\bar{p}n$ - system between ~5 and 6 GeV. The spectator proton reflects the motion of the neutron at the time of the interaction. For a constant beam momentum its kinematic quantities determine the mass of the X^- to an accuracy of ~15 MeV/c^2 (on the average). The momentum of the proton is obtained with high precision from its range, its angle with the beam track is found by a special method that constrains the curvature of the track according to its momentum.

Counter experiments[4] measure the total neutron cross section on a deuterium target at fixed beam energies, thus averaging over a wide region of $\bar{p}n$ CM- energies. Any resonance in the $\bar{p}n$ - system is a member of an I = 1 triplet; I-spin invariance predicts that its neutral equivalent is formed in $\bar{p}p$ interactions. The counter experiments[5] that measure the $\bar{p}p$ total cross section in the CM- energy range between 5 and 6 GeV do not observe any narrow structure (see Fig.18). However, their resolution, given by the width of the beam momentum, is

roughly 50 MeV and since the $\bar{p}p$ system couples to I = 0 states as well, the density of resonant states may be higher. This experiment provides a continuous range of CM- energies, whereas the average spacing of the discrete counter data is 100 MeV. Although the bubble chamber experiment cannot compete in the amount of measured events, the systematic errors - especially between different counter experiments - are in the same order as the statistical errors of this experiment.

2. DATA ACQUISITION

2.1. SCANNING AND MEASURING

A total of 63300 pictures from the second run were scanned for events with a stopping proton. Scanning and measuring was performed concurrently on Vanguard film plane digitizers. Because the measuring is relatively simple for this experiment a separate scan did not prove to be more efficient.

According to the experience with the preliminary experiments (chapter 6) and due to the considerations in chapter 5 about contaminating reactions the film was searched for all events with more than 2 outgoing prongs (even or odd numbered), where at least one of the tracks is a stopping proton and for 2-pronged events with a stopping proton, where the other track forms an angle of more than 2 degrees with the beam track in at least one view. The scanning rule for the 2-prongs was chosen to eliminate essentially all elastic and quasi-elastic scatters as well as 2-prongs with a charged leading particle; most of these reactions are peripheral with not much interest for this experiment.

A stopping proton was defined as a heavily ionizing track, consistent with being positive (straight or opposite curvature to that of beam tracks), which stops

in the chamber in the region visible on the Vanguard screen when the production vertex is on the cross hair (center of the screen) and which does not kink or interact. The rules required the scanner to test whether the proton leaves the chamber at the front glass or through the back wall. Clearly associated V^0s, gammas and neutron stars were recorded.

The only tracks measured for each event are the beam track, the stopping proton and, if available, a "pointing track". 3 points were measured along the beam track with the last point near the vertex in a clear region. Up to 8 points were measured on the stopping proton track, depending on its length. In high multiplicity events it is often hard to measure the vertex precisely. In many cases the position of the vertex can be determined better by intersecting one of the outgoing tracks with the beam track. This track was called a pointing track and was defined on a view to view basis as a clear track with close to minimum ionization, forming an angle of more than 20 degrees with the beam track. If the event had a pointing track in the particular view it was measured instead of the vertex as a 3 point track with the first point close to the vertex in a clear region. If there was more than one pointing track the one most nearly perpendicular to the beam was measured.

Events with a missing view and events with a

proton track shorter than 1 mm in all 3 views were defined as unmeasurable.

2.2. RECONSTRUCTION

The measurements were checked weekly with preliminary versions of the reconstruction program. The quick feed-back to the measurers helped to reduce the number of logical errors and misinterpretations of the scanning and measuring rules, the quality of the reconstruction provided a monitor for the measuring accuracy as well as for the functioning of the data encoding - decoding system. In addition all raw data were processed through a program to check the last two digits of the recorded coordinates for randomness.

For reconstruction the program NP54 [6] was modified to make various checks on the data and the scanning information and to perform the operations needed for the special technique to reconstruct short stopping protons (section 3.5). The beam track is reconstructed in the normal way. For the reconstruction of the proton track the vertex is first determined in each view. If a pointing track was measured the circle through the three points on the beam and the circle through the 3 points on the pointing track are intersected. The error of the intersection perpendicular to the stopping proton $\sigma_\perp$ is

calculated from

$$\sigma_{\perp}^2 = \sigma^2 \frac{\sin^2\alpha + \sin^2\beta}{\sin^2\gamma} \qquad (2\text{-}1)$$

where σ is the measuring error,

α is the angle between the beam and the proton,

β is the angle between the pointer and the proton,

γ is the angle between the beam and the pointer

and is used to determine the error of the proton angle. The error in direction of the proton $\sigma_{\parallel}$, with

$$\sigma_{\parallel}^2 = \sigma^2 \frac{\sigma_{\perp}^2}{2\sigma_{\perp}^2 - \sigma^2} \qquad (2\text{-}2)$$

is used for the calculation of the error of the proton momentum (obtained from range). The vertex and the endpoint are reconstructed as corresponding points. If more points were measured on the proton track the vertex with weight $(\sigma/\sigma_{\perp})^2$ and the other points with weight 1 are reconstructed either as a straight line track or if the distance between vertex and endpoint in the xy - plane (parallel to the chamber glass) is greater than 5 cm, as a helix.

A successfully reconstructed track is tested as to whether its endpoint is inside the chamber. Track length and angles are averaged with the corresponding point data and the corrections for the azimuthal angle (angle in the xy - plane) are added (section 3.5).

If a pointing track was measured in more than one view an attempt is made to reconstruct it. Since the pointer is not necessarily the same track in the 3 views a failure to reconstruct it does not imply that it was measured incorrectly.

The failing events were grouped into the following categories:

1: Initialization trouble
(e.g. wrong number of points; wrong number of tracks; wrong fiducials measured).

2: Proton track does not stop in the chamber.

3: Vertex failure
(e.g. failure of intersection routine; bad pointing track that produces a weight less than 0.1 for the vertex and the stop point is the only point measured on the proton track).

4: Illegal use of the missing point flag.

5: Reconstruction failure on beam or proton
(beam tracks were rejected if the discrepancy dz in the z - coordinates calculated from the 3 pairs of views was greater than 0.3 cm, the requirement for proton tracks was dz < 0.2 cm).

6: Beam is inconsistent with having negative charge.

7: RMS of fit to proton track is too high
(for the straight line fit the limit was length dependent).

2.3. SUMMARY OF DATA GATHERING

Scanning efficiency was checked on a random basis. Appearance (or disappearance) of narrow structures in m_x is not directly influenced by low or biased scanning efficiency. The data will clearly be biased by a low efficiency for short forward protons in high multiplicity events. Also short extremely backward protons will have a low detection probability. The overall efficiency depends on the length cut-off and is generally low because the film is very crowded with tracks from primary and secondary interactions.

Special emphasis was given to the accuracy of the measurements which, especially for the short proton tracks, is crucial for good resolution.

Results of the data acquisition are summarized in table 1. The number of frames was determined from the last frame scanned on each roll and the number of lost frames as recorded by the measurers. The distribution of gaps in the frame numbers of consecutive events was checked for all gaps greater than 35 frames. It was found to be in excellent agreement with the theoretical random distribution:

(# of gaps of more than G frames) =

(total # of events) * exp(-G * (# of events per frame)).

Tab. 1: SUMMARY OF THE DATA ACQUISITION

Frames scanned	63300	
Events measured	10188	
Events per frame	0.16	
Scanning efficiency (for spectator length > 2mm)	75	%
Events reconstructed	9530	
Reconstructed events per frame	0.15	
Pass rate	93.5	%
RMS of mass error Δm_x (for $\Delta m_x < 50$ MeV/c^2)	12	MeV/c^2
Accuracy in xy - plane	0.010	cm

Rejects :

type	1	2	3	4	5	6	7
number of events	19	50	114	12	373	10	78

Failures to reconstruct the pointer if it was measured in more than one view: 112

3. RESOLUTION

3.1. THE VARIABLES

The mass of the X^- in reaction (1-1)

$$\bar{p}d \longrightarrow p_s X^-$$

depends on the kinematic quantities of the beam and the spectator proton as described by equation (5-3). Typical uncertainties of the 3 relevant variables - the beam momentum p_b, the spectator momentum p_{sp} and the angle ϑ between beam and spectator - and their propagations towards the error of the mass m_x are summarized in table 2. The error of the beam momentum is quoted according to the specifications of the beam line (and is consistent with the value found in chapter 4), the errors of the spectator quantities depend on the measuring accuracy, the geometry of the specific event and on the quality of various constants for the bubble chamber and the optics.

Angle and momentum of the spectator proton are extracted from the space coordinates of the first point (vertex) and the last point (end point) of the reconstructed track. Since these two points are corresponding points in the three views, the errors of their space coordinates do not depend strongly on the geometry (e.g. angles in respect to the intercamera lines,

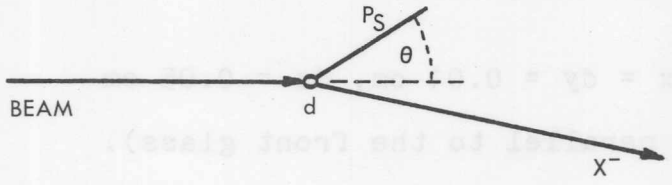

Typical ERROR of VARIABLE	PROPAGATION	Δm_X [MeV/c²]
$\Delta\theta = 3°$	$\frac{\partial m_X}{\partial \theta} = \frac{p_B p_{SP} \sin\theta}{m_X}$	15
$\Delta p_{SP} = 5$ MeV/c	$\frac{\partial m_X}{\partial p_{SP}} \simeq \frac{m_X - m_0}{p_{SP}} - \frac{p_{SP}(E_B + m_d)}{2 m_P m_X}$	12
$\Delta p_B = 0.1$ GeV/c	$\frac{\partial m_X}{\partial p_B} \simeq \frac{m_X}{m_P} + \frac{m_X - m_0}{p_B}$	17

$m_0 = m_X(p_{SP}=0)$

Tab.2 : Expected Resolution in the Mass m_X

dip angle); variations in accuracy with the position in the chamber are neglected. Therefore, constant errors for the space coordinates are assumed:

$$dx = dy = 0.01 \text{ cm}, \quad dz = 0.05 \text{ cm} \qquad (3\text{-}1)$$

(the xy - plane is parallel to the front glass).

These errors depend not only on the one-view measuring accuracy, but also on the optical constants for the three-dimensional reconstruction.

3.2. OPTICAL CONSTANTS

The optical constants were determined with the program CONGEN[7] on the measurements of 18 front fiducials, 4 back fiducials and 6 corresponding points (bubbles) in the chamber. The data of two pictures were used for each fit. The front fiducials were constrained to the nominal values[8] with an uncertainty of 0.01 cm for the x- and y- coordinates and with an uncertainty of 0.05 cm for their z- coordinate. The z- coordinate of the back fiducials was constrained to the nominal value with an error of 0.1 cm. Constraining the x- and y- coordinates of the back fiducials did not prove to be useful because the relative orientation between the front and back fiducials is unknown.

Initial studies on the photographs of one roll

(#603) did not include distortion parameters; the quality of the fits was poor. When Berkeley-type (B) distortion parameters (2 tilts, pincushion and film stretch) were included in the fit the χ^2 did not improve as expected. Graphically it was found that the major distortion was a constant curvature in the x- direction (along the beam). With this single distortion parameter (R1) a significant improvement for the fit was achieved. Finally the combination (R5) of B- distortions and the R1- distortion produced a satisfactory result.

Tab. 3: COMPARISON OF DIFFERENT SETS OF DISTORTIONS

Distortions	χ^2	χ^2 expected
none	334	204
B	275	195
R1	235	202
R5	130	193

The optical constants were determined for 3 more rolls. The distortion coefficients (especially R1) varied considerably from roll to roll, probably depending on the camera pack used. Nevertheless, for the reconstruction of the spectator events only one set of constants has been used. Though the change of distortions is non-negligible over the whole range of the chamber, the effect is

insignificant locally. Most spectators are very short compared to the dimensions of the chamber, so that the mass m_x depends only on measurements in a small region. A random sample of 20 events was reconstructed both with and without the use of distortion coefficients; the maximum difference found in m_x was only 2 MeV/c^2.

The form of the distortions finally used (R4) consists of 4 parameters (a,b,c,d) :

$$x' = x + a \cdot u^2 + b \cdot u \cdot v \qquad (3\text{-}2)$$
$$y' = y + a \cdot u \cdot v + b \cdot v^2 + c \cdot u^2 + d \cdot v^2$$

where $u = (x - x_{camera}) / z_{camera}$

$v = (y - y_{camera}) / z_{camera}$

(a and b are film tilts)

The constants listed in table 4 are given in a right handed coordinate system with the positive x- axis in direction of the beam, parallel to the front glass and the positive z- axis in the viewing direction of the cameras, perpendicular to the front glass. The origin is defined as in reference 8 for x and y (roughly the center of the front glass), the average z- coordinate of the front fiducials is the origin of the z- axis. This coordinate system is used everywhere in this experiment.

The fiducials used for fitting the constants are those 18 of the total of 22 front fiducials that are

Tab.4 : OPTICAL CONSTANTS

		SET 1 with distortions		SET 2 without distortions	
Index of refraction of					
Liquid		1.105		1.097	
Glass		1.513		1.513	
Thickness of glass		19.675		19.634	
-z of cameras		215.3		215.3	
Cameras		x	y	x	y
1		-25.702	0.230	-23.050	2.961
2		33.373	-31.489	35.832	-28.976
3		33.411	32.099	35.901	34.582
Apparent positions (not distorted) of fiducial :					
1	VIEW 1	-64.358	0.069	-64.498	-0.028
1	VIEW 2	-66.595	1.208	-66.752	1.104
1	VIEW 3	-66.595	-1.071	-66.767	-1.180
2	VIEW 1	22.517	0.055	22.367	-0.043
2	VIEW 2	20.577	1.086	20.477	0.985
2	VIEW 3	20.576	-0.978	20.443	-1.070

Distortions

VIEW	1	2	3
a	0.44	0.11	0.25
b	-0.64	0.02	0.04
c	0.29	0.22	0.19
d	1.40	0.00	0.35

visible in all 3 views; fiducials 4a,3d,4d,4 (in the nomenclature of Ref.8) are not used. The reference fiducials for the measurements of the spectator events are 1e (fiducial 1) and 3e (fiducial 2) ; their apparent positions are given in table 4.

3.3. RANGE - MOMENTUM RELATION

The momentum of the spectator protons is determined from their range. The momentum - range relation was obtained from fitting range - energy data[9] for protons in deuterium at kinetic energies T between 3 and 80 MeV (corresponding to momenta between 77 and 387 MeV/c) :

$$p(s) = 125.03*s^{1/4} + 129.61*s^{0.3} + 0.135*s^{2} \qquad (3\text{-}3)$$

where $s = \rho \cdot l$ (3-4)

and s is the range in g/cm^2,
ρ is the density of the liquid deuterium,
l is the track length,
p is the momentum in MeV/c.

The fit to the 12 data points has an accuracy of 0.12 MeV/c with the maximum deviation of 0.27 MeV/c at T = 3 MeV.

For the determination of the charge density of the liquid deuterium, measurements of stopping pions - identified by π-μ-e decay - are used. The advantage of this method over the standard procedure using muons is

that the long range of the pions provides a good accuracy for the range measurement, even if the pion decays at a small speed rather than at rest. The disadvantage is that the momentum has to be determined from curvature and therefore depends on the magnetic field (section 3.4). Not including possible systematic errors in the field value the density was determined to an accuracy of 2.5 % with only 8 pion tracks.

The measurements were performed in the following way : stopping pions with a small dip angle and with a track length between 36 and 70 cm (momentum between 100 and 135 MeV/c) were selected. 7 points were measured on the first 15 cm of the track for the determination of the momentum (from curvature). To obtain the length, the track was divided into segments with reasonably constant curvature in a way that δ - rays marked the end points of each segment. Each segment was measured as a separate track; the length of the pion track is the sum of the lengths of its segments.

For convenient analysis of the measurements pion range - momentum data[9] were fit in the narrow region of p = 90 MeV/c to p = 140 MeV/c to the simple function

$$p = a \cdot s^{1/4} + b \cdot s^{1/2} \qquad (3\text{-}5)$$

which, using (3-4), can be solved analytically for the

density ρ :

$$\rho = \frac{1}{l}\left(\frac{\sqrt{a^2+4bp} - a}{2b}\right)^4 \qquad (3\text{-}6)$$

(the fitted values are a = 47.08, b = 16.04)

The average density found from the 8 pion tracks is

$$\rho = 0.134 \pm 0.0035 \text{ g/cm}^3 \quad . \qquad (3\text{-}7)$$

The quoted error is from the Gaussian standard deviation and does not include the error on the scaling factor for the magnetic field.

3.4. MAGNETIC FIELD

For the purpose of determining the deuterium density the value of the magnetic field was checked; otherwise the field value is of minor importance for the resolution, because only corrections to the proton angle and the measurement of the central value of the beam momentum depend on it.

Measurements of Λ- particle decays were used in a simple method that does not require any fitting and that is free of ambiguous background. The film was scanned for charged decays of slow Λ- particles, i.e. it was scanned for neutral vees with the positive track having the ionization and curvature of a slow proton track. The low Q - value for the decay and the selection of slow Λ´s has

the advantage that the curvature of the outgoing tracks will be high enough to get an accurate measurement of their momenta, which is a basic requirement for good sensitivity to the field. The possibility of identifying the proton on the scan table and the low propability for other charged decay modes guarantees a much cleaner sample of events at the scan level than the analysis of neutral K- mesons can provide.

19 neutral V´s were measured on one roll (# 615) and were reconstructed with NP54 with a set of optical constants specially determined for this roll. For the reconstruction the nominal magnetic field[10] H_n (with a central intensity of 17.563 kG) was used. If the true magnetic field H is

$$H = S \cdot H_n \qquad (3\text{-}8)$$

then, ignoring the constraints from the primary vertex,

$$m_\Lambda^2 = m_p^2 + m_\pi^2 + 2\sqrt{(m_p^2+S^2p_p^2)(m_\pi^2+S^2p_\pi^2)} - 2S^2p_pp_\pi\cos\vartheta \qquad (3\text{-}9)$$

where p_π and p_p are the momenta of the pion and proton as given by the reconstruction,

$m_\Lambda = 1.11557\ \mathrm{GeV/c^2}$ is the mass of the Λ,

ϑ is the opening angle of the V^0.

A mass plot for m_Λ with the scaling factor S set to 1 is shown in figure 1; the lambdas are clearly separated from other V^0s. The 12 events with

$$1.11\ \mathrm{GeV/c^2} < m_\Lambda < 1.12\ \mathrm{GeV/c^2}$$

were selected, equation (3-9) was solved for S and S was calculated for each event. The error of S was calculated from the errors of the measured quantities and was used for the weight in averaging the scaling factor. The result

$$S = 1.0013 \pm \begin{cases} 0.0079 & \text{from error propagation} \\ 0.0096 & \text{from standard deviation} \end{cases} \qquad (3\text{-}10)$$

is consistent with a scale factor of S = 1.0 and the unmodified field was accepted.

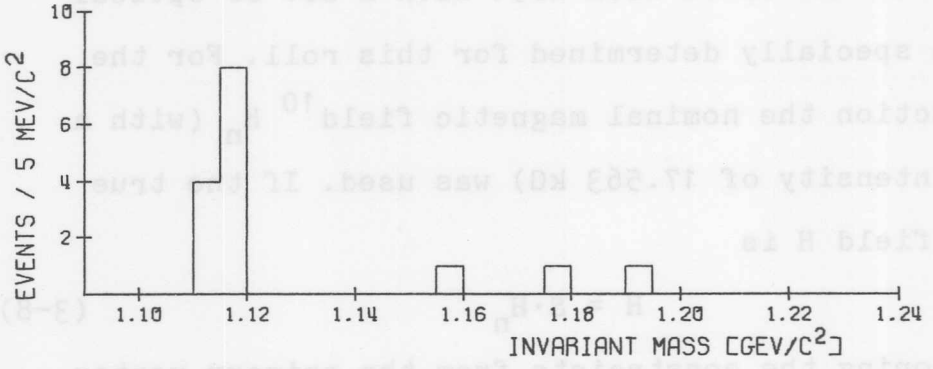

Fig.1 : V^0 Mass Distribution

3.5. AZIMUTHAL ANGLE

For most events the mass m_x is very sensitive to the angle between the beam and the spectator. The errors in the angles of the beam track are negligible compared to the errors of the dip and especially the azimuth of the spectator. In usual reconstruction techniques the azimuthal angle is found from 3- parameter circle fits

in the xy- plane. For stopping particles the momentum is determined by the range l and can provide a constraint for the fit. The fit with only 2 parameters reduces the error of the fitted angle considerably. For example, the 0- constraint fit of 2 points to a straight line has the error in the fitted angle $\sqrt{13}$ times smaller than the 0- constraint fit of 3 equally spaced points to a circle. In general the gain in accuracy will be even greater, if the points are not equally spaced and if in the two parameter fit extra points are used as constraints. For the 2- point, 2- parameter determination of the angle φ its error $d\varphi$ is

$$d\varphi = \sqrt{2}\,\frac{dy}{l} \qquad (3\text{-}11)$$

(here the y-direction is normal to the track).

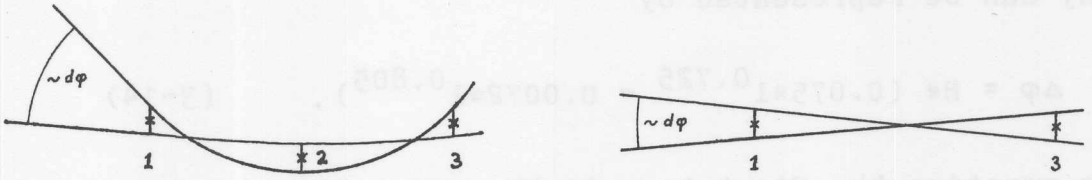

Fig.2 : Track Angle φ in the Circle Fit and the Straight Line Fit.

For a track with 3 equally spaced points the angle φ at point # 1 (see Fig.2) is

$$\varphi = \frac{1}{l} (-3y_1 + 4y_2 - y_3) \qquad (3\text{-}12)$$

and

$$d\varphi = \sqrt{26}\,\frac{dy}{l} \qquad (3\text{-}13)$$

The sagitta of a proton track with a projected length of less than 5 cm in the xy- plane is less than 8 times its measuring error. Therefore, for those tracks a straight line fit to the measured data is sufficient for a reasonable description of the data. To get the initial azimuthal angle of the spectator the fitted angle has to be corrected according to the curvature and the change in curvature due to energy loss along the track. The corrections $\Delta\varphi$ were found by a Monte Carlo method. Curves of stopping protons were generated using the range - momentum relation. 7 equally spaced points on each of these curves were fit to a straight line. The differences $\Delta\varphi$ between the initial angle and the fitted angle found this way can be represented by

$$\Delta\varphi = H * (0.075 * l^{0.725} - 0.0072 * l^{0.805}). \qquad (3\text{-}14)$$

In this equation the first term is the correction due to the curvature, the second one is due to the energy loss. The formula is independent of the dip angle; the field H is to be chosen positive if the track curves counter - clockwise (from positive x- axis to positive y- axis).

The measured points on the track will generally not be evenly spaced. A first order deviation from

constant spacing is

$$D = c_1 + c_2 \cdot s \qquad (3\text{-}15)$$

(s is the distance from the vertex).

This represents constantly changing separation D between adjacent points. The fitted angle will then deviate from that obtained by equally spaced points by

$$\Delta\varphi_s = 0.4\ \delta \qquad (3\text{-}16)$$

with

$$\delta = \gamma\left(\frac{\bar{s}}{l} - 0.5\right)$$

where $\bar{s}$ is the average distance of the measured points from the vertex,
γ is the turning angle of the track.

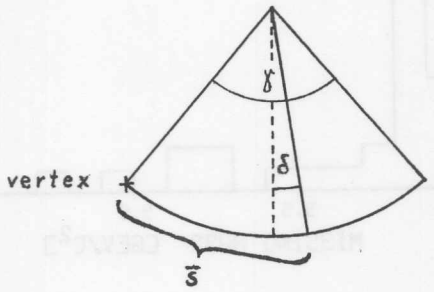

To check the quality of the procedure for the angle determination the stopping protons of 6 events of elastic scattering on a 1.25 GeV/c $\bar{p}p$ - film were measured and reconstructed with this technique. For elastic scatters the angle can be predicted from the momentum of the proton recoil. The agreement between the measured and the predicted angle was within errors and in all cases better than 0.4 degrees.

The resolution can also be checked with elastic

events in the film of this experiment. The sample of events will not be pure elastic $\bar{p}d$ scattering mainly because of a background of quasi-elstic scatters.
32 events looking like elastic scatters were measured and reconstructed like spectator events. The quantity m_x, calculated with a constant beam momentum (14.9 GeV/c), for these events is histogrammed in figure 3. It shows the elastic peak (section 5.2.2.) with a resolution better than 20 MeV/c^2.

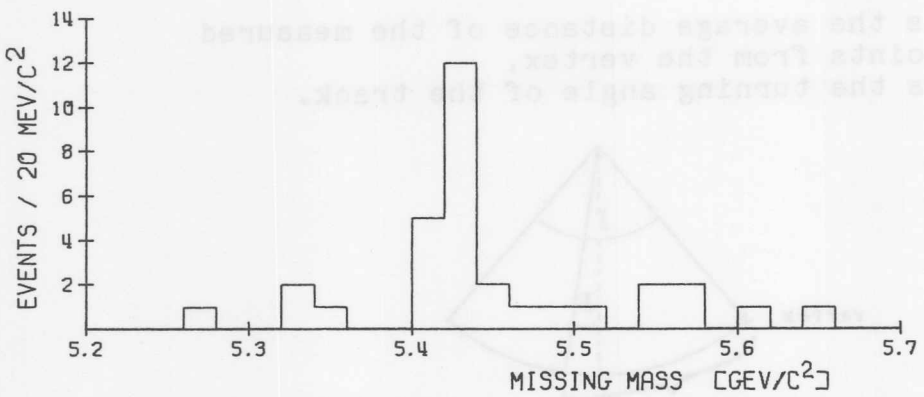

Fig.3 : m_x for Elastic Scatters

The width of the elastic peak mainly tests the resolution due to the accuracy of the angle measurement. According to table 2 the error of m_x due to the error in the spectator momentum is small near $m_x = m_0$. This can also be seen directly from equation (5-3): the term $2\ p_b\ p_{sp}\ \cos\vartheta$ is small for elastic events that have ϑ near 90°. The kinematics of elastic events makes m_x

insensitive to variations of the real beam momentum as long as a constant value of p_b is used for the calculation of m_x (if the real values of the beam momentum are used the mass m_x changes as given in table 2).

3.6. BEAM MOMENTUM

The momentum of the beam track of each event cannot be determined with sufficient accuracy; the measuring accuracy for a long track of 160 cm is still about 200 MeV/c. Some average value for the beam momentum has to be assigned to each event. The error in the value of the total average $\bar{p}_b$ of the beam momentum does not effect the resolution; it only produces a constant translation of the whole spectrum by $\Delta\bar{p}_b \cdot m_p/m_0$ and an almost negligible magnification of the mass scale as given by the term $\Delta\bar{p}_b \cdot (m_x - m_0)/\bar{p}_b$.

The resolution, however, is very sensitive to changes in the difference between the true and the assigned value of the beam momentum (see table 2). For constant conditions the beam line is specified with a momentum bite of ± 1.2% corresponding to a standard deviation of 70 MeV/c. The quality of the beam is discussed in detail in the next chapter.

4. THE BEAM

4.1. THE BEAM LINE

The AGS was operated in a bubble chamber - only mode, i.e. no other experiments had to be serviced by the beam in the main ring. 2 extractions from the proton beam were made for each accelerator cycle. The beam of 15 GeV/c antiprotons was provided to the 80" bubble chamber by RF - particle separation through beam line #4 [11]. The proposed revision[12] - a third separator cavity - was installed but not operating. The detailed layout of the beam line can be found in references 11,12; a simplified schematic is given in figure 4. Momentum selection is achieved by horizontal deflections (z- direction), particle separation operates by vertical deflections (y- direction). During the run all magnet currents were repeatedly read under computer control and a warning message was given if any significant change was detected.

Antiprotons have to be separated from π^- and K^- mesons. With the two- cavity system exact double contaminant rejection cannot be achieved for antiprotons above 6.5 GeV/c. However, above 15 GeV/c the phase between the two cavities can be adjusted to a compromise for the cancellation of deflection angles for both unwanted particles. The phasors for a beam momentum of 15 GeV/c [13]

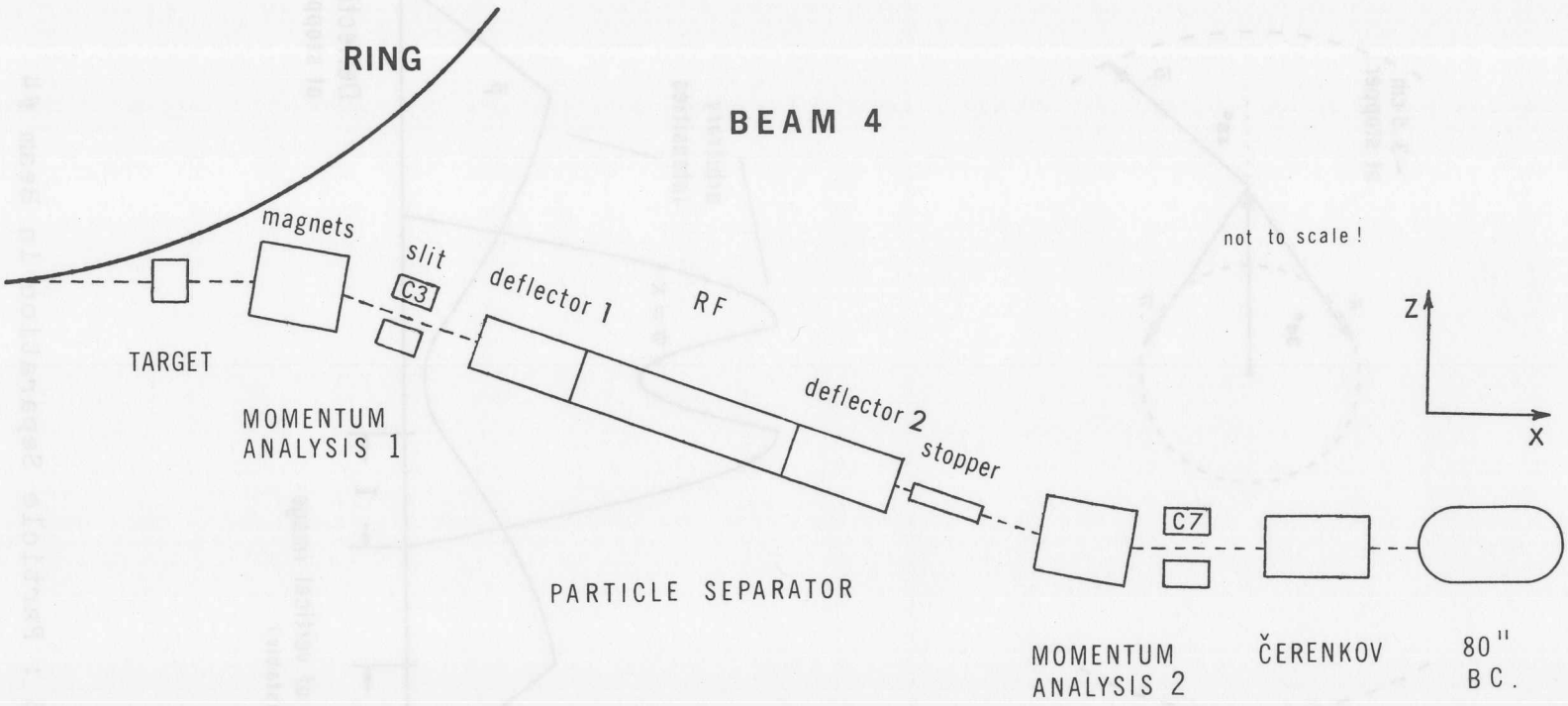

Fig.4 : Schematic of the Beam Line

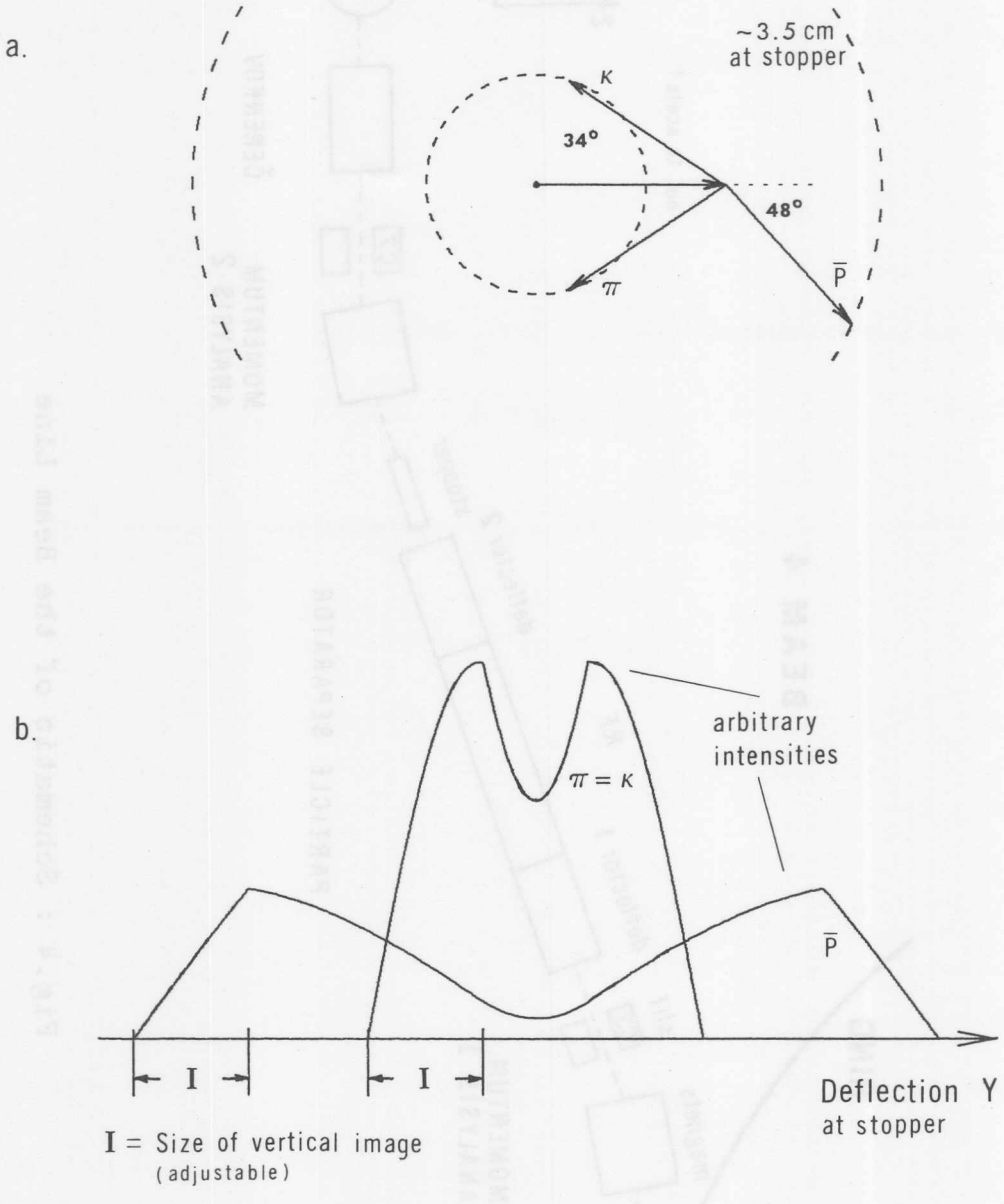

Fig.5 : Particle Separation in Beam #4

are shown in figure 5a, the relative intensities at the stopper are shown as a function of the deflection y in figure 5b. This particle separation technique splits the beam into two bunches which remain well separated along the beam transport into the bubble chamber (Fig.11). The elimination of the mesonic beam component depends on the stability of the phase difference between the oscillations in the two RF- cavities and, to a small degree, on the beam momentum p_b. The size of the stopper determines the tolerance for the phase. Flux - phase curves were measured several times during the run; the tolerance was found to be greater than ± 10 degrees, the stability was 2 degrees. The particle phase angle is proportional to $1/p_b^2$ and it changes by 0.1° for pions and by 1.5° for kaons at a change of 1% in beam momentum. The amount of mesonic contamination as measured with the Čerenkov counter was 7%. During the run the Čerenkov counter was set up to veto a picture if more than 30% of the particles going into the bubble chamber were triggered as mesons. The resulting average contamination is estimated to 5%.

The momentum analysis system is designed to select a momentum band of 1% of the central beam momentum. Analysis section 1 provides the stated momentum selection, whereas the main purpose of section 2 (post analysis section) is the purification of the beam from unwanted off-momentum particles (e.g. muons from decayed pions).

The horizontal size of the target used was 0.15", so that the size of the horizontal image at the slit of the first momentum analysis (collimator C3) was 0.35 cm. The opening of the collimator is 0.46 cm, the same size as the dispersion of the bending magnets for 1% of momentum deviation. Assuming a perfect optical system and a uniform illumination of the target the momentum profile behind the slit has a trapezoidal shape (Fig.6) with 68% of the area within ± 0.43% of momentum deviation. (With the standard target size of 0.2" the profile is triangular.) It is estimated that the beam optics increases the width by ~20%. The second momentum analysis section has about the same resolution as the first one with a large dispersion of 1.2 cm/% momentum deviation. The beam leaves the slit C7 with a correlated deflection - momentum phase space (Fig.6). In the bubble chamber the correlation is mostly destroyed due to the angular divergence of the beam.

4.2. THE BEAM MOMENTUM

4.2.1. THE MOMENTUM DEVIATIONS

It was pointed out before (section 3.6.) that knowledge of deviations from a constant beam momentum is essential for the resolution in this experiment. Differences in the momenta of beam particles may be grouped into 3 categories according to their origin or

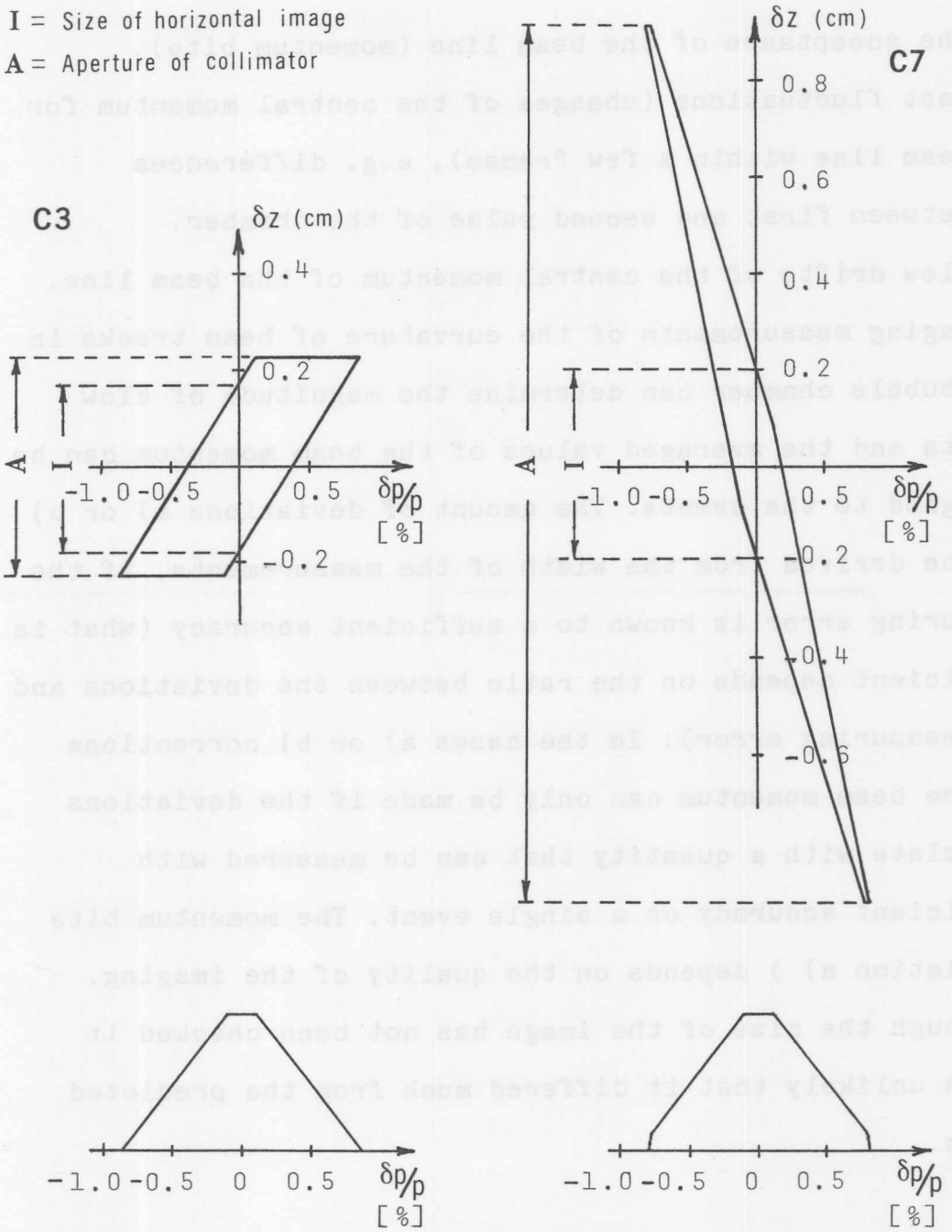

Fig.6 : Momentum - Deflection Phase Space
at Collimators C3 and C7

appearance:

a) The acceptance of the beam line (momentum bite).

b) Fast fluctuations (changes of the central momentum for beam line within a few frames), e.g. differences between first and second pulse of the chamber.

c) Slow drifts of the central momentum of the beam line.

Averaging measurements of the curvature of beam tracks in the bubble chamber can determine the magnitude of slow drifts and the averaged values of the beam momentum can be assigned to the events. The amount of deviations a) or b) can be derived from the width of the measurements, if the measuring error is known to a sufficient accuracy (what is sufficient depends on the ratio between the deviations and the measuring error). In the cases a) or b) corrections to the beam momentum can only be made if the deviations correlate with a quantity that can be measured with sufficient accuracy on a single event. The momentum bite (deviation a)) depends on the quality of the imaging. Although the size of the image has not been checked it seems unlikely that it differed much from the predicted value.

4.2.2. BEAM TRACK MEASUREMENTS

To determine differences in the momenta of beam particles by measuring beam tracks on the bubble chamber

film one wants a method that provides a sufficient number of measured points on each track to detect small kinks and as many measured tracks as possible so that one can detect drifts with the best time resolution. The systematic errors should be constant for all measurements within ~50 MeV/c. The use of the curvature for the determination of the beam momentum relies on the stability of the chamber field, which is expected to be sufficiently good so that fluctuations can be ignored. As mentioned in chapter 3.2. the optical distortions are not constant; The differences found amount to a change of the measured momentum by as much as 200 MeV/c. Therefore, along with the track measurements the distortions have to be determined. When using conventional measuring machines no other systematic errors are encountered but the number of coordinates to be measured is limited by the measuring effort (compare chapter 6).

To be able to measure a large number of non-interacting beam tracks it was decided to use the Rutgers-Stevens PEPR device in a fully automatic mode. This electronic encoding system has the disadvantage that, though the local reproducibility of a measurement within a short time is ~5 times better than the resolution of a Vanguard film plane digitizer, its global accuracy is considerably worse: distortions depend not only on the x and y coordinates but, since PEPR measures with a line

element (bite), they also depend on the angle of the track and on various scan conditions. Since the error is systematic it does not average to zero and it may drift in time or may be different for each calibration of the system. The PEPR hardware drift as well as the change of optical distortions (other than those caused by the liquid) can be traced by measuring fiducials and the track measurements can be corrected according to the deviations from the given apparent locations of the fiducials. (Apparent positions are defined with respect to the position of the camera lens which is not changed with film changes).

20 of the 22 fiducial marks on the front glass of the bubble chamber were measured on each frame. Their apparent positions were calculated from their space coordinates[8] with CONGEN[7] using the optical constants and distortions of roll 615 (compare sections 3.2 and 3.4). For an increase in accuracy the calibration routine for the hardware was improved, the hardware was readjusted and in order to reduce angle dependent errors the fiducials were measured with half the maximum line length (bite); most fiducial arms are at ± 45°, while beam tracks are near 0 degrees. The fiducials were fit to 10 parameters : a general linear transformation, 2 film tilts, a pincushion and the curvature term $y \propto x^2$ (section 3.2). Agreement with the predicted positions within 1.6 to 2.0 μ

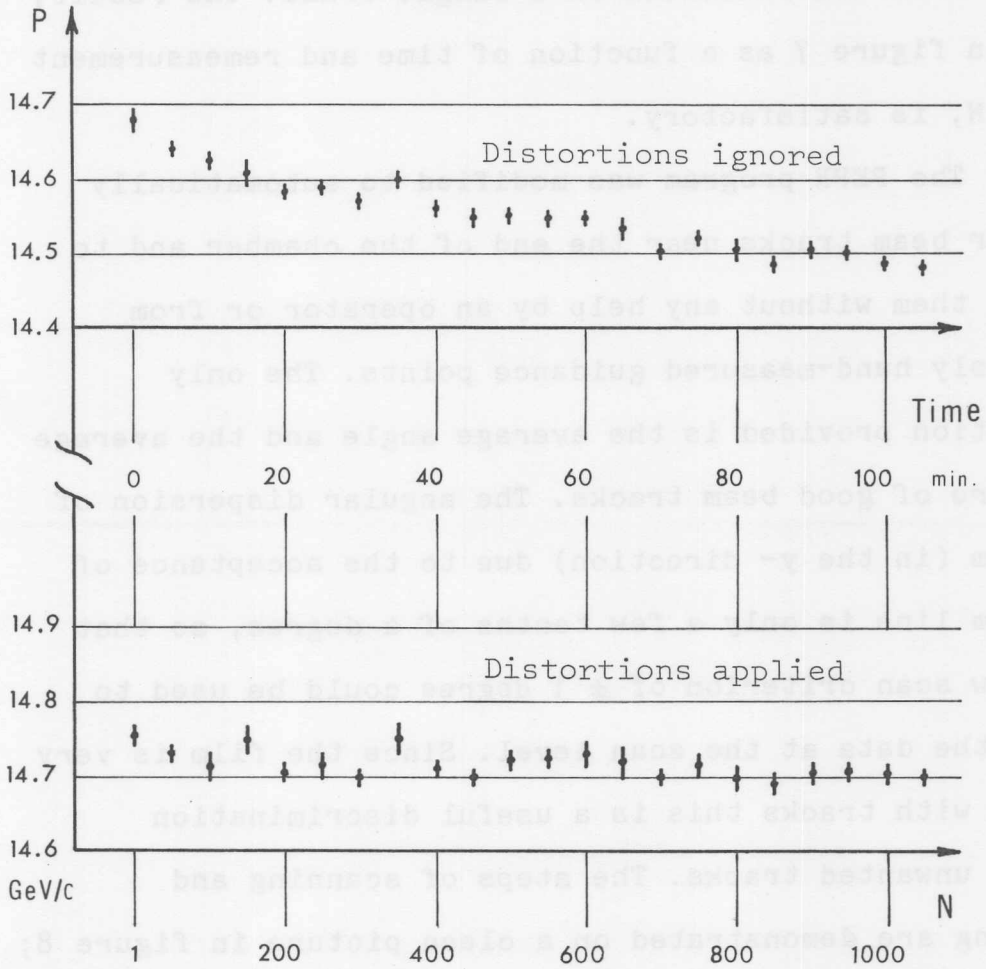

Fig.7 : Momentum of a Beam Track from Repeated Measuring of a Single Frame with PEPR

on film was obtained. The effectiveness of the method to compensate for drifts was tested by repeatedly measuring a beam track and fiducials on a single frame. The result, shown in figure 7 as a function of time and remeasurement number N, is satisfactory.

The PEPR program was modified to automatically scan for beam tracks near the end of the chamber and to measure them without any help by an operator or from previously hand-measured guidance points. The only information provided is the average angle and the average curvature of good beam tracks. The angular dispersion of the beam (in the y- direction) due to the acceptance of the beam line is only a few tenths of a degree, so that a narrow scan criterion of ± 1 degree could be used to purify the data at the scan level. Since the film is very crowded with tracks this is a useful discrimination against unwanted tracks. The steps of scanning and measuring are demonstrated on a clean picture in figure 8; the result of track following on a more typical picture is shown in figure 9.

Matching of beam tracks in 3 views and - since PEPR was not set up to read frame numbers - possible necessity for matching frames can be a difficult problem. However, the beam position in z- direction is defined by the beam line collimators to ± 1.5 cm in the chamber which is a sufficiently small deviation to determine the momentum

a.

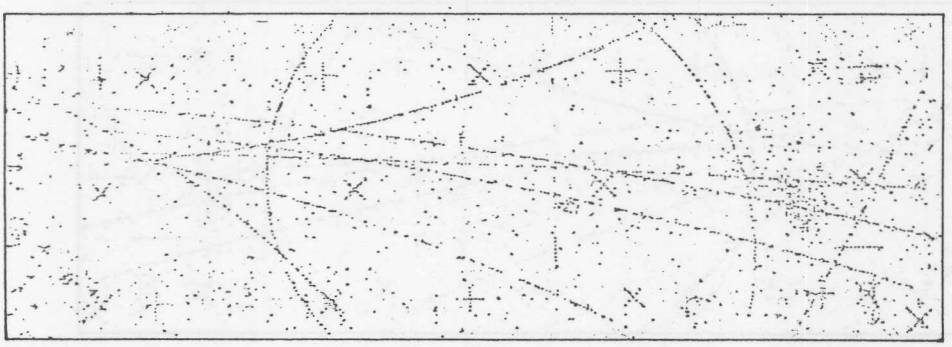

TV - Scan

b.

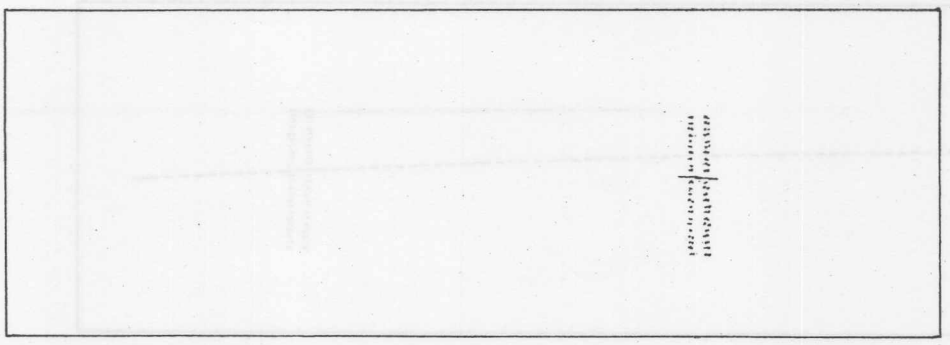

Scanning for Beams

c.

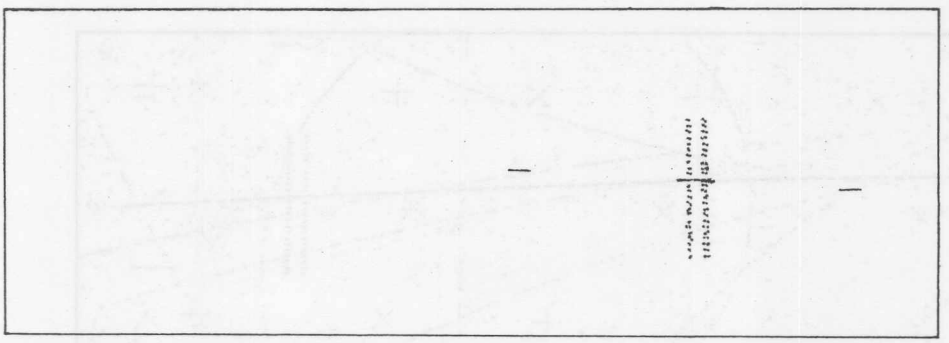

Prediction and Verification

Fig.8 : Operation of PEPR in Automatic Mode for the Measuring of Beam Tracks. Part 1

d.

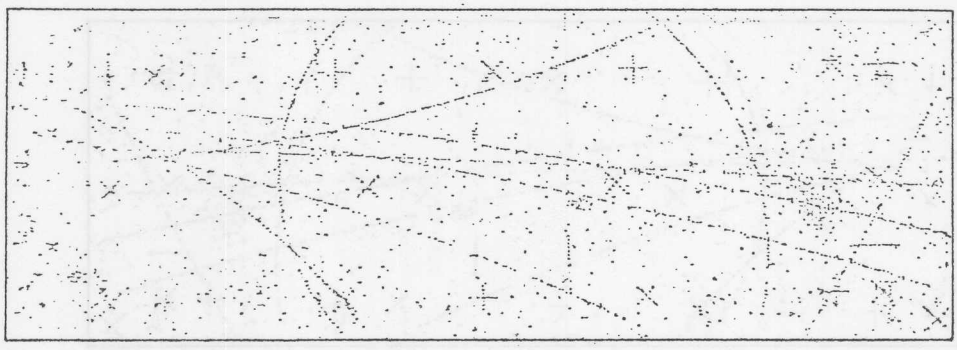

TV - Scan

e.

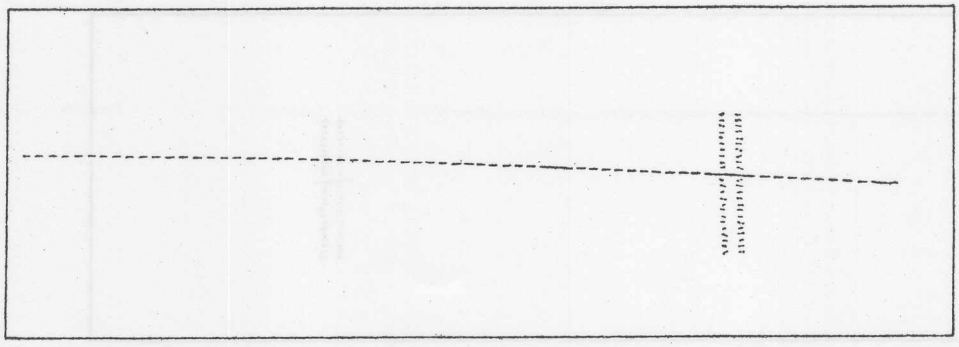

Track Following

f.

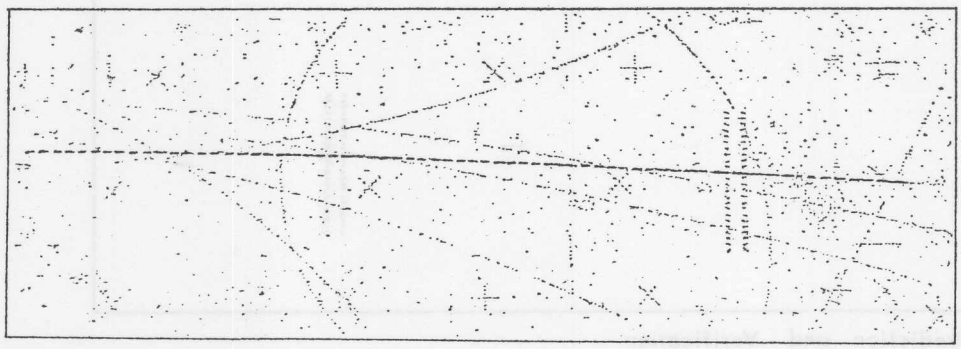

Result

Fig.8 : Operation of PEPR in Automatic Mode for the Measuring of Beam Tracks. Part 2

a.

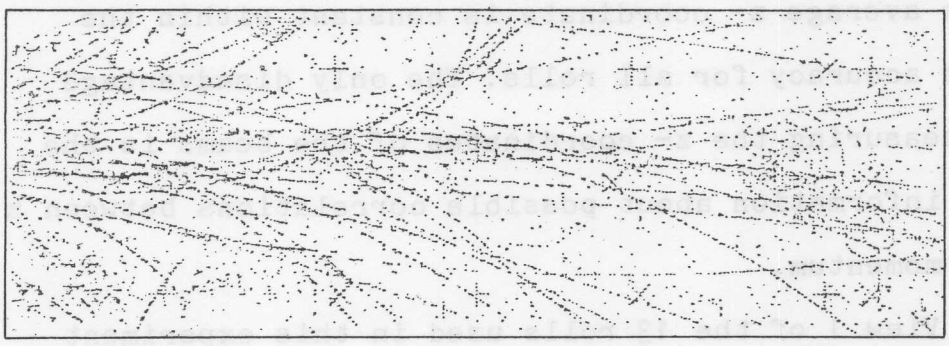

TV - Scan

b.

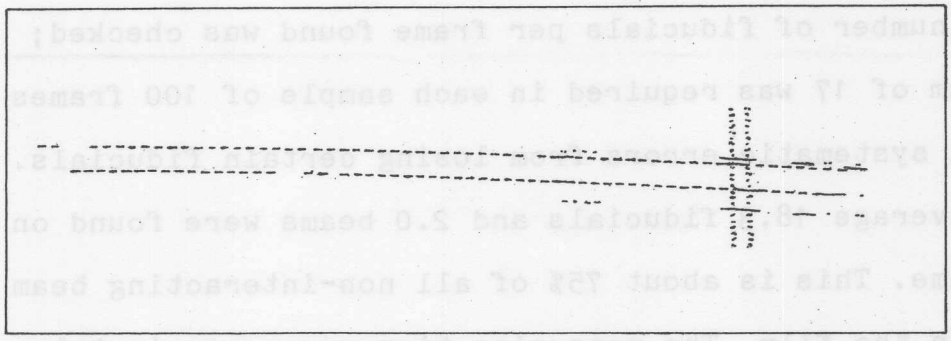

Scanning and Track Following

c.

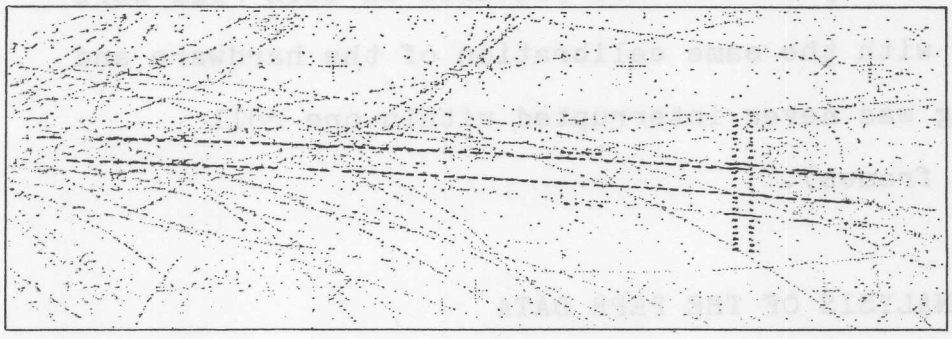

Result

Fig.9 : Automatic Scanning and Track Following of Beam Tracks with PEPR on a Typical Picture

from one view only using the same z_0 (= z at x=0) and the same dip angle for all beam tracks. In figure 10 it is verified from the measurements of the spectator events that the average z- coordinate is constant within the required accuracy for all rolls. The only disadvantage of not measuring the z- coordinates of the beams is the loss of information about possible correlations between z and the momentum.

View 1 of the 13 rolls used in this experiment was measured. During the operation every 100 frames the average number of fiducials per frame found was checked; a minimum of 17 was required in each sample of 100 frames to avoid systematic errors from losing certain fiducials. In the average 18.3 fiducials and 2.0 beams were found on each frame. This is about 75% of all non-interacting beam tracks on the film. The measuring time was approximately 1000 pictures per hour. All pictures on each roll were measured with the same calibration of the hardware and measuring was never interrupted within one roll (of 5000 frames).

4.2.3. ANALYSIS OF THE PEPR DATA

The PEPR output is reconstructed with the program PBFIT. On each event, defined as a frame with at least one measured beam track, the fiducials were fit as described

before. The resulting transformations and distortions are applied to the track data points. The x- and y- space coordinates are calculated using the optical constants and the z(x) dependence from the Vanguard measurements as mentioned above. The space coordinates are fit in the xy-plane to a circle; deletion of up to 20% of the points with residuals greater than 3 sigma is used in a standard way. The attempt to delete the PEPR scan point causes the track to fail the reconstruction. The momentum is calculated from the radius and an average value of the magnetic field as provided by a simplified field routine. An example for the statistics of a PBFIT - run is shown in table 5. If on a roll the measuring error for the fiducials, as calculated from the fiducial fit, was greater than 2.3 μ the data were rejected and the roll was remeasured.

Figure 11 shows a fraction of the results in a scatter plot of the momentum and the y- coordinate. The split in y caused by the particle separator can be seen.

The momenta are averaged and plotted as a function of the frame number in figure 12. A search for systematic fast fluctuations by Fourier transform techniques gave no evidence for periodic changes in momentum. In the search for correlations a difference of 25 MeV/c in average momenta for the upper and lower beam was found. This deviation may be due to a systematic measuring error

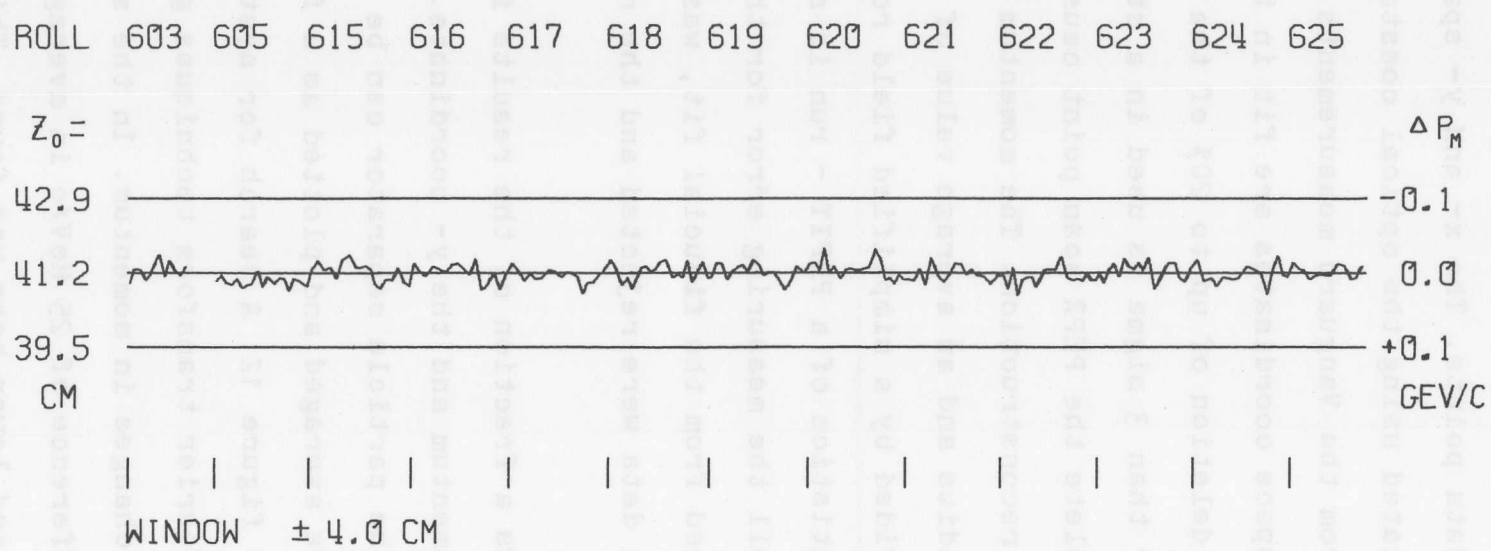

Fig.10 : z_0 for the Beam Tracks of Spectator Events

```
 PBFIT SUMMARY FOR  1 ROLL  PROCESSED ON  01/27/75

ROLL NUMBER    623

  4570 EVENTS READ .              Ø OF THEM REJECTED BY FIDUCIAL FIT .

REJECT REASON          TOO FEW FIDS     TOO MANY BAD FIDS     BAD CHISQUARED        OTHERS
NUMBER                       Ø                 Ø                  Ø                Ø

 QUALITY OF THE FIDUCIALS IN THE  4570 EVENTS KEPT :

FID #        1    2    3    4    5    6    7    8    9   10   11   12   13   14   15   16   17   18   19   20
NOT FOUND  342   45  314 2016  111   51  107 3405  424  119   49  136  144   89   58  168  148  128   85  254
BAD         74    7   44   97    5    5   14    Ø    Ø   24   14   16   23   27   12   14   27   39   28   27

      9.Ø % MISSED BY PEPR ,    Ø.6 % OF THOSE FOUND WERE REJECTED BY PBFIT.

ACCURACY (FOR NOT REJECTED EVENTS) :
FOR ALL MEASURED FIDUCIALS : Ø.ØØ6 CM  IN SPACE    OR 2.1 MICRON ON FILM
FOR ALL ACCEPTED FIDUCIALS : Ø.ØØ5 CM  IN SPACE    OR 1.8 MICRON ON FILM .


 SUMMARY FOR THE  1Ø699 TRACKS READ FROM PEPR TAPE

 22.1 % OF THE TRACKS WERE LOST OR REJECTED
LOST BY FID.FIT FAIL     TOO SHORT     GAP AND BAD FIT    # OF BAD POINTS >    CP #1 BAD       CH12 BAD       FIT ERROR >
          Ø                117             275               1156               3Ø7             277             235

THE   8332 GOOD TRACKS
HAVE AN AVERAGE OF 14.6 GOOD POINTS ;    8.6 %  OF POINTS WERE DELETED .
# OF TRACKS WITH      Ø      1    2,3   4 TO 7    DELETED POINTS
                    21Ø4   4855  1335     38

AVERAGE LENGTH OF TRACKS 143.Ø CM
       ACCURACY : .ØØ8 CM SPACE  OR  2.6 MICRON ON FILM
```

Tab.5 : Example of a PBFIT Summary

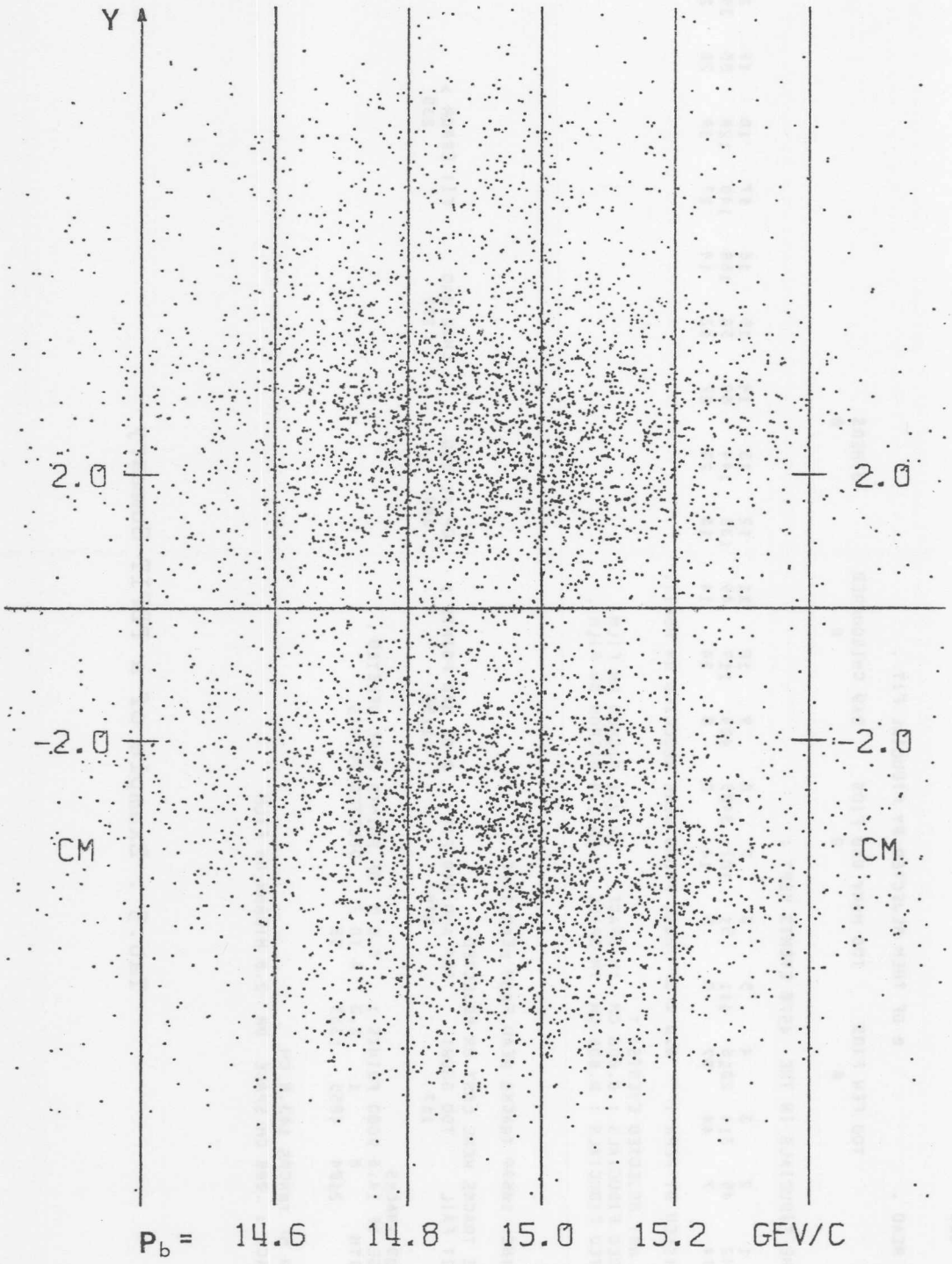

Fig.11 : Deflection y versus Momentum for Beam Tracks Measured with PEPR

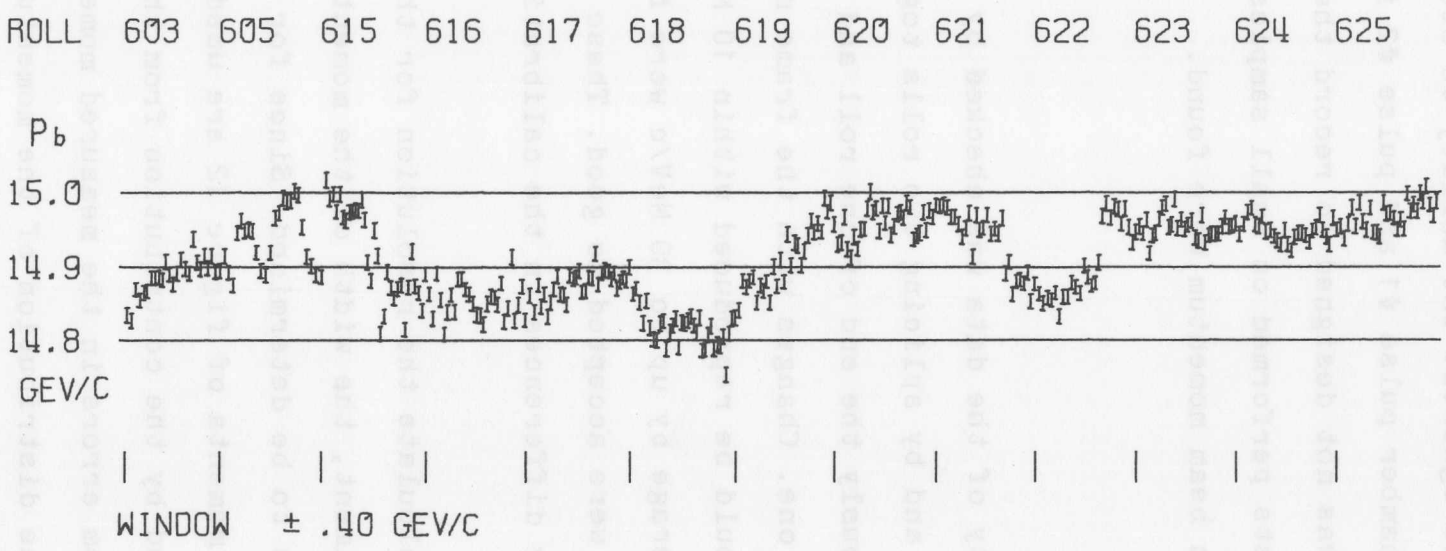

Fig.12 : Beam Momentum as Obtained from the PEPR Data

and to correlations in kinking tracks and, since it is negligibly small, it is ignored. The ability to study differences between chamber pulse #1 and pulse #2 is limited because PEPR was not designed to record the pulse number. In the few tests performed on small samples of data no differences in beam momentum were found.

4.2.4. ERROR ANALYSIS

The reliability of the data was checked by remeasuring some film and by splicing two rolls together and measuring continuously the end of one roll and the beginning of the next one. Changes with the frame number in the measurements could be reproduced within 10 MeV/c but offsets of the average by up to 30 MeV/c were found on measurements which were accepted as good. These offsets are probably caused by differences in the calibration of the hardware.

In order to calculate the resolution for the mass m_x in this experiment, the width of the momentum spread of the beam has to be determined. Since for the calculation of m_x the momenta of figure 12 are used, the width has to be reduced by the contribution from the slow drifts, i.e. the random errors in the measured momenta are investigated on the distribution of the momentum differences from the local average $\bar{p}_n$ (local being defined

as the averages shown in figure 12). The contributions to the width of this distribution of $(p - \bar{p}_n)$ are :

Random error of fiducial fit	± 60 MeV/c
Random error of track point measurements	± 80 MeV/c
Spread in the z- coordinate of the beam	± 70 MeV/c
Coulomb multiple scattering error	± 120 MeV/c
Strong interaction single scattering error	(± 800 MeV/c)
Internal spread of the beam	?

The error due to hadronic single scattering is dominant and its effect is commonly reduced by track rejection techniques. To get a meaningful estimate for the internal spread of the beam the technique has to provide an accurate prediction for the remaining width. The cut-off method on a detectable kink[14] (like rejects of bad circle fits) is not very effective at 15 GeV/c; a scatter in the middle of the track by only 0.1° varies the sagitta by 10%. The cut-off on a visible recoil[15] is not suitable for an automatic scan that is incapable of detecting recoils. On beam measurements, where the momentum of the track is known a priori to much better accuracy than the single scattering error, a cut-off on the measured momentum is possible. This method is especially effective because the single scattering error distribution is non-Gaussian with a very narrow peak at zero, containing more than half of the data, (tracks that do not scatter or tracks that are fixed up correctly or almost correctly by the circle fitting routine) and long tails extending over several GeV/c. For a numerical investigation the PEPR output of a

perfect beam track of 15 GeV/c was simulated and modified by kinks as obtained from a Monte Carlo of momentum transfers with a probability e^{bt}. The reconstruction with PBFIT failed 55% to 65% of these kinking tracks, depending on the value of b (b = 11, 15, 20, 25 $(GeV/c)^{-2}$ were tried). The momentum distributions are almost independent of the value of b and, assuming a cross section of 40 mb for kinks (elastic scattering and events with leading particles), its width (in agreement with reference 14) is about 800 MeV/c.

The width $\sigma_w = \sqrt{\overline{(p-\bar{p}_n)^2}}$ after rejection of data outside a window $\pm p_w$ of the measured momentum is plotted as a function of p_w in figure 13 for the Monte Carlo data of kinking tracks (curve 1) and for the real data (curve 2). The fraction of tracks in the real data that are kinking is determined by subtracting (squared) a fraction of curve 1 from curve 2 so that the resulting curve has a horizontal asymptote for high values of p_w. The correct fraction of curve 1 is plotted as curve 6; it is the single scattering error as a function of the cut-off p_w.* Curve 4 is the result of the subtraction. Its shape is consistent with a Gaussian within 0.002 GeV/c

* The fraction obtained by this subtraction is the probability for a track to have a kink, corresponding to a cross section of 90 mb; this means that more than half of the kinks are actually caused by track following mistakes.

in the vertical scale of figure 13; the asymptotic value, 205 MeV/c, is its width.

Now the unfolding of the internal width of the beam momentum is straight forward. The result of 110 MeV/c ± 25 MeV/c is consistent with the specifications for the momentum bite of the beam line.

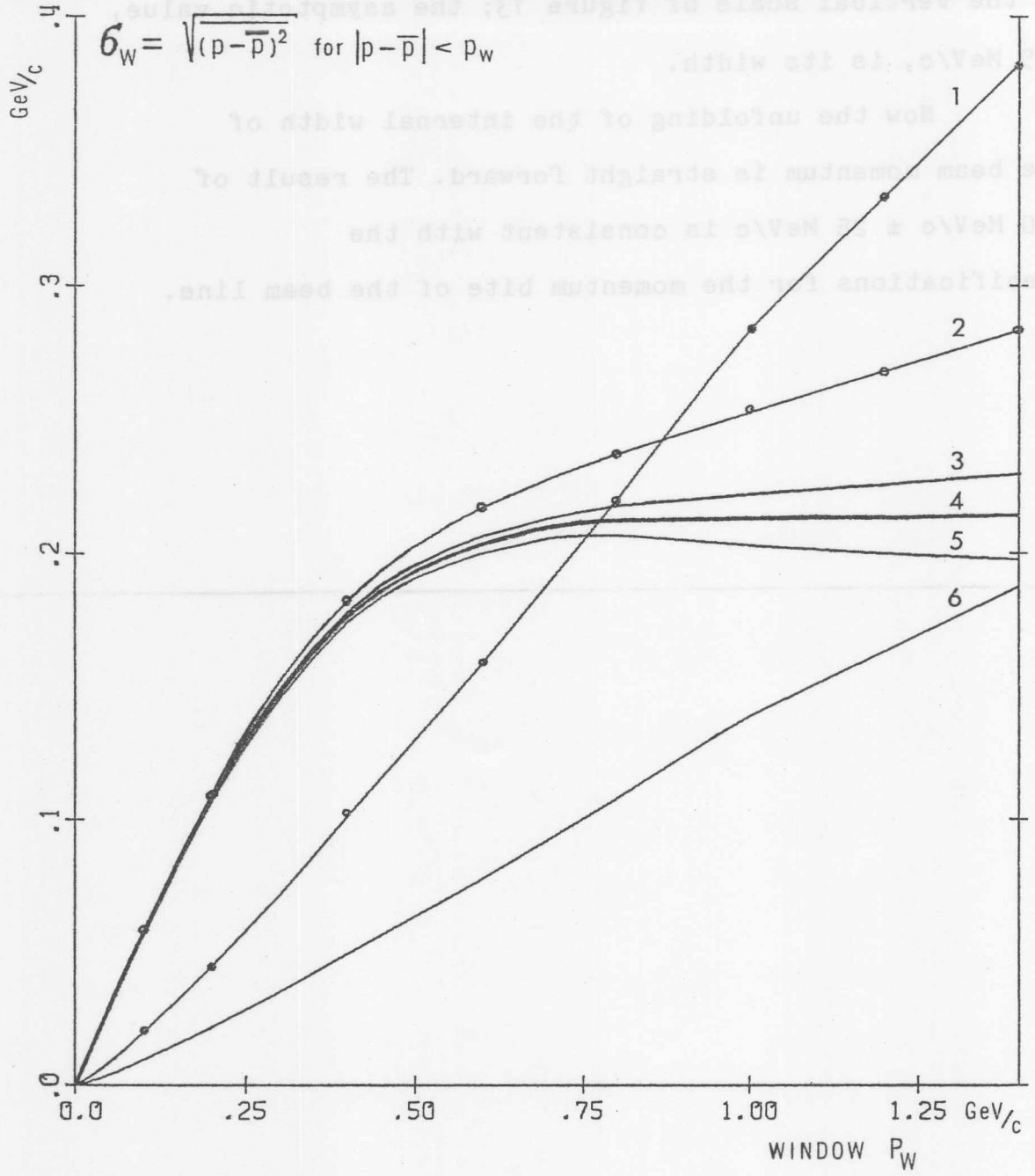

Fig.13 : Error Curves for PEPR Beam Measurements

5. KINEMATICS

The use of deuterium as a neutron target introduces difficulties for the following reasons:

a) The neutron target is not at rest and its momentum at the time of the interaction can only be determined by the use of models (e.g. impulse model). The presence of Fermi motion, which usually is an undesired difficulty, is of essential importance for this experiment. The kinematics of interactions with a moving target is discussed in section 5.1.

b) The target is not a pure neutron target. The neutron interactions must be separated from proton interactions and double (or coherent) scattering. The contaminations from interactions involving the target proton are discussed in section 5.2.

c) The neutron is bound to the proton. Although the binding energy is only -2.23 MeV there may be noticeable differences between interactions with free neutrons and interactions with a neutron that is slightly off the mass shell. The separation of the nucleons in the deuteron is not much larger than their radii and therefore causes non-negligible "screening".[17,18] The fact that the neutron is in a bound system is of no disadvantage for the study of the missing mass m_x. The implication on the cross sections is discussed in chapter 8.

5.1. THE TARGET MOTION

In the approximation of the impulse model[16] ~90% to 95% of the inelastic interactions can be described as scattering from free neutrons and free protons; the measurement of the reaction (1-1)

$$\bar{p}d \longrightarrow p_s X^-$$

is equivalent to the study of the process

$$\bar{p}n \longrightarrow X^-$$

if p_s is really a spectator with no scattering or rescattering off the proton in the deuteron.
The CM-energy $\sqrt{s}$ of the $\bar{p}n$- system for an incident beam momentum of 14.9 GeV/c with the target neutron at rest is equivalent to a mass of

$$m_0 = 5.45 \text{ GeV}/c^2 . \qquad (5\text{-}1)$$

The Fermi motion of the nucleons in the deuteron sweeps the CM- energy with a probability that is obtained from the deuteron wave function, thus providing a continuous spectrum of CM- energies $m_x c^2 = \sqrt{s}$ in a range of about

$$5.0 \text{ to } 6.0 \text{ GeV} . \qquad (5\text{-}2)$$

m_x is determined by the momentum $\vec{p}_{sp}$ of the spectator proton using energy - momentum conservation for the reaction (1-1) :

$$m_x^2 = m_d^2 + 2m_p^2 + 2m_d E_b - 2E_{sp}(m_d+E_b) + 2\vec{p}_b\cdot\vec{p}_{sp} \qquad (5\text{-}3)$$

or

$$m_x^2 = m_0^2 - 2T_{sp}(m_d+E_b) + 2\vec{p}_b\cdot\vec{p}_{sp} \qquad (5\text{-}3')$$

where m_p is the proton or antiproton mass,
m_d is the deuteron mass,
p_b, E_b are the laboratory beam momentum and energy,
E_{sp} is the laboratory energy of the spectator and
T_{sp} is its kinetic energy.

The kinematic boundary according to equations (5-3) and (5-1) is shown in figure 14 (solid lines). The dashed line represents p_{sp} versus m_x at $\cos\vartheta = 0$ (ϑ is the angle between the spectator momentum and the beam). Masses greater than m_0 can only be obtained from forward going spectators; a small region below m_0, approximately 0.1 GeV/c^2 wide, is populated by both forward and backward spectators; masses below that region are only produced by backward spectators.

Among the various approximations[18,19,20] to the numerical deuteron wave functions[21] the most popular one is the Hulthén wave function for the S- wave, neglecting the ~4% D- wave contribution[19] :

$$\Phi(\vec{p}) \propto \frac{1}{(p^2+a^2)(p^2+b^2)} \quad . \qquad (5\text{-}4)$$

Ignoring the flux factor and assuming a constant total cross section for $\bar{p}n$- scattering in the range (5-2) of $\sqrt{s}$

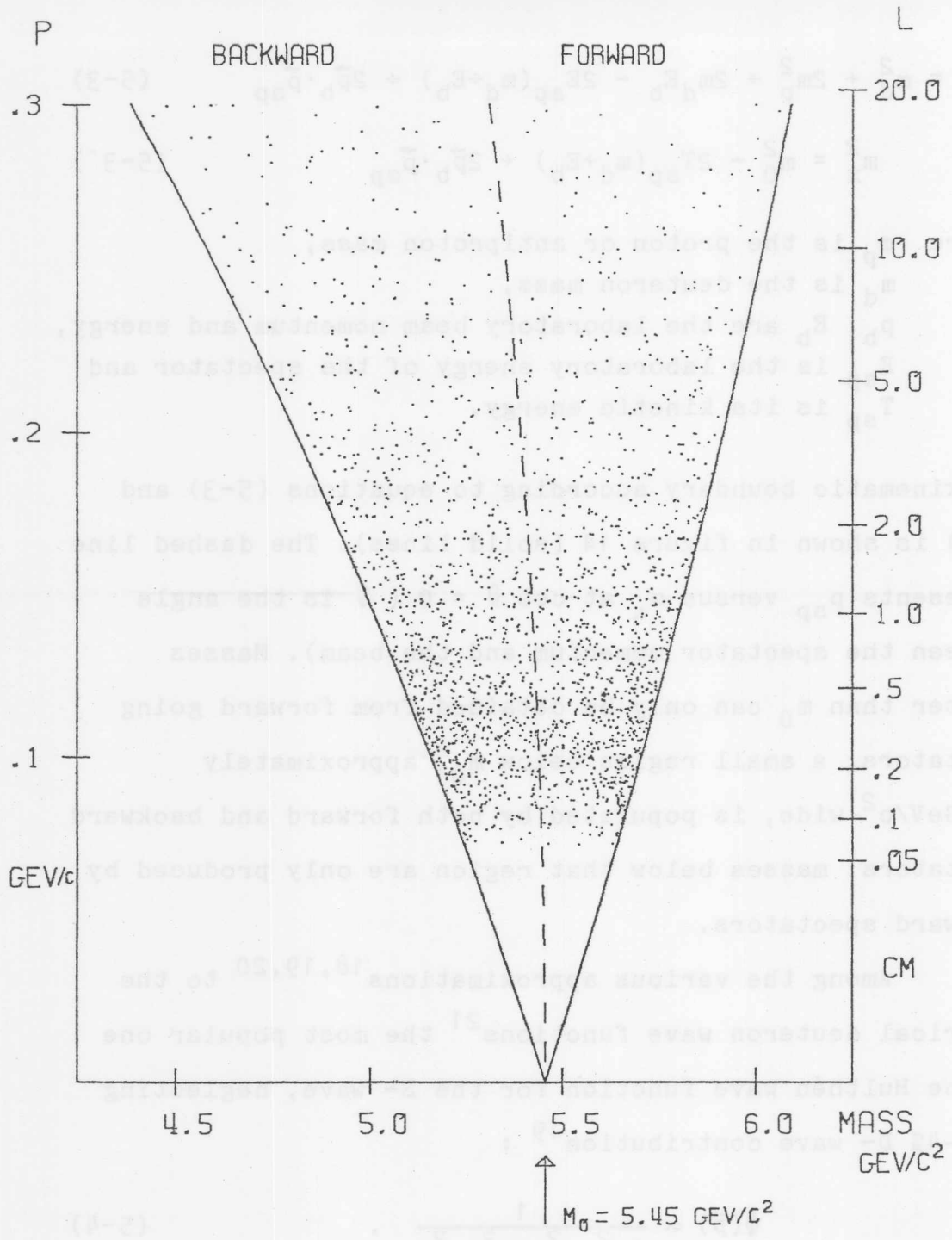

Fig.14 : Kinematic Region for m_x and a Scatter Plot of Monte Carlo Events

the momentum distibution n(p) is obtained by integrating Φ^2 over the solid angle Ω :

$$n(p) = A \cdot \frac{p^2}{((p^2+a^2)(p^2+b^2))^2} \quad . \qquad (5\text{-}5)$$

The area $\int_0^\infty n(p)\, dp$ is normalized to 1 with

$$A = \frac{4}{\pi}\, ab\, (a+b)^3 \quad . \qquad (5\text{-}6)$$

Monte Carlo events are plotted in figure 14 using this approximation with a = 45.7 MeV/c, b = 237 MeV/c and the following visibility cut-off for slow spectators (for $p < 100$ MeV/c) : the momentum vector of the spectator is projected into a plane parallel to the beam. Events with a projected momentum p_{xy} of less than 70 MeV/c are rejected, events with p_{xy} between 70 and 100 MeV/c are accepted with a Gaussian probability centered at 100 MeV/c with a half width of 20 MeV/c. This visibility cut-off reduces the number of events around $\cos \vartheta = 0$ for the low momentum spectators.

The relation between the cross section σ and the number of events N is given by

$$dN = \rho_n' \cdot \frac{L_T}{v_b} \cdot F \cdot \sigma_{\bar{p}n}\, d\vec{p}_n \qquad (5\text{-}7)$$

where L_T is the total track length of the beam,

$\vec{p}_n = -\vec{p}_{sp}$ is the neutron momentum,

ρ_n' is the density of neutrons with momentum $\vec{p}_n$,

F is the Møller[22] flux factor given by

$$F = ((\vec{v}_b - \vec{v}_n)^2 - (\vec{v}_b \times \vec{v}_n)^2)^{1/2} \qquad (5\text{-}8)$$

with $\vec{v}_b$, $\vec{v}_n$ being the beam and neutron velocities. The neutron density ρ_n' can be expressed by the Hulthén distribution (5-5) and the particle density ρ_n in the target, the $\bar{p}n$- cross section can be approximated by

$$\sigma_{\bar{p}n} = \sigma_0(1-c(s-s_0)) \qquad (5\text{-}9)$$

where σ_0 is the $\bar{p}n$- cross section at $s_0 = m_0^2 c^4$

c is the slope $\frac{d\sigma}{ds}$ of the cross section at $s = s_0$.

Then

$$dN = L_T \cdot \rho_n \cdot \sigma_0 \cdot A\ ((p^2+a^2)(p^2+b^2))^{-2}$$

$$\cdot \frac{1}{v_b}\sqrt{(\vec{v}_b-\vec{v}_n)^2-(\vec{v}_b\times\vec{v}_n)^2}\ p^2\ dp\ \frac{1}{2}\,d\cos\vartheta\ . \qquad (5\text{-}7')$$

Here $\frac{A}{2}\ p^2\ ((p^2+a^2)(p^2+b^2))^{-2}\ dp\ d\cos\vartheta$ is the normalized probability density for a neutron to have the momentum p and the angle ϑ with respect to the beam. Integration over $\cos\vartheta$ can be done in a closed form and provides the momentum distribution. Results of the integration are used for fits and predictions of the measured data (Fig.19,20). Angular distributions were obtained by numerical integration (Fig. 21 to 23).

5.2. CONTAMINATIONS

5.2.1. DEVIATIONS FROM THE IMPULSE MECHANISM

For the study of the process (1-1) as a missing mass experiment, deviations from the impulse mechanism are unimportant as long as one does not want to extract free $\bar{p}n$- cross sections. The fact that the neutron is slightly off mass shell and that additional momentum transfers (Fig.15) to the proton are possible may even enhance a resonant X^- state.

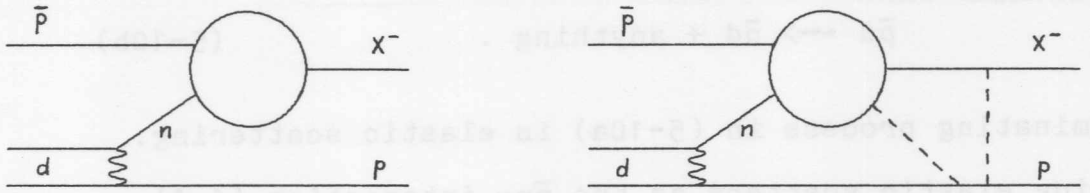

Fig.15 : The Impulse Mechanism (left) and Possible Resonant Double Interactions (right)

As an exchange of an I-spin 1 particle is possible the otherwise pure I-spin 1 state of the X^- can contain a small admixture of I=2 states.

Deviations from the impulse process are not considered as contaminations in this experiment if the antiproton interacts mainly with the neutron and if the track identified as a spectator is really a proton.

5.2.2. PARTICLES MISIDENTIFIED AS A PROTON

Antiprotons may look like a spectator proton if they interact near the vertex of the event and form a 0- pronged secondary event. These events are rare though and could be distinguished by a check on charge conservation for the primary interaction.

The only important contribution from particles mistaken as protons comes from stopping deuterons :

$$\bar{p}d \longrightarrow \bar{p}d + \text{anything} \qquad (5\text{-}10a)$$

$$\bar{p}d \longrightarrow \bar{n}d + \text{anything} \; . \qquad (5\text{-}10b)$$

The dominating process in (5-10a) is elastic scattering. Mistaking elastic scatters as the $\bar{p}n$- interaction (1-1) generates a missing mass m_x according to equation (5-3′) constrained by $2T_{sd}(m_d+E_b) = 2\vec{p}_b \cdot \vec{p}_{sd}$ to the kinematics of the elastic scattering of

$$m_x \simeq m_0 + \frac{E_b+m_d}{2m_0} \cdot p_{sp}\left(\frac{p_{sd}}{m_d} - \frac{p_{sp}}{m_p}\right) \qquad (5\text{-}11)$$

in non-relativistic approximation. Here p_{sd} is the momentum of the spectator-like deuteron, T_{sd} is its kinetic energy and p_{sp} is the momentum that a proton of the same range would have. For deuteron momenta around 0.2 GeV/c

$$p_{sd} \simeq 1.7\, p_{sp}$$

and

$$m_x \simeq m_0 - 0.25\, p_{sp}^2 \quad . \qquad (5\text{-}11')$$

Equation (5-11′) shows that elastic scattering events will contaminate the missing mass spectrum m_x in a narrow region near m_0 with a half width of $\Delta m_x = 0.25\, \Delta p_{sp}^2 \simeq 5$ MeV/c^2. Experimental results are shown in figure 17 and figure 3. The scattering angle is close to and always less than 90° in the lab.

Among the other interaction channels in (5-10) the only one studied at $p_b = 15$ GeV/c is the reaction $\bar{p}d \longrightarrow \bar{p}d\pi^+\pi^-$ with a cross section of 0.3 mb [23]. The total cross section for inelastic coherent deuteron events is estimated to be 1.5 to 2.0 mb. The resonance productions

$$\bar{p}d \longrightarrow \bar{N} + d \qquad (5\text{-}10c)$$

are constrained in the quantity m_x in a similar way as elastic scattering by $2T_{sd}(m_d+E_b) = 2\vec{p}_b\cdot\vec{p}_{sd} - (m_N^2-m_p^2)$. In equation (5-11′) m_0 is replaced by m_{0N} with

$$m_{0N} \simeq m_0 + R\cdot(m_N^2-m_p^2)/2m_x \qquad (5\text{-}12)$$

where m_N is the mass of the $\bar{N}$ - resonance,

R is essentially the ratio $p_{sp}/p_{sd} \simeq 0.59$

(its more accurate form also contains the ratio between the beam momentum used in the calculation and the true beam momentum) .

The width of the $\bar{N}$ - resonance reduces to a width in m_X by the factor $0.59\ m_N / m_x$, which is approximately one sixth for the low N^* states. Therefore these events will produce narrow peaks in the m_x - spectrum if the beam momentum is constant or a constant beam momentum is used for the calculation of m_x. A change of 1% in the true value of the beam momentum varies only the factor R by 1%, whereas adjusting the value p_b by 1% changes m_0 by 1/2 %. The kinematic region for the coherent deuteron events is in the forward hemisphere only; the sample of events with backward spectators is free of deuteron contamination.

5.2.3. PROTON INTERACTIONS

Interactions of the antiproton with the proton can produce a low momentum proton p_L which looks like a spectator, while the neutron is the true spectator :

$$\bar{p}d \longrightarrow n_s\ \bar{p}\ p_L + \text{anything} \qquad (5\text{-}13a)$$

$$\bar{p}d \longrightarrow n_s\ \bar{n}\ p_L + \text{anything}\ . \qquad (5\text{-}13b)$$

These interactions are the major source of contaminations. Reactions (5-13a) contain $\bar{p}p$ quasi-elastic scattering. The missing mass m_x of these events is like in $\bar{p}d$ elastic scattering still centered near m_0 but because of the Fermi motion of the proton it spreads over a much larger region in the missing mass spectrum. Resonant channels in

the proton interactions of the type

$$\bar{p}p \longrightarrow \bar{N} + p_L \qquad (5\text{-}13c)$$

will also resonate in the quantity m_x with

$$m_x = m_0 + (m_N^2 - m_p^2)/2m_x - T_L(m_d - m_p)/m_x \qquad (5\text{-}14)$$

if the Fermi motion of the target proton is ignored. (the energy T_L of the low momentum proton varies m_x only by ± 3 MeV/c^2). The target motion, though, causes the resonance to be spread out over several 100 MeV/c^2 in the X^- - mass. The center of the peak does not coincide with the peak caused by the equivalent reaction in (5-10c).

The kinematics of the inelastic channels in the reactions (5-13) can be understood with the results from a $\bar{p}p$ - experiment[24] at 12.1 GeV/c at the CERN 2m bubble chamber, which studied the reaction

$$\bar{p}p \longrightarrow \bar{p}p\pi^+\pi^- \; . \qquad (5\text{-}15)$$

The distribution of the laboratory momentum p_{Lp} for the proton is shown in figure 16a, the angular distibution (Fig.16b) is obtained under the restriction $0.11 \text{ GeV/c} < p_{Lp} < 0.36 \text{ GeV/c}$ to eliminate detection biases and most protons that do not stop in the chamber. (All data were read from graphs).

The kinematic limit for $\cos \vartheta$ in reaction (5-15) is approximately (for $p_b >> m_p$)

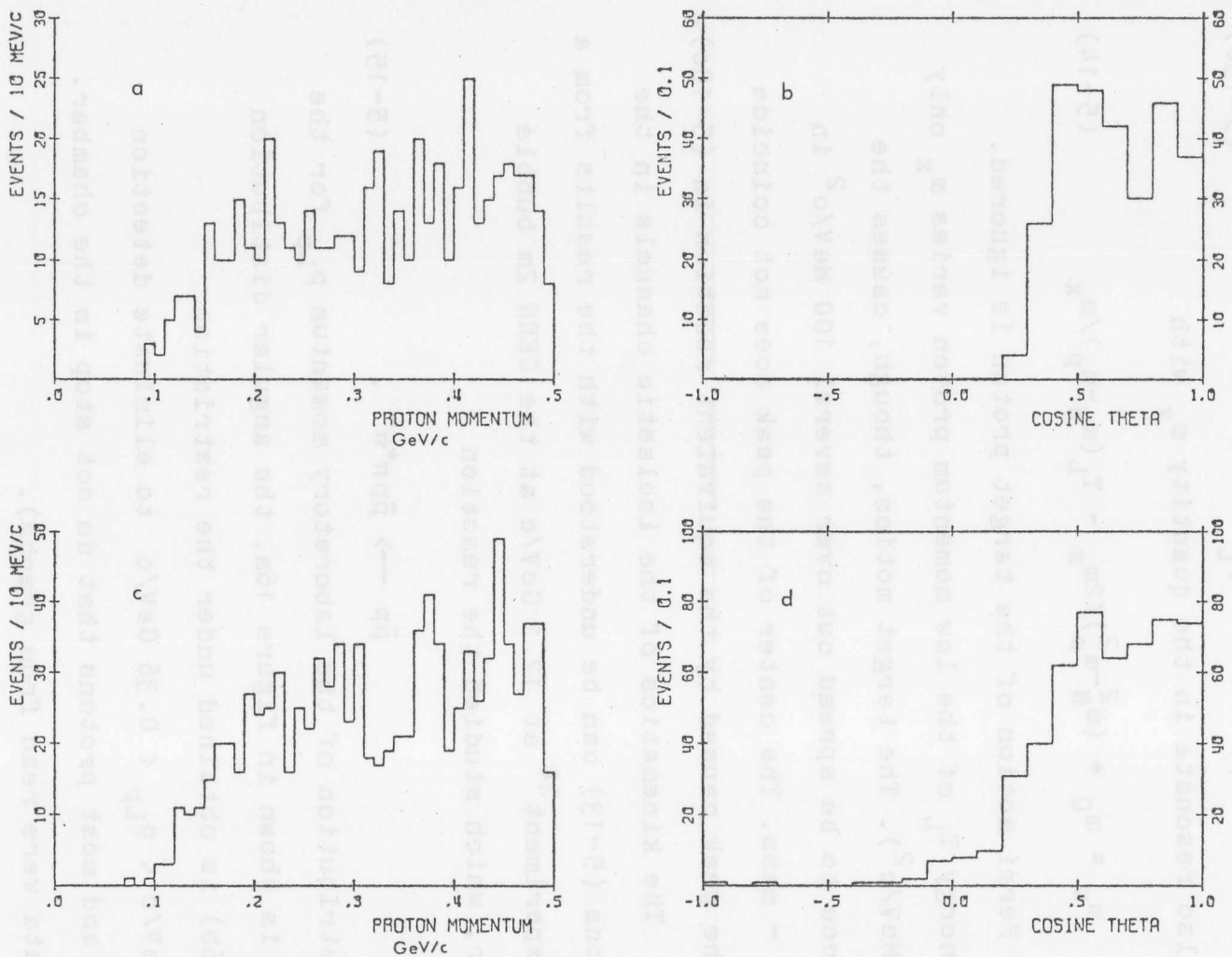

Fig.16 : $\bar{p}p$ Data at 12 GeV/c (a, b) and their Distributions after Random Transformation by Spectator Momenta (c, d)

$$(\cos\vartheta)_{min} \approx \sqrt{\frac{\Delta m}{2p_b}\,(1+\Delta m/m_p)} \qquad (5\text{-}16)$$

where Δm is the mass of the $(\pi^+\pi^-)$ - system.
The threshold for this 4-prong reaction is at $\Delta m = 2\,m_\pi$ and $(\cos\vartheta)_{min} \approx 0.12$.
The lower limit for $\cos\vartheta$ due to visibility in the bubble chamber is higher than the kinematic limit. The value of

$$\cos\vartheta = \frac{2T_L(E_b+m_p) + m_p\Delta m + (\Delta m)^2}{2p_b p_{Lp}} \qquad (5\text{-}17)$$

at $p_{Lp} = 0.11$ GeV/c is $(\cos\vartheta)_{min} = 0.19$.

To apply the above results to the inelastic $\bar{p}d$ - cross sections (5-13) the proton momenta have to be transformed by the Fermi momentum of the proton target. For this purpose spectator momenta have been generated randomly with a Hulthén distribution and are used as Lorentz transformation for the measured momenta of reaction (5-16). If the resulting proton is too slow to be visible in the bubble chamber the event is rejected (a smooth cut-off is applied for momenta below 110 MeV/c).

The momentum distribution (Fig.16c) is almost flat above 0.2 GeV/c, the angular distribution for momenta between 0.11 GeV/c and 0.36 GeV/c (Fig.16d) shows the original nearly rectangular shape with the slope at threshold smeared by the width of the Hulthén distribution. In general one can expect the angular distribution for each channel in (5-13) to have a similar behavior with the

flat portion restricted to higher values of $\cos\vartheta$ as $(\cos\vartheta)_{min}$ increases with higher missing masses.

The total angular distribution for all inelasic channels is the sum of these distributions and should therefore be continuously rising up to $\cos\vartheta = +1$.

5.2.4. EVENTS WITH 2 SLOW PROTONS

In the interactions with the neutron (proton spectator events) a slow proton may be produced, usually as a charge transfer to the neutron :

$$\bar{p}d \longrightarrow p_s\ p_L + \text{anything} . \qquad (5\text{-}18)$$

Either of the two proton tracks may be too short to be visible in the bubble chamber; in most cases the invisible one is the spectator, because a large part (~70%) of the Hulthén distribution is below the visibility limit. If one of the tracks is going backwards, it is most likely the spectator according to distribution figure 16d. The interactions (5-18) can easily be distinguished as being even pronged events with two slow proton tracks or odd pronged events with one visible proton.

5.2.5. BEAM AND TARGET IMPURITIES

Beam contaminations by π^- and K^- mesons are approximately 5% (chapter 4); the hydrogen impurity of

the deuterium amounts to 2% by weight. Mesonic beam contaminations are negligible; their cross sections are only half the antiproton cross section so that only 2.5% of the events are induced by π or K mesons.

The target impurity simply adds to the contaminations (5-13) for the channels not resonating in the mode (5-13c). Reactions (5-13c) off a free proton will produce resonances in m_x in the 2- and 4- prong data and, because of the absence of Fermi motion, they will be narrow. The amount of hydrogen admixture is so small though that one cannot expect to observe any of these resonances.

6. PRELIMINARY EXPERIMENTS

The film of 98000 photographs from the first run in June 1970 was divided equally for analysis among the Strasbourg group and the Rutgers - Stevens group. For a survey 25000 pictures were scanned for all interactions with an outgoing clear proton which stopped in the chamber. Track coordinates that are necessary to reconstruct the momentum (from range) and the angle of the proton track with respect to the beam track were measured on an image plane digitizer. The mass m_x recoiling against the proton was calculated from energy-momentum conservation and is plotted in figure 17. The apparent structure in this mass distribution is the elastic peak on top of a broader peak of events of quasi-elastic scattering off the proton in the deuteron (compare chapter 5).

Subsequently another 40000 pictures of the total film with the best quality regarding contrast and focus were also scanned for events with stopping protons and measured on a film plane digitizer. In this scan all 2-pronged events were ignored because this class of events is dominated by elastic and quasi-elastic scattering. Partial results were presented at an APS - meeting[25] in 1972; the final data of this scan are contained in the mass plot figure 18.

For comparison the $\bar{p}p$ total cross section data

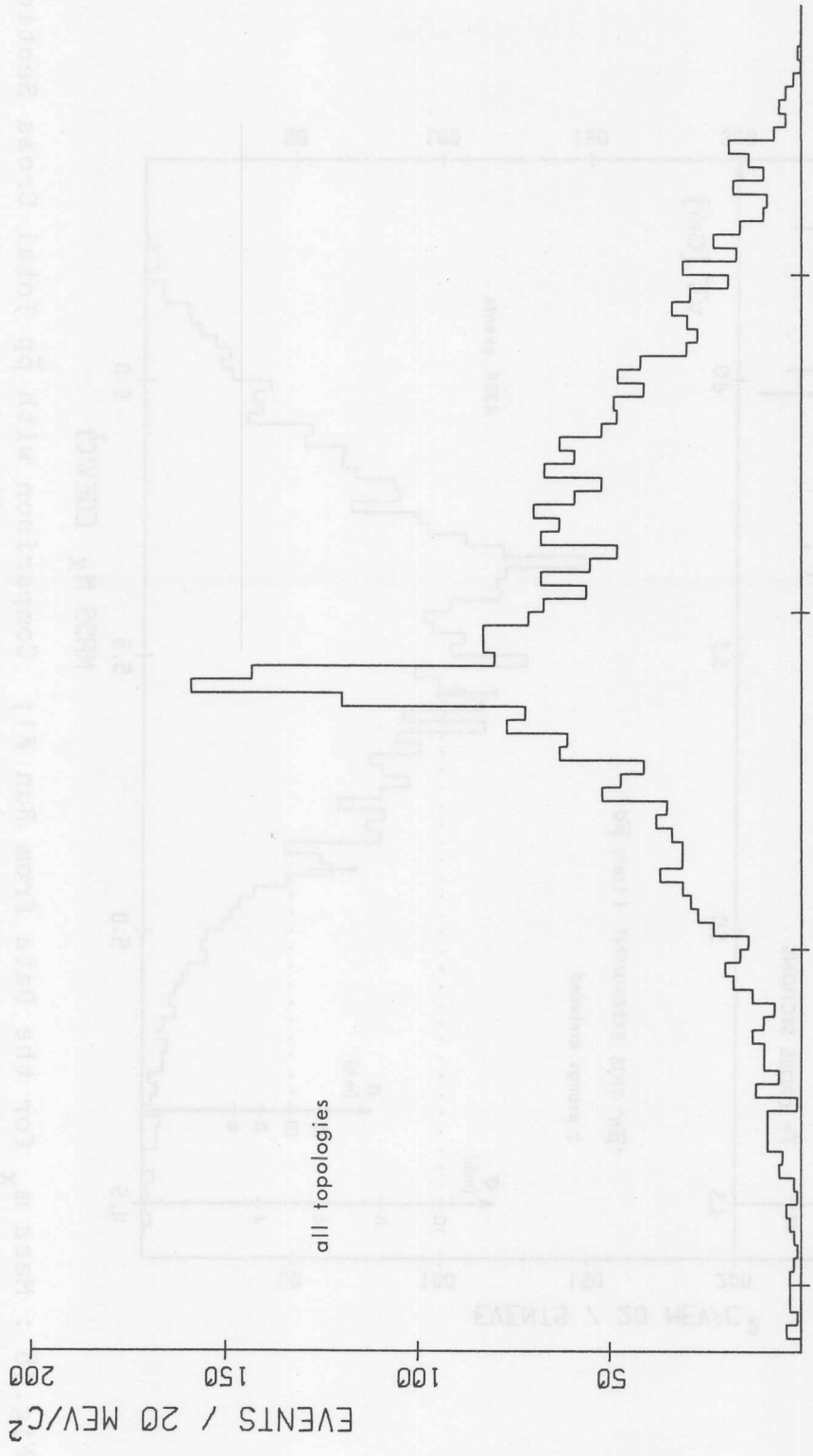

Fig.17 : The Mass m_x for all Topologies (IPD-Data)

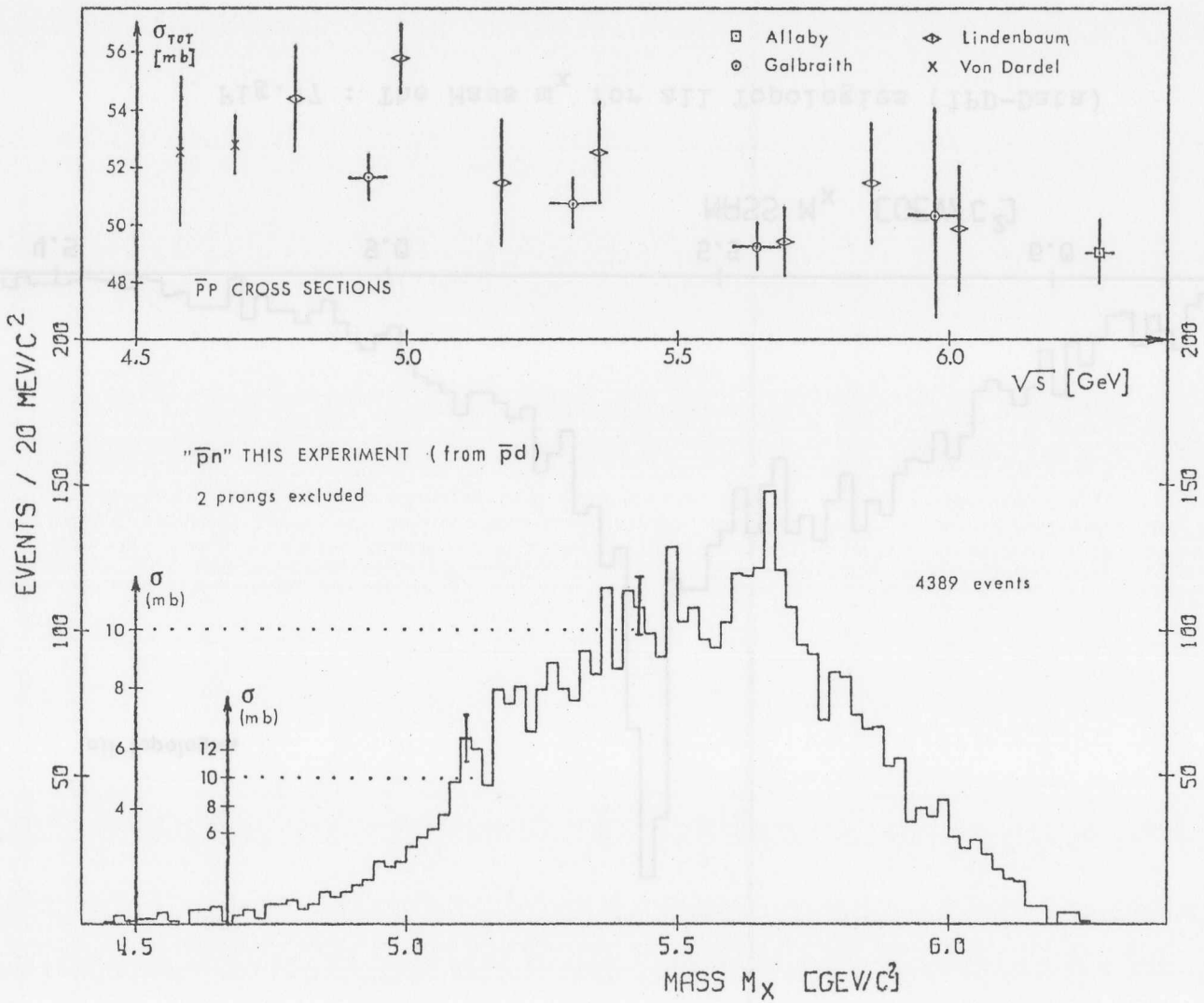

Fig.18 : Mass m_x for the Data from Run #1; Comparison with $\bar{p}p$ Total Cross Sections

are shown in the upper part of the graph. The separation of the data points is large compared to the resolution of this experiment. The comparison of the cross sections can only be considered as an estimate : the $\bar{p}d$- data in the lower histogram do not contain elastic scattering or any other 2-pronged event. Double scattering and contaminating events (chapter 5) contribute mainly at masses greater than 5.5 GeV/c^2. The flux for the $\bar{p}n$ interactions depends on the value of s for the $\bar{p}n$- system, mainly determined by the deuteron wave function. The requirement of a visible spectator reduces the flux largely around $m_x = m_0$. Two examples for approximate scales of cross sections are drawn into the plot. For a more rigorous discussion of cross sections refer to chapter 8.

Indications of changes in the momentum of the beam were observed in these data. Instabilities in the incident momentum of more than 100 MeV/c affect the resolution for the mass m_x noticeably. Various studies were performed, including investigations of beam tracks on the measured events for this experiment and other experiments[23,26] on the same film as well as measurements of non-interacting beam tracks.

On 4 of the rolls (5000 pictures per roll) 15 beam tracks were measured every 500 frames. An F-test[27] for the 8 samples of beam data for each half roll revealed a probability of less than 1% that the 8 samples derive

from a common distribution. Mainly due to the multiple scattering error and due to the single hadronic scattering[14] (small kinks) in the chamber or upstream, the error of the average momentum of a 15 track sample is about 100 MeV/c. To reduce this source of error one can select beam tracks that are parallel to each other within a very tight tolerance. 500 beam tracks on 3/4 of the film used in figure 18 have been measured this way to provide an average momentum with an accuracy of 40 MeV/c every 2500 frames. The results, showing differences of up to 300 MeV/c, confirm the hypothesis of variations in the beam momentum. The data have been used - where available - for the calculation of the mass in figure 18.

All the above methods for monitoring the beam momentum lack sufficient statistics. When the film from the second run of 125000 pictures in February 1973 was available, it was decided not to proceed on the analysis of the beam momentum in the first run. The quality of the new film was considerably better so that automatic measurements with the PEPR-device were conceivable. In addition, further exchanging of film of the first run between Europe and the United States did not seem worthwhile.

The data of run #2 were treated separately and in the following chapters only these data are discussed. Although most of the techniques, data gathering and

processing procedures apply to run #1 as well, some differences in the scanning rules and especially a systematic uncertainty of about 300 MeV/c in the relative values of the beam momenta in the two runs motivated the decision not to combine the data.

7. SPECTATOR DISTRIBUTIONS

Angular and momentum distributions for the measured spectator protons are compared with the predictions in chapter 5. The distribution of the momenta p_{sp} for all events, shown in figure 19, cannot be described by the Hulthén function because of the presence of contaminations. As explained in chapter 5, the contaminations should be negligible for backward going protons. The momenta of the backward going protons are plotted in figure 20; the shape of the distribution agrees with the theory (Hulthén wave function with a = 45.7, b = 260 MeV/c; $d\sigma/ds = -2.5$ $\mu b/GeV^2$; other corrections as in section 5.1; amplitude fitted) in the momentum interval of 120 to 220 MeV/c. Below 120 MeV/c the detection efficiency decreases and approaches zero for spectator tracks shorter than 1 mm. The sudden increase of the cross section above 220 MeV/c has been observed by other experiments with various beam energies and particles[28,29]. The D - wave of the deuteron wave function averages at slightly higher spectator momenta[19] but its shape is very similar to the shape of the S - wave distribution, so that it cannot explain the excess of spectators with high momenta. Most likely the enhancement above 220 MeV/c is caused by double scattering with an exponential probability for the momentum transfer $|t|$ to the proton. The number of events

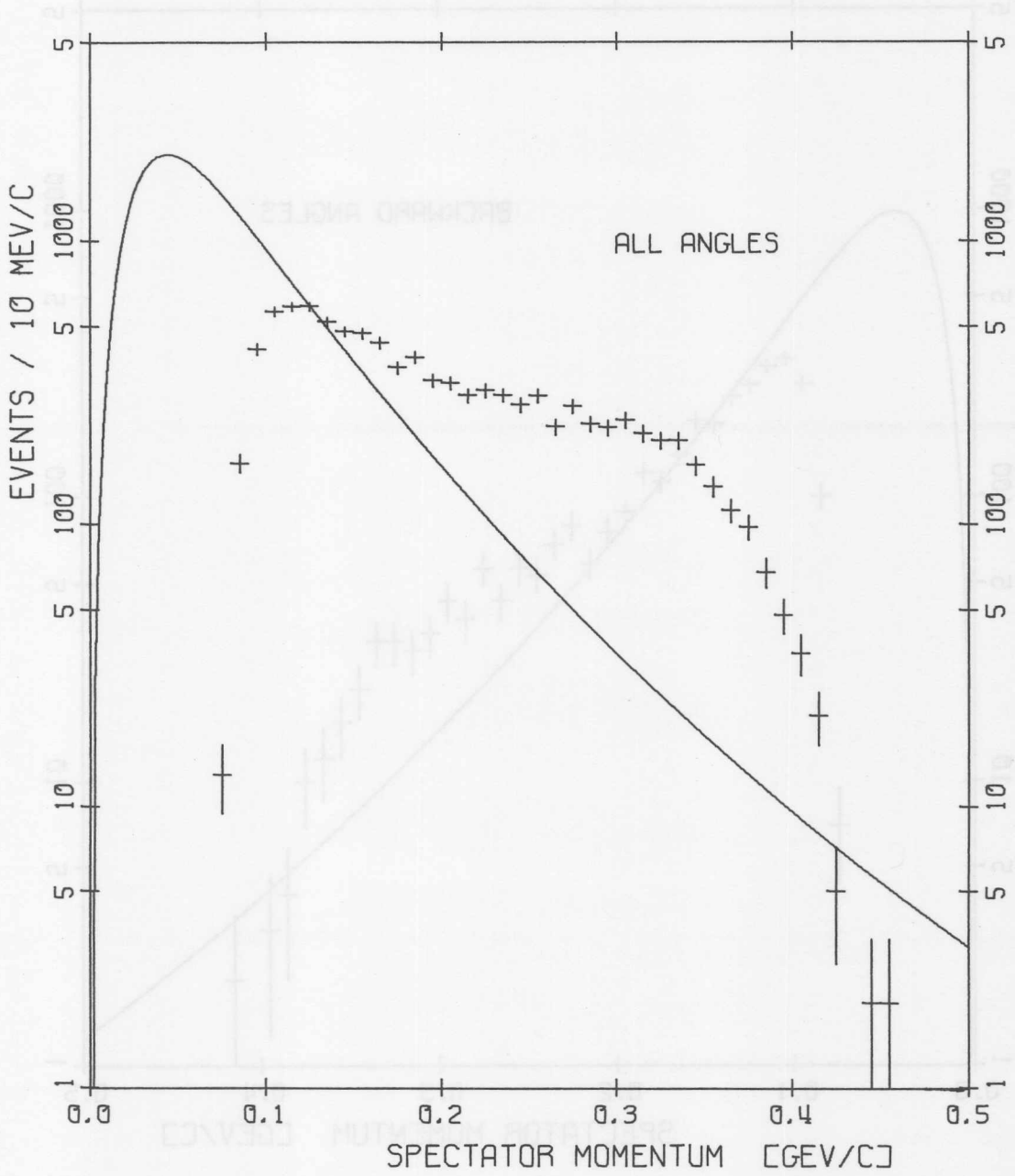

Fig.19 : The Spectator Momentum for all Events

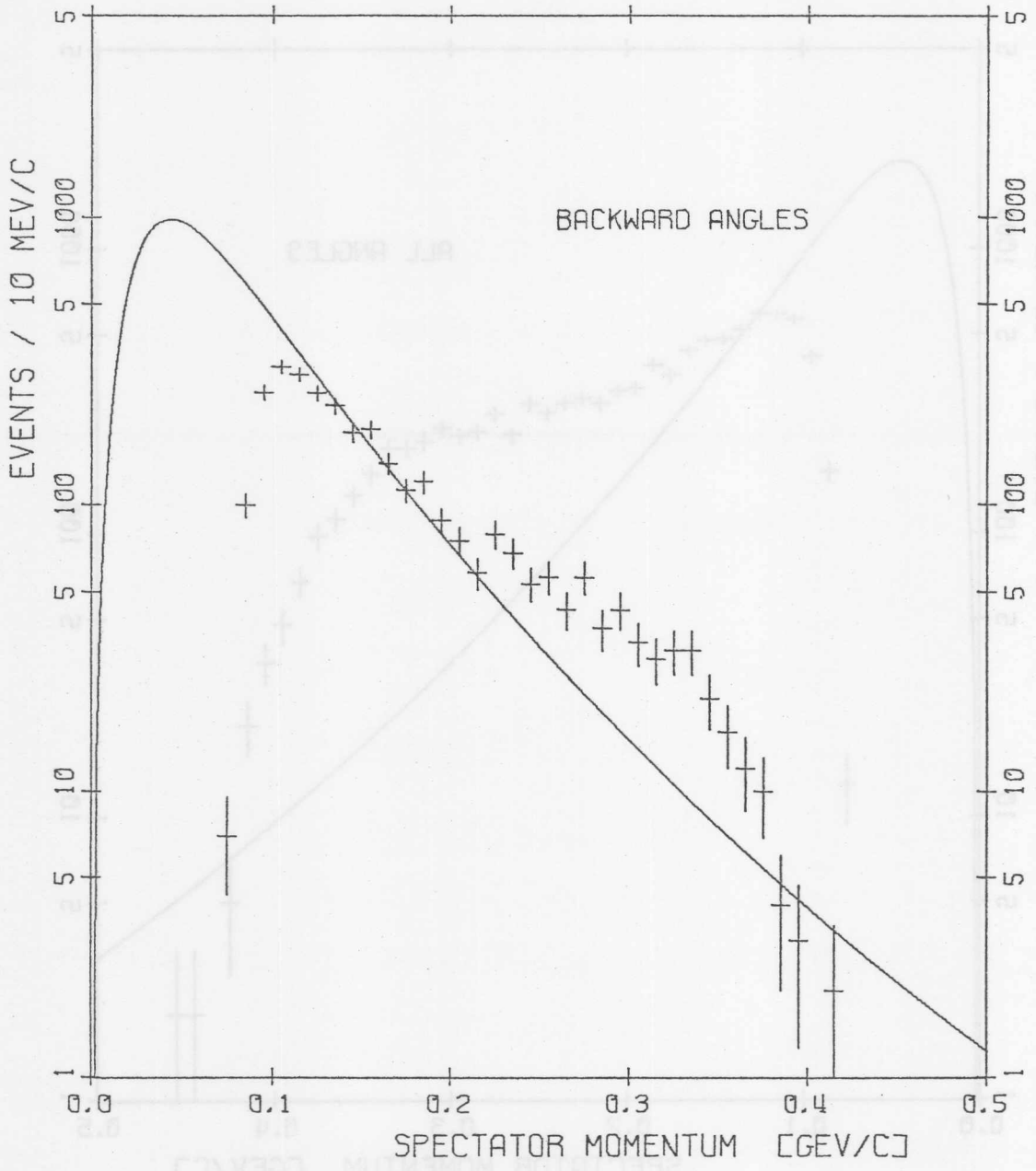

Fig.20 : The Spectator Momentum for Events with a Backward Going Spectator

with $p_{sp} > 350$ MeV/c drops rapidly with the increasing probability for the track to leave the scan volume. The fitted amplitude of the distribution of the backward going spectators was used to predict the curve in figure 19.

The angular distribution is shown in figure 21 for events with $110 \text{ MeV/c} < p_{sp} < 360 \text{ MeV/c}$; this restriction is to eliminate most of the detection and stopping condition biases. The shaded histogram is the angular distribution for events with $110 \text{ MeV/c} < p_{sp} < 150 \text{ MeV/c}$, a momentum region that is reasonably well described by the Hulthén prediction (Fig. 19). The angular behaviour of this fraction of the data can also be described by the impulse model with only a slight excess of events in the forward direction. The curve that is supposed to describe the angular distribution for the events with p_{sp} between 110 and 360 MeV/c is a prediction using the scaling factor of the fit in figure 20. Even in the backward direction there is a slight excess of events arising from the excess seen in figure 20. The increase of the number of events above the curve in the far backward direction may indicate the presence of a pion exchange mechanism from the antiproton to the deuteron as described by R.Poster et al.[30]. The distribution for the events with $p_{sp} > 220$ MeV/c was investigated and for $\cos \vartheta < 0$ no discrepancy with the impulse hypothesis was found. This result suggests that

these events are real spectators, although it is possible that an almost flat angular distribution in the backward hemisphere can be produced by a mixture of pion exchange mechanism[30] and rescattering with small momentum transfer.

60% of the events with forward going protons are not spectator events in the sense of the impulse approximation. The shape of their angular distribution is in agreement with the shape predicted for the contaminations (5-13) from neutron spectator events. For better comparison the distribution for 4-pronged events is plotted in figure 22 (upper histogram); the theoretical curve is drawn to fit the left half of the plot. The distribution of events above this line agrees well with the one in figure 16d (note that Fig.16d contains only one of all possible 4-prong channels).

The lower histogram in figure 22 shows the angular distribution for 2-pronged events; it proves the effectiveness of the rejection of elastic and quasi-elasic type of events, which should peak at a positive value of $\cos\vartheta$ near $\cos\vartheta = 0$. A remainder of the tail of quasi-elastic events extending to $\cos\vartheta = 0.4$ can be seen.

The amount of contamination from non-spectator events decreases with increasing charged multiplicity. As an example the angular distribution for events with 8 or more prongs is shown in figure 23.

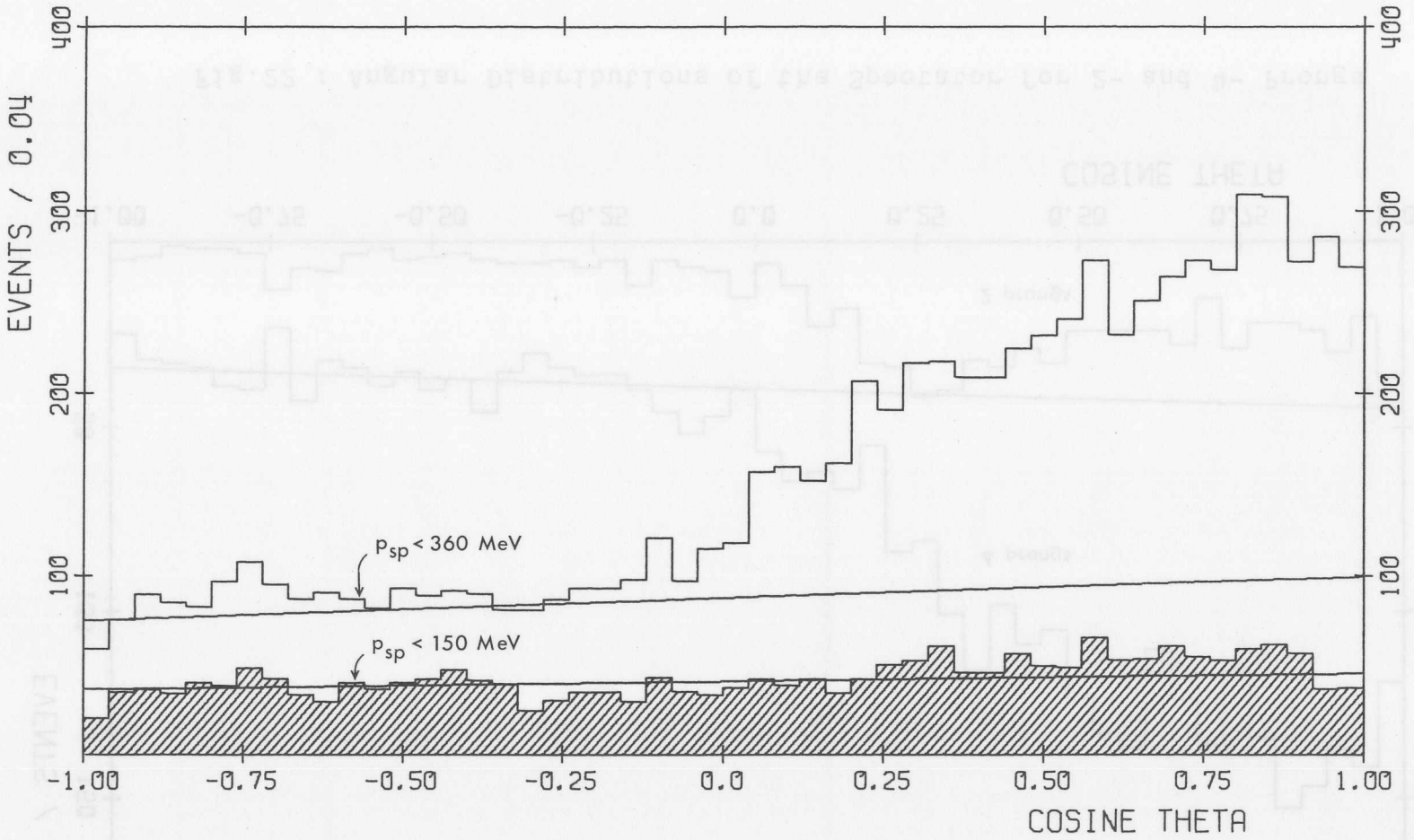

Fig.21 : Angular Distributions for $p_{sp} < 360$ MeV/c and for $p_{sp} < 150$ MeV/c

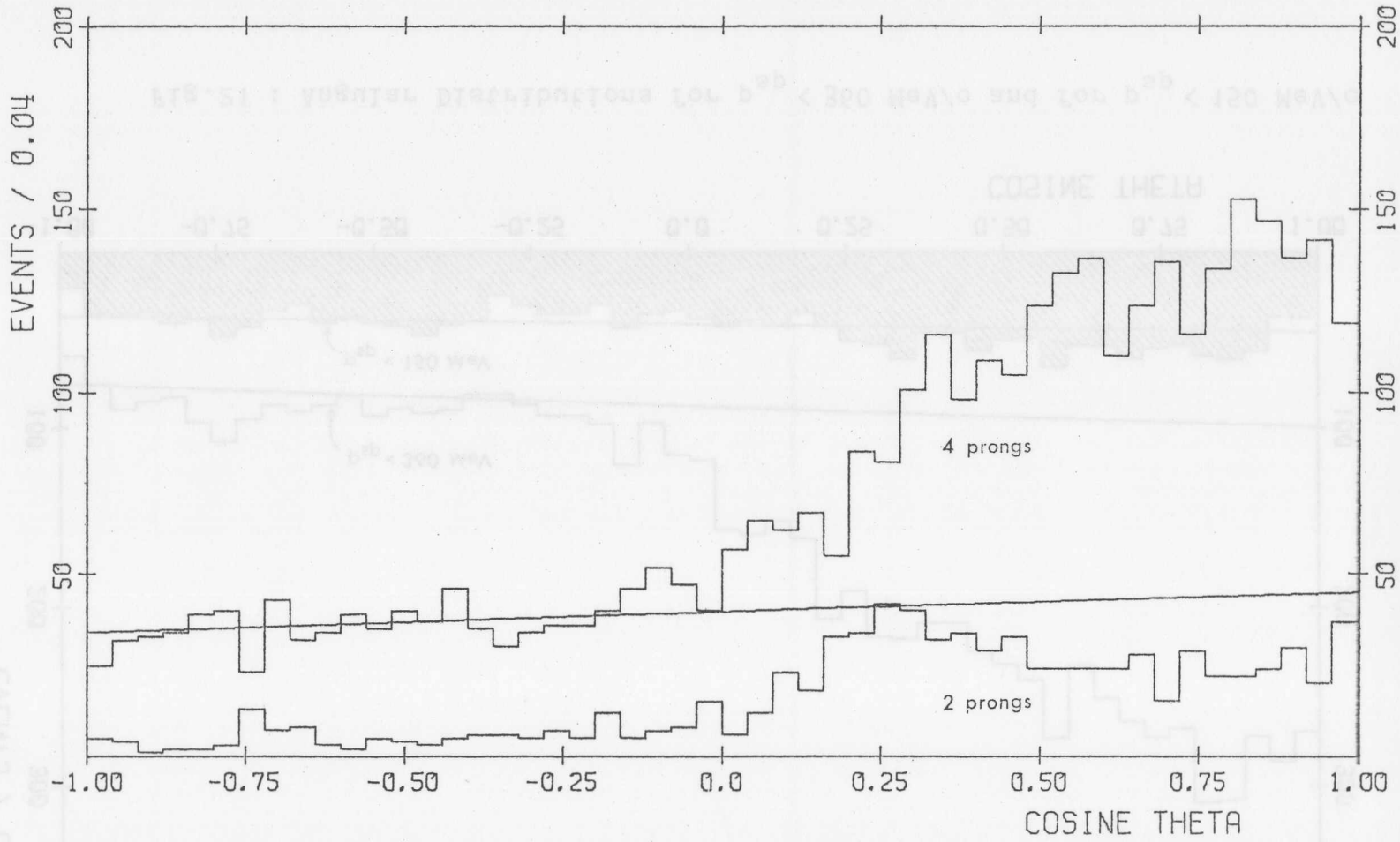

Fig.22 : Angular Distributions of the Spectator for 2- and 4- Prongs

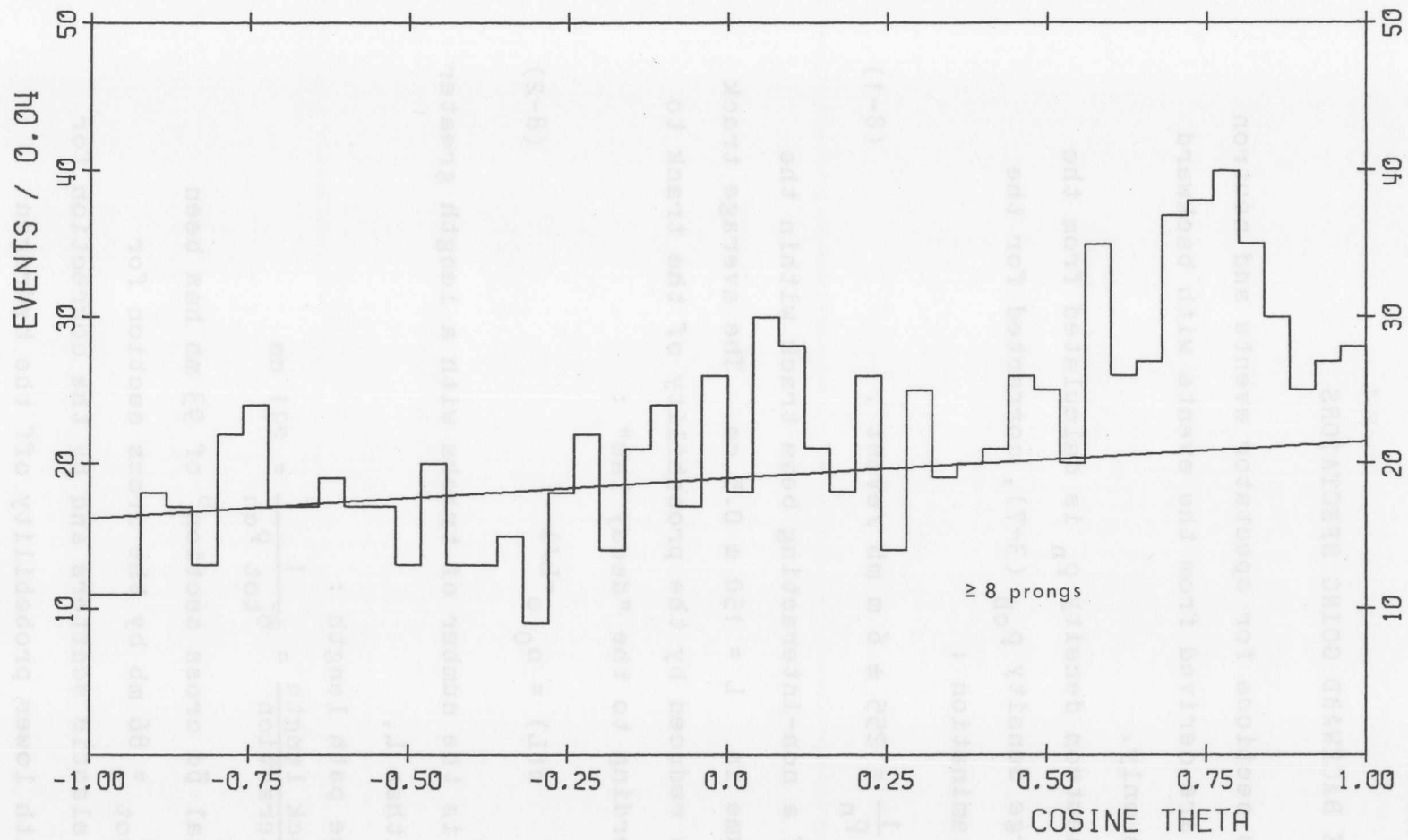

Fig.23 : Angular Distribution of the Spectator for Events with 8 and more Prongs

8. CROSS SECTIONS

8.1. VISIBLE BACKWARD GOING SPECTATORS

Cross sections for spectator events and neutron interactions are derived from the events with backward going protons only.

The neutron density ρ_n is calculated from the measured charge density ρ_{ch} (3-7), corrected for the hydrogen contamination :

$$\frac{1}{\rho_n} = 255 \pm 6 \text{ m mb /event} . \qquad (8\text{-}1)$$

The length of a non-interacting beam track within the fiducial volume is $L = 150 \pm 0.5$ cm. The average track length $\langle L \rangle$ is reduced by the probability of the track to interact according to the "decay law" :

$$n(L) = n_0 \, e^{-L/\lambda} \qquad (8\text{-}2)$$

where $n(L)$ is the number of tracks with a length greater than L,

λ is the free path length :

$$\lambda = \frac{\text{track length}}{\text{interaction}} = \frac{1}{\sigma'_{tot} \, \rho_{ch}} = 291 \text{ cm}$$

where the total $\bar{p}d$ cross section[5] of 93 mb has been reduced to $\sigma'_{tot} = 86$ mb by the cross section for undetectable elastic scatters and by the correction for scattering with lower probability off the hydrogen

impurity in the chamber. The result for the average track length is *

$$\langle L \rangle = \lambda(1 - e^{-L/\lambda}) = 117 \pm 1 \text{ cm} . \qquad (8\text{-}3)$$

The number of beam tracks entering the fiducial volume was counted on 2% of the used frames. An average of 4.68 ± 0.06 beam tracks per frame was obtained. This determines the total track length

$$L_T = 350 * 10^3 \pm 7 * 10^3 \text{ m}$$

and the flux $F = 1350 \pm 20$ events/mb for neutron interactions.

The topological cross sections for events with a visible backward going spectator (visible defined as $p_{sp} >$ 110 MeV/c) are listed in table 6a. Odd pronged events have been added to the next higher class of events. The number of events has been corrected for misidentification of the spectator in events with 2 stopping protons, for losses caused by secondary interactions of the spectator, for beam contamination, for reconstruction rejects that are not due to a violation of the scanning rules and for scanning efficiency. The number of Dalitz pairs is estimated from the number of detected γ - ray conversions and is also included in the corrections.

* The commonly used approximation $\langle L \rangle = L \cdot (1 - \frac{L}{2\lambda}) = 111$ cm is inaccurate for this experiment.

8.2. NEUTRON CROSS SECTIONS

For the attempt to calculate free neutron cross sections from the events with visible spectators the total number of spectator proton events is determined with the assumption of the impulse model and the Hulthén momentum distribution. The momentum distributions of backward going spectators are fit in the region of p_{sp} between 120 MeV/c to 220 MeV/c to dn/dp as obtained by integrating equation (5-7´) over cos ϑ from 0 to 1 (forward neutron) with the cross section as the only free parameter. The number of Hulthén - type spectator events, obtained as scaling factor of the fitted curve, and the corresponding cross sections $\sigma_n^{(d)}$ are listed in table 6b. Because the fits do not follow the reduction of scanning efficiency below p_{sp} = 130 MeV/c an increased efficiency of 80% was derived for the calculation of these cross sections. Otherwise the same corrections were applied as before.

These cross sections have to be corrected for Glauber screening and all scattering that is not described by the impulse approximation with a Hulthén wave function, to obtain neutron cross sections. Glauber theory by itself cannot predict this correction; additional assumptions or models have to be included.

In an attempt to experimentally find the correction D, defined by

$$\sigma_n = \sigma_n^{(d)} (1+D) \qquad (8-4)$$

400 frames of the film have been scanned carefully for all interactions. 628 clearly inelastic events and 157 possibly elastic 2- and 1- prongs were found ("possibly elastic" defined as a scattering by less than 2 degrees for the fast track).* The number of neutron interactions in the class of "possibly elastic" events was obtained by subtracting the estimated number of elastic deuteron events (a cross section of 6 mb was guessed) and dividing the remaining number by 2, with the assumption of equal cross sections for $\bar{p}n$ and $\bar{p}p$ "possibly elastic" scattering. The 286 events with an odd number of prongs or with a visible spectator were corrected for the reactions (5-13) by the fraction obtained from figure 21. This procedure determined the total number of neutron interactions to 280 ± 30, yielding a cross section of 32 ± 3.5 mb and with[4] $\sigma_n = 53$ mb

$$D = 0.65 \pm 0.15 \ .$$

A different approach was tried ignoring all events with 2 or less prongs. These 260 events, after being corrected for 3- and 4-prongs with Dalitz pairs and for reactions (5-13), correspond to a cross section of 22 ± 3 mb and are to be compared with $\sigma_n^{(>2)}$, the total inelastic $\bar{p}n$

* Estimating that 20% of the elastic and quasi- elastic events are undetectable a total $\bar{p}d$- cross section of 90 ± 4 mb was found).

cross section reduced by the inelastic 1- prong cross section (here the spectator is not counted as a prong). Neither cross section has been measured near 15 GeV/c. The elastic cross section can be approximated by the $\bar{p}p$-elastic cross section[31] of ~9 mb. The 1- prong cross section is estimated from the $\bar{p}p$ 2- prong cross section[32] of 12.6 mb at 15 GeV/c and the various exclusive $\bar{p}p$ cross sections[33] at 6.9 GeV/c. The data at 6.9 GeV/c show that 2- prong annihilations are negligible and that the four classes of 2- prong interactions have comparable cross sections:

$$\bar{p}p \longrightarrow \bar{p}p\ (\pi^\circ)$$
$$\bar{p}p \longrightarrow \bar{n}p\ \pi^-\ (\pi^\circ)$$
$$\bar{p}p \longrightarrow \bar{p}n\ \pi^+\ (\pi^\circ)$$
$$\bar{p}p \longrightarrow \bar{n}n\ \pi^+\pi^-\ (\pi^\circ)\ .$$

For the $\bar{p}n$ interactions only 2 of the equivalent channels have a 1- prong topology :

$$\bar{p}n \longrightarrow \bar{p}n\ (\pi^\circ)$$
$$\bar{p}n \longrightarrow \bar{n}n\ \pi^-\ (\pi^\circ)\ .$$

Therefore it is assumed that the $\bar{p}n$ inelastic 1- prong cross section is roughly half the $\bar{p}p$ inelastic 2- prong cross section. Then $\sigma_n^{(>2)} = 37.7$ mb and

$$D = 0.7 \pm 0.3\ .$$

For comparison, the value of D found by B.Y.Oh et al. for $\bar{p}n$ scattering[28] between 1.09 and 3.45 GeV/c by scaling exclusive $\bar{p}p$ cross sections as obtained from a deuteron

target (neutron spectator) up to the $\bar{p}p$ cross sections as obtained with a hydrogen target was D = 0.7.

A theoretical prediction of the correction is attempted starting with the Glauber model :

$$\sigma_d = \sigma_n + \sigma_p - \delta\sigma \qquad (8\text{-}5)$$

where σ_d, σ_n, σ_p are the total cross sections for deuteron, neutron and proton scattering.

$\delta\sigma$ is the screening of one nucleon in the deuteron by the other; its simplest form[17] is

$$\delta\sigma = \frac{\langle r^{-2} \rangle}{4\pi} \sigma_n \sigma_p \qquad (8\text{-}6)$$

where $\langle r^{-2} \rangle$ is the mean inverse square separation of the nuclei in the deuteron.

$\langle r^{-2} \rangle$ is usually derived from charge symmetry and the four cross sections for (particle - proton), (particle - deuteron), (antiparticle - proton) and (antiparticle - deuteron) interactions[17,4]. The measured values of $\langle r^{-2} \rangle$ at various beam momenta up to 20 GeV/c have been reviewed by Galbraith[34] in 1969, Serpukhov data are included in reference 35. $\langle r^{-2} \rangle$ appears to rise with increasing beam momentum. At 15 GeV/c its value is 0.04 mb^{-1}. Theoretical values are energy independent; the highest value of 0.03 mb^{-1} is obtained from a deuteron wave function with hard core[18].

Writing from the experimental point of view

$$\sigma_d = \sigma_n^{(Hu)} + \sigma_p^{(Hu)} + \Delta\sigma \qquad (8\text{-}7)$$

where $\sigma_n^{(Hu)}$, $\sigma_p^{(Hu)}$ are the cross sections for events with a Hulthén - type spectator proton or neutron, $\Delta\sigma$ contains coherent scattering from deuterons, double scattering and single scattering which is different from the Hulthén - impulse model. Equation (8-7) may be rewritten as

$$\sigma_d = (\sigma_n^{(Hu)} + \tfrac{1}{2}\delta\sigma + \tfrac{1}{2}\Delta\sigma) + (\sigma_p^{(Hu)} + \tfrac{1}{2}\delta\sigma + \tfrac{1}{2}\Delta\sigma) - \delta\sigma$$

and may be interpreted as equation (8-5), i.e.

$$\sigma_n = \sigma_n^{(Hu)} + \tfrac{1}{2}\delta\sigma + \tfrac{1}{2}\Delta\sigma \qquad (8\text{-}8)$$

or

$$\sigma_n\,(1 - \tfrac{1}{2}\delta\sigma/\sigma_n - \tfrac{1}{2}\Delta\sigma/\sigma_n) = \sigma_n^{(Hu)} \; . \qquad (8\text{-}8')$$

The factors of 1/2 are based on the assumption that protons and neutrons have similar cross sections and screening properties.

In the geometrical interpretation[17] of the Glauber model the term $\frac{1}{2}\frac{\delta\sigma}{\sigma_n} = \frac{1}{2}\frac{\langle r^{-2}\rangle}{4\pi}\cdot\sigma_p$ is the probability for a beam to hit the proton in the deuteron after it intersected (without interacting) with the neutron (= screening, shadow). Encouraged by the success of this model one may estimate double scattering $\Delta\sigma'$ in a similar way :

$$\tfrac{1}{2}\Delta\sigma'/\sigma_n \approx \frac{1}{2}\frac{\langle r^{-2}\rangle}{4\pi}\sum_i A_i\sigma_p(x_i) \qquad (8\text{-}9)$$

where x_i are the particles produced by the $\bar{p}n$

interaction with intensities A_i.

For a crude estimate of the sum in (8-9) the total $\bar{p}n$ cross section is divided into an absorptive part and a scattering part :

$$\sum_i A_i \sigma_p(x_i) = \frac{1}{2}\cdot\sigma_p(\text{"}\bar{p}n\text{"}) + \frac{1}{2}\cdot(\sigma_p(\text{"}\bar{N}\text{"})+\sigma_p(N)) \quad .$$

The rescattering $\sigma_p(\text{"}\bar{p}n\text{"})$ of the absorptive component has the quantum numbers of a $\bar{p}n$ - system for the projectile; its cross section should be roughly the deuterium cross section of 100 mb. The other component consists of a slow nucleon recoil and a fast component with the quantum numbers of an antinucleon. Setting the cross section for the fast component to 50 mb and the cross section for the slow nucleon to the nucleon - nucleon cross section around 0.5 GeV/c of 150 mb

$$\sum_i A_i \sigma_p(x_i) \simeq 150 \text{ mb} \simeq 3\sigma_p$$

and $$\Delta\sigma' = 3\,\delta\sigma \qquad (8\text{-}10)$$

If deviations from the Hulthén wave function and coherent deuteron events that cannot be described by double scattering are ignored $\Delta\sigma' = \Delta\sigma$ and

$$\sigma_n = \sigma_n^{(Hu)} + 2\,\delta\sigma \quad . \qquad (8\text{-}11)$$

With $\langle r^{-2}\rangle = 0.04\ \text{mb}^{-1}$, $\sigma_p = 50$ mb one gets $\delta\sigma = 8.3$ mb and $D = 0.5$.

Considering the assumptions made in this derivation the

result is in good agreement with the values of D found from the scan data. The topological neutron cross sections calculated with the same value of D = 0.65 ± 0.15 for all topologies are listed in table 6b.

Tab.6 : TOPOLOGICAL CROSS SECTIONS

a) For Events with a Visible Spectator in Backward Direction
110 MeV/c < p_{sp} < 360 MeV/c

Charged Multiplicity	2 *	4	6	8	10	12	more	total
Events N_V	147	960	765	350	83	12	2	2319
Corrected # of Events **	285	1482	1182	540	126	18	3	3594
Cross Section [mb]	0.19	1.10	0.88	0.40	0.09	0.01	-	2.66
Error (statistical) [mb]	0.016	0.036	0.032	0.022	0.010	0.003	-	0.055

b) Model Dependent Corrections of Neutron Cross Sections

Charged Multiplicity	1 *	3	5	7	9	more	total
Extrapolation in p_{sp} : Events N_{Hu}	1350	7600	6550	3300	700	150 ***	19600
Corrected Cross Section [mb]	1.66	8.26	7.06	3.54	0.75	0.16	21.4
Error	0.20	0.38	0.36	0.27	0.15	0.06	0.6
Corrections for Screening and Double Scattering : $\bar{p}n$ Cross Section [mb]	2.7	13.6	11.6	5.8	1.2	0.25	35.3
Error (random) [mb]	0.3	0.6	0.6	0.4	0.2	0.1	1.0
Error (systematic) [mb]	0.4	2.0	1.8	0.9	0.2	0.05	5.3

* Clearly inelastic events only . ** Systematic error ~5 % .
*** Not fitted; from extrapolation in multiplicity of the ratio N_V/N_{Hu} .

9. RESONANCE SEARCH

9.1. THE $\bar{p}n$ - SYSTEM

The mass m_x recoiling against the spectator proton p_s in the reaction (1-1)

$$\bar{p}d \longrightarrow p_s X^-$$

is plotted for all events in figure 24. The error in m_x due to the inaccuracy in the measurements is calculated for each event by the reconstruction program; their distribution is shown in figure 25.

Events with short spectator tracks are restricted to a region around m_0 as shown in figure 14. The events at the high and low mass tails of figure 24 have spectator tracks with a length around 30 cm. For these events the measuring accuracy is unimportant; multiple scattering errors and more systematic errors like distortions become more relevant in this region. The best resolution is found around 5.2 GeV/c^2 and 5.8 GeV/c^2. However, for most events the effect of the error in the spectator quantities is small compared to the error introduced by variations in the beam momentum, which is almost constant (~20 MeV/c^2) over the whole mass region. Therefore the rejection of events with a geometry that causes high errors in figure 25 will not improve the total resolution significantly.

Except for the enhancement above 5.6 GeV/c^2

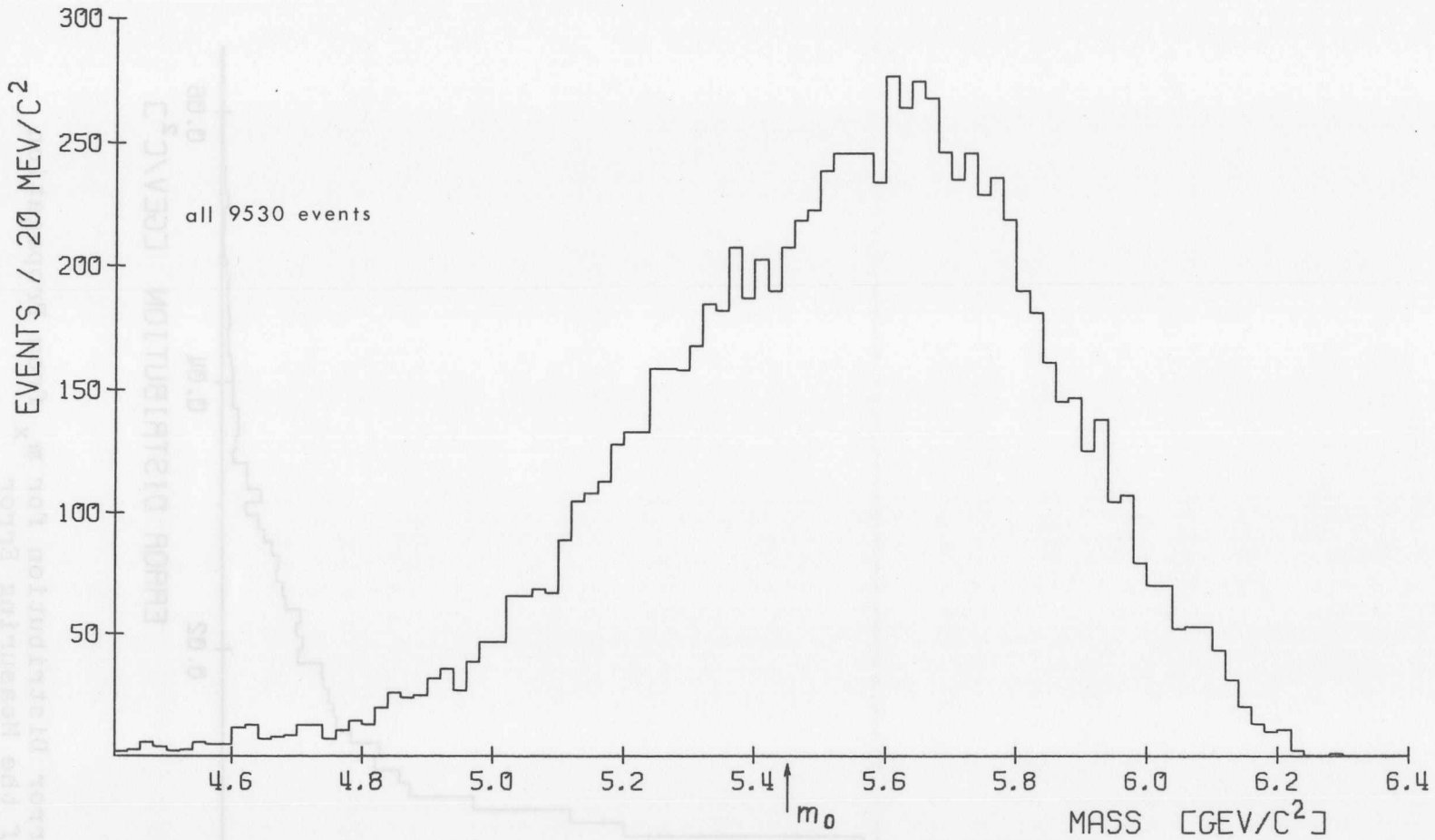

Fig.24 : Mass of the X^-; all Events

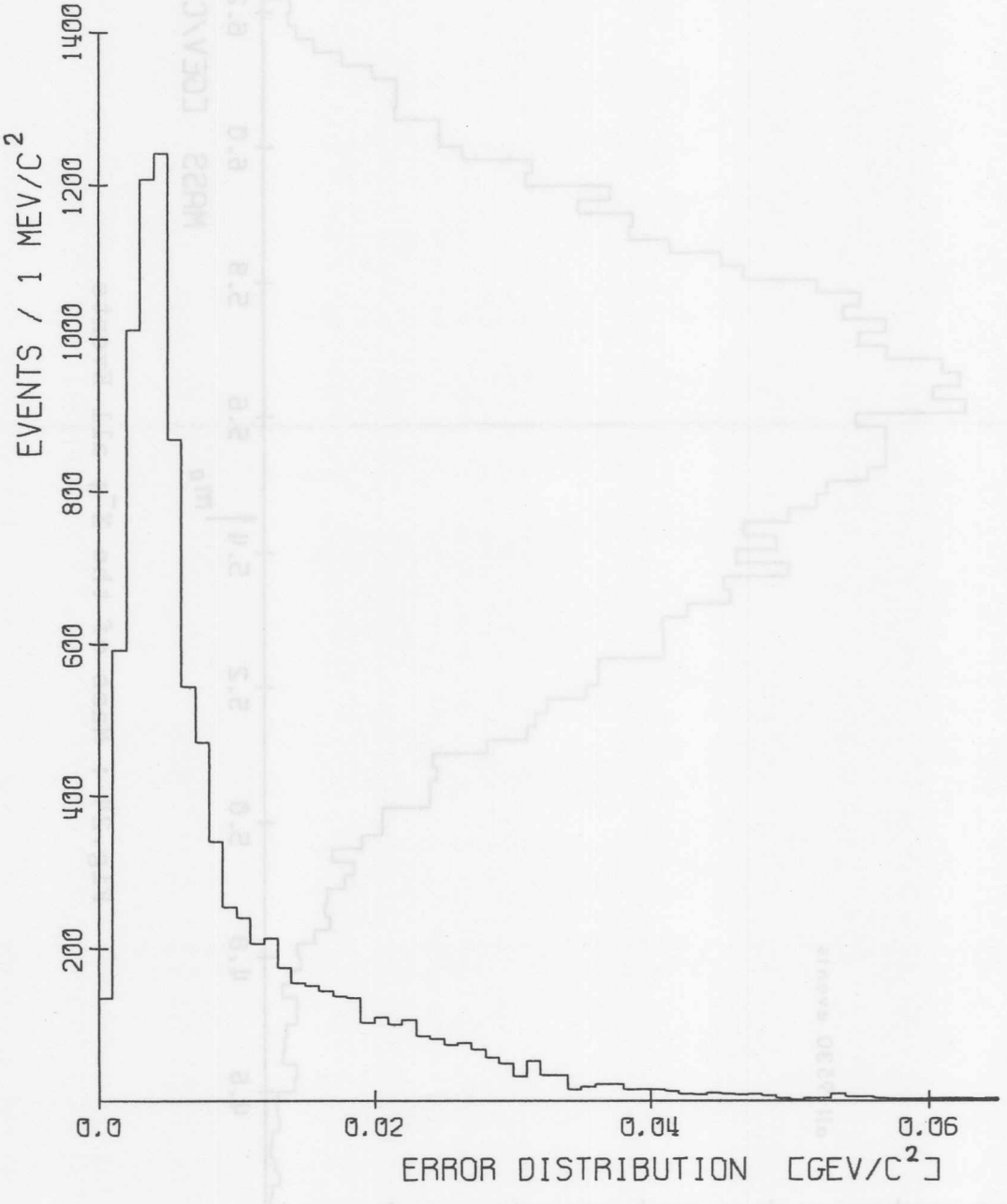

Fig.25 : Error Distribution for m_x from Propagation of the Measuring Error

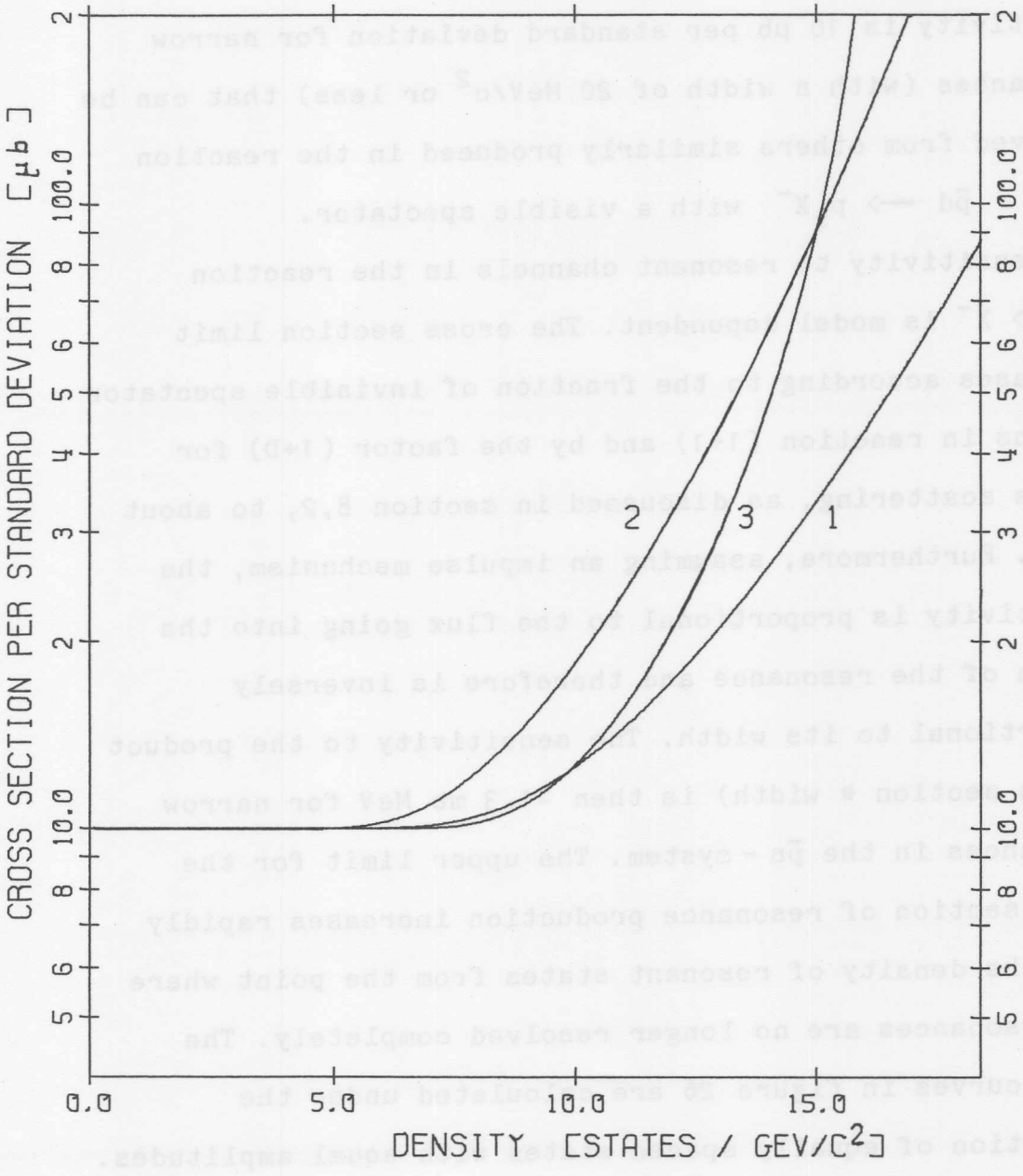

Fig.26 : Upper Limits of the Cross Section for Resonance Production as a Function of the Density of States

- which will be discussed later - the mass distribution is smooth. The largest fluctuations (at 4.62 and 5.37 GeV/c^2) have a significance of less than 2 standard deviations. For the region near 5.4 GeV/c^2 (with ~200 events/bin) the sensitivity is 10 μb per standard deviation for narrow resonances (with a width of 20 MeV/c^2 or less) that can be resolved from others similarly produced in the reaction

(1-1) $\bar{p}d \longrightarrow p_s X^-$ with a visible spectator.

The sensitivity to resonant channels in the reaction $\bar{p}n \longrightarrow X^-$ is model dependent. The cross section limit increases according to the fraction of invisible spectator protons in reaction (1-1) and by the factor (1+D) for double scattering, as discussed in section 8.2, to about 65 μb. Furthermore, assuming an impulse mechanism, the sensitivity is proportional to the flux going into the region of the resonance and therefore is inversely proportional to its width. The sensitivity to the product (cross section * width) is then ~1.3 mb MeV for narrow resonances in the $\bar{p}n$ - system. The upper limit for the cross section of resonance production increases rapidly with the density of resonant states from the point where the resonances are no longer resolved completely. The three curves in figure 26 are calculated under the assumption of equally spaced states with equal amplitudes. Curves 1 and 2 are obtained for Gaussians with half-widths of 20 MeV/c^2 and 25 MeV/c^2 respectively, curve 3 derives

from the convolution of a flat distribution with a σ of 17 MeV/c^2 (a possible approximation for the distribution of beam momenta) and a Gaussian with σ = 12 MeV/c^2 (measuring error). In the Regge model[36] with a slope of 1 GeV^{-2} for the trajectory the density ot states near 5.5 GeV/c^2 is ~11 (GeV/c^2)$^{-1}$; a gain of resolution from 25 to 20 MeV/c^2 improves the sensitivity for the detection of Reggeons by almost a factor of 2.

For events of neutron interactions by the impulse mechanism the distribution of the mass m_x should have its maximum near m_0 (Fig.14). Double scattering from both nucleons in the deuteron and contaminations by proton and deuteron interactions (5-13, 5-10) preferentially produce the "spectator" particle in the forward direction and therefore increase the number of events with $m_x > m_0$. It was shown in chapter 7 that the amount of contamination decreases with increasing charged multiplicity; this is reflected in the change of the shape of the mass distributions (Fig.27) for different prong topologies. These histograms show that the enhancement in the mass plot (Fig.24) above 5.6 GeV/c^2 is mostly due to events with 4 prongs.

The information about the presence of a pointing track in an event can be used for further investigation of the contaminations. In peripheral excitations of the beam particle the decay products of the resonance have a

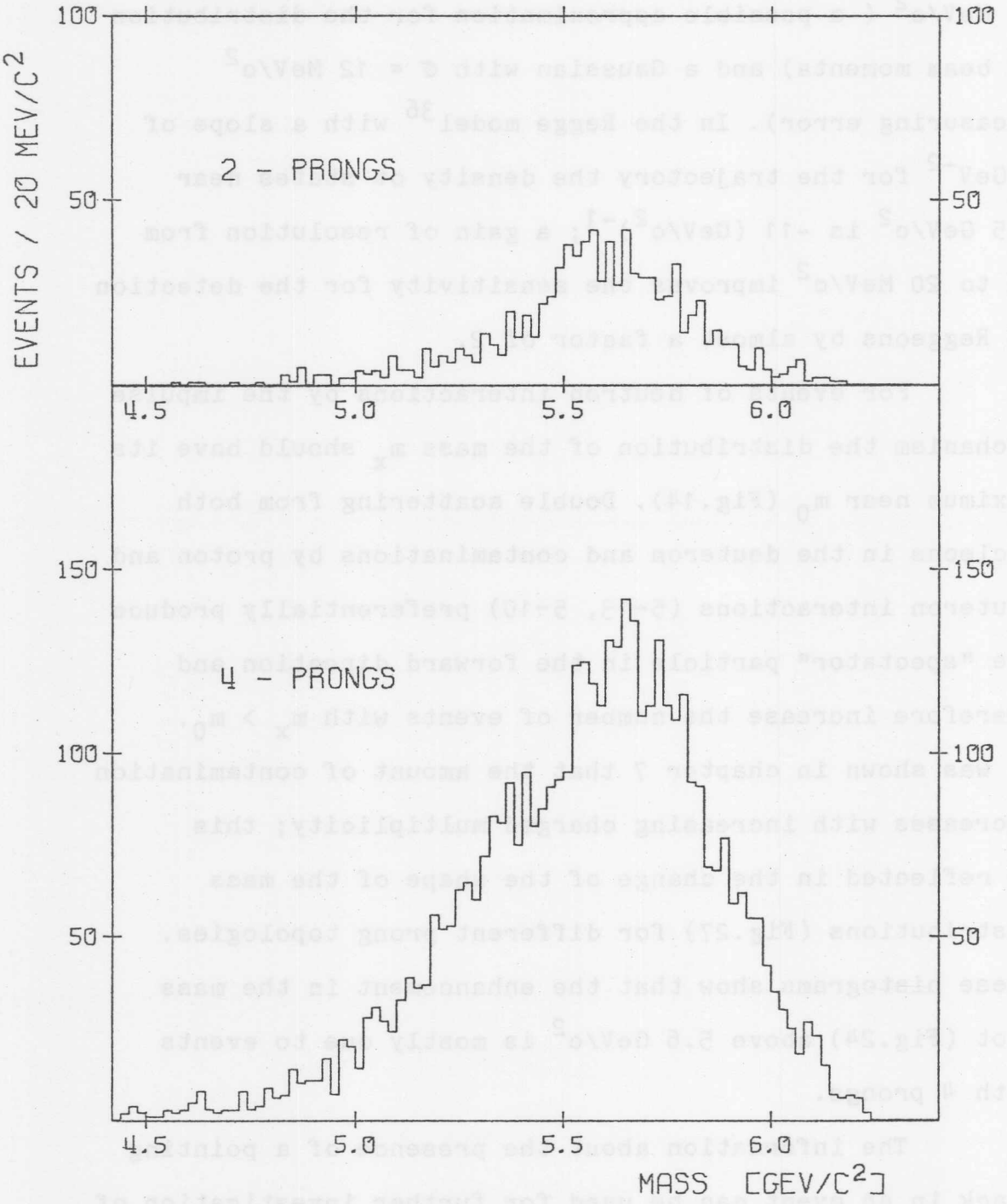

Fig.27 : Mass of the X^- for the Topological Channels
Part 1

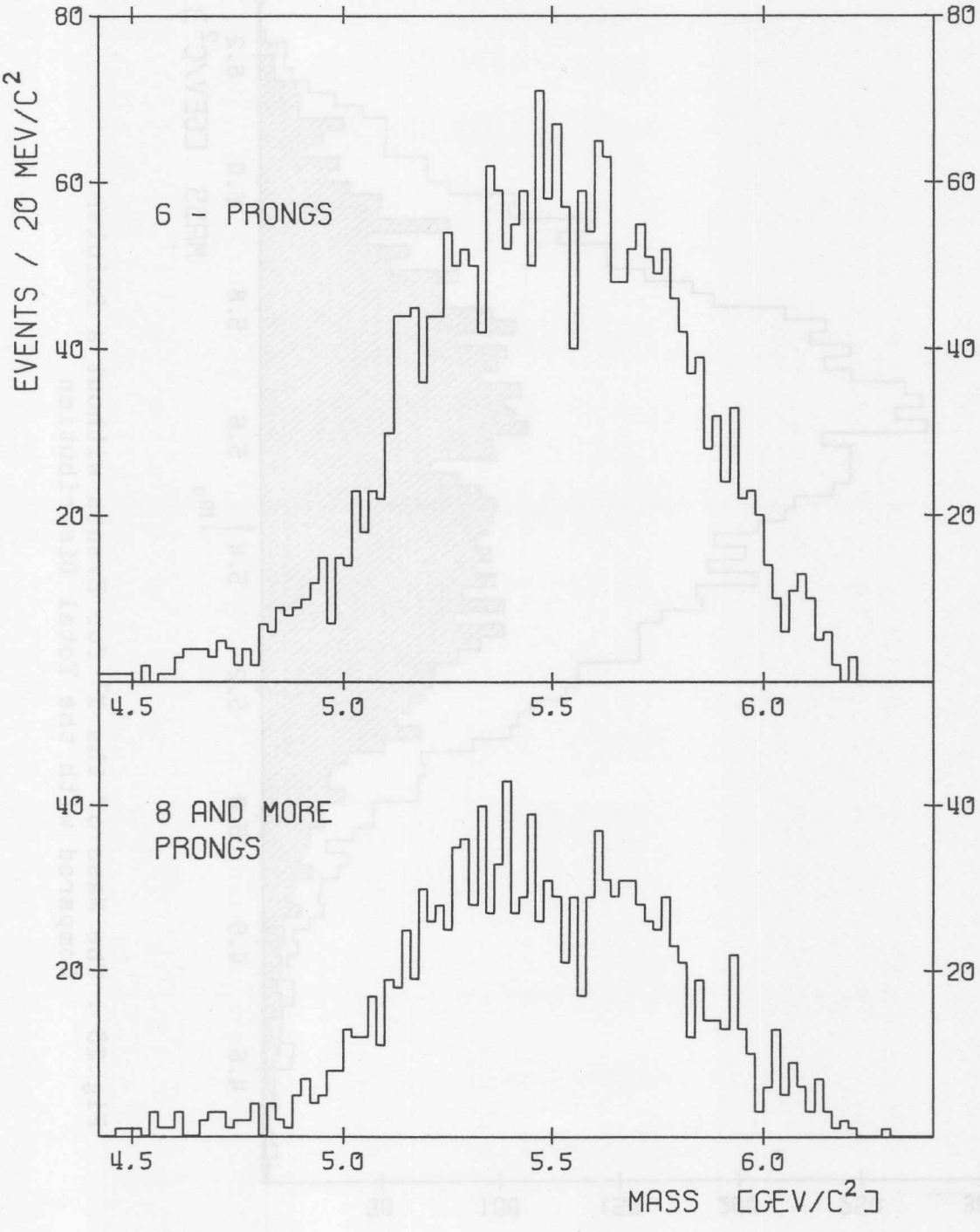

Fig.27 : Mass of the X^- for the Topological Channels Part 2

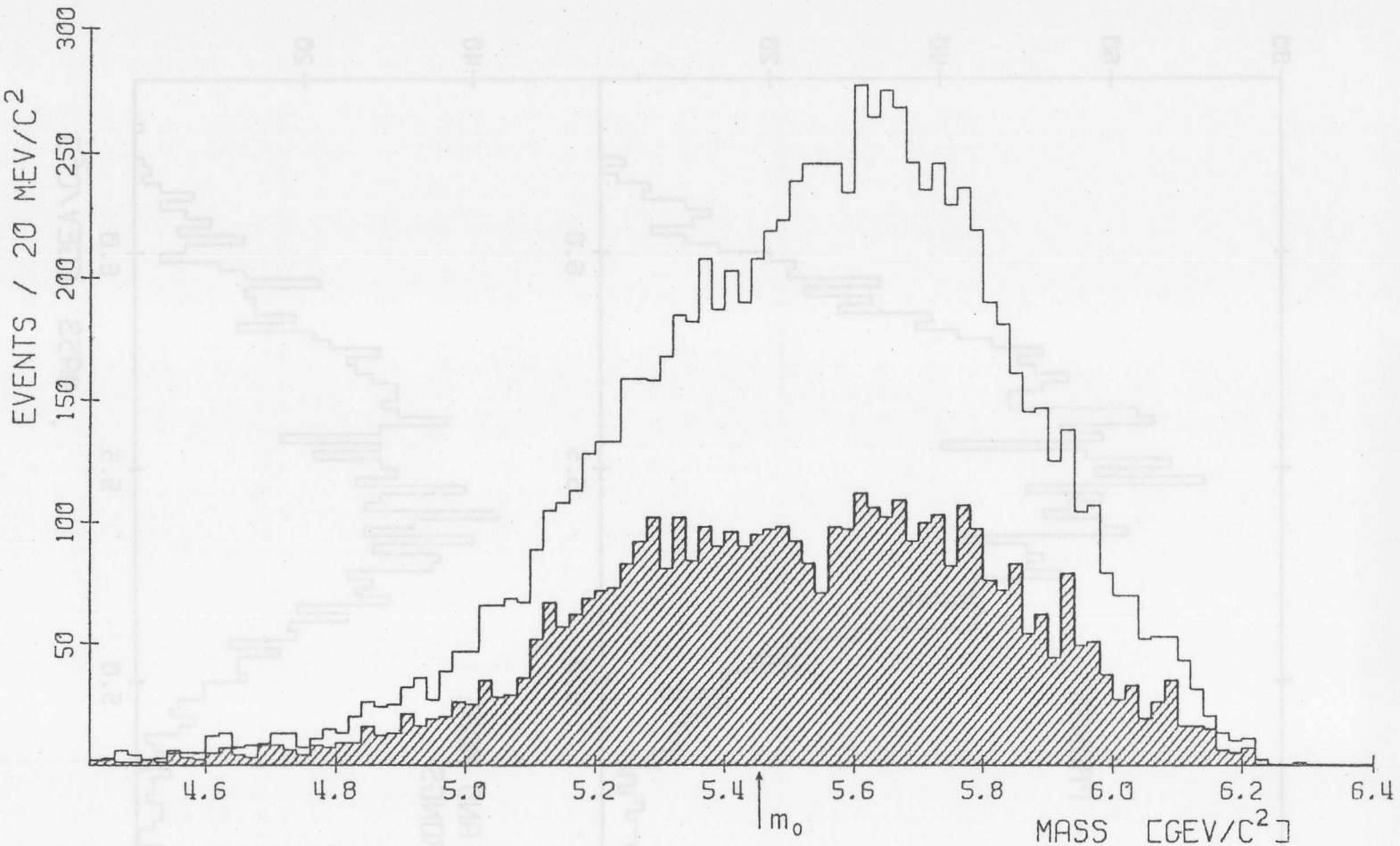

Fig.28 : The Mass of the X^- for Events without a Pointer Compared with the Total Distribution

rapidity which is close to the rapidity of the projectile. Therefore the contaminant reactions

$$\bar{p}d \longrightarrow \bar{N}^- \text{ "d"}$$

(here N stands for any non-strange baryon,
"d" stands for deuteron or
an unbound neutron-proton pair)

should not be associated with a pointing track. Figure 28 shows the distribution of m_x for events with a pointing track shaded into the total distribution. The reduction of the ratio between events with $m_x > m_0$ and events with $m_x < m_0$ is apparent. The excess of events with forward spectators is still large mainly due to the symmetric process of peripheral excitations of the target nucleons. The amount of contamination from target excitation is smaller though, because the relatively large Q-value for the N- decays (except for the $\Delta(1232)$) tends to produce protons that are too fast to qualify as spectators. In addition excited states of the proton can have a neutron in the final state, in which case the event would not be among the events of this experiment.

Peripheral production of baryon resonances at either the beam or the target produce events with 2 or 4 prongs. The 6 and 8 pronged events may contain events with both the beam and the target excited to an (anti-) baryon state. The excess in the number of 4 pronged events (Fig.27) above 5.6 GeV/c^2 shows indications of structure.

It was shown in chapter 5 that the reactions (5-10c)

$$\bar{p}d \longrightarrow \bar{N}^{-} d$$

can produce resonances in m_x. In figure 29 the 4 pronged events are separated into events with a pointing track and events without a pointing track. The plot for the events without a pointer has been modified according to the considerations in chapter 5.1. to use a constant beam momentum of 14.9 GeV/c for the calculation of m_x; for a reduction of background events with a "spectator" momentum greater than 300 MeV/c have been eliminated and for an improvement of the resolution events with a "spectator" track shorter than 2 mm have been omitted. The histogram shows peaks at 5.55 and 5.65 GeV/c^2. Assuming that the peaks are caused by the coherent deuteron interactions (5-10c) the corresponding masses of the $\bar{N}$ are calculated from equations (5-11) and (5-12) as m_N = 1.67 GeV/c^2 and 2.18 GeV/c^2. The lower resonance is consistent with the interpretation as the N(1700) or the Δ(1650) or any N - resonance inbetween. Surprising is the absence of any indication for N(1470) - production. If the peaks were produced by the proton interactions (5-13c) with a spectator neutron the masses of the $\bar{N}$ would be given by equation (5-15) as m_N = 1.40 and 1.77 GeV/c^2. The width in m_x introduced by the Fermi motion of the proton target was found from Monte Carlo events to be 200 MeV/c^2 (full width); it is inconsistent with the observed widths and it

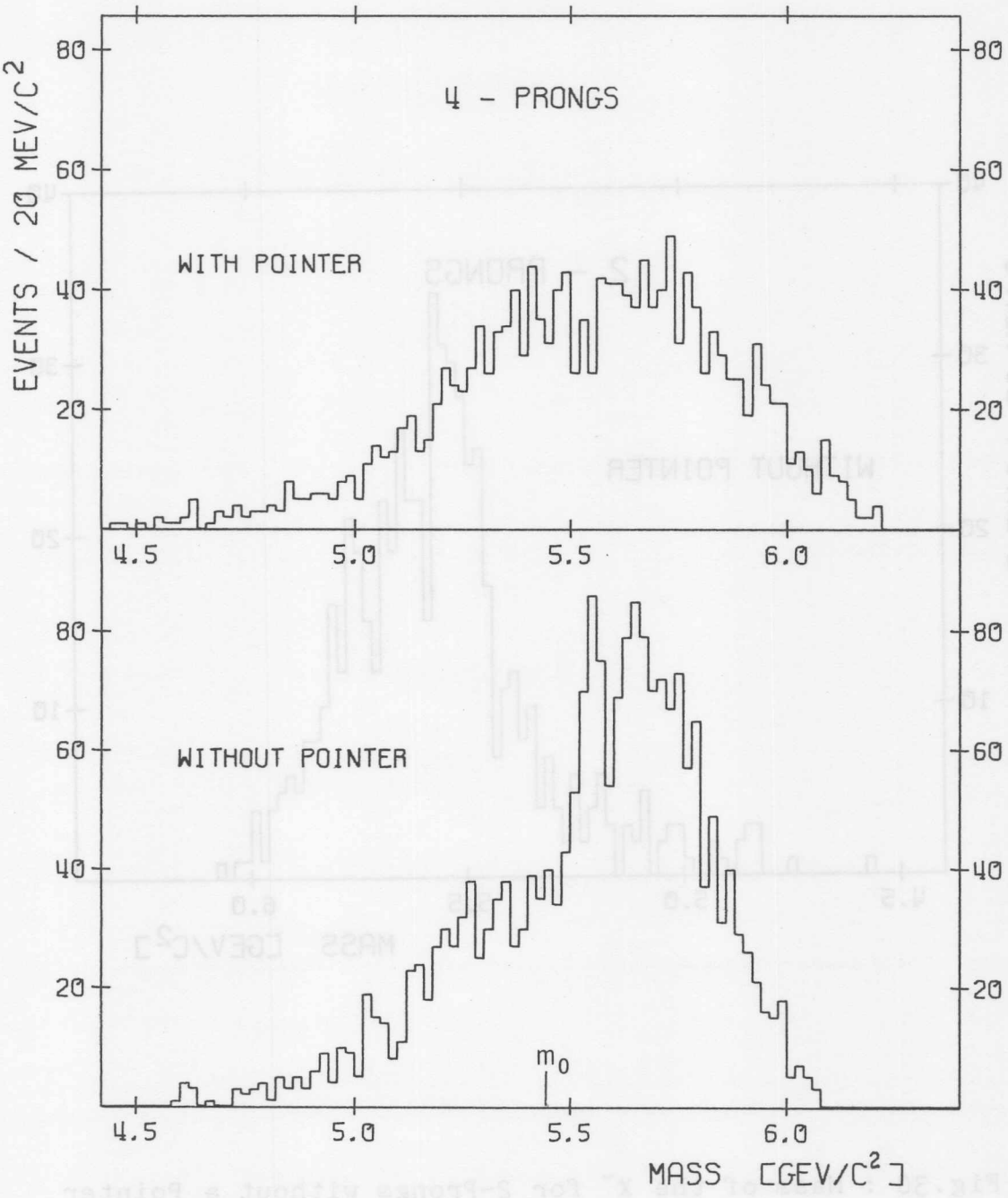

Fig.29 : Mass of the X^- for 4-Prong Events; Separated into Events with a Pointer and Events without a Pointer

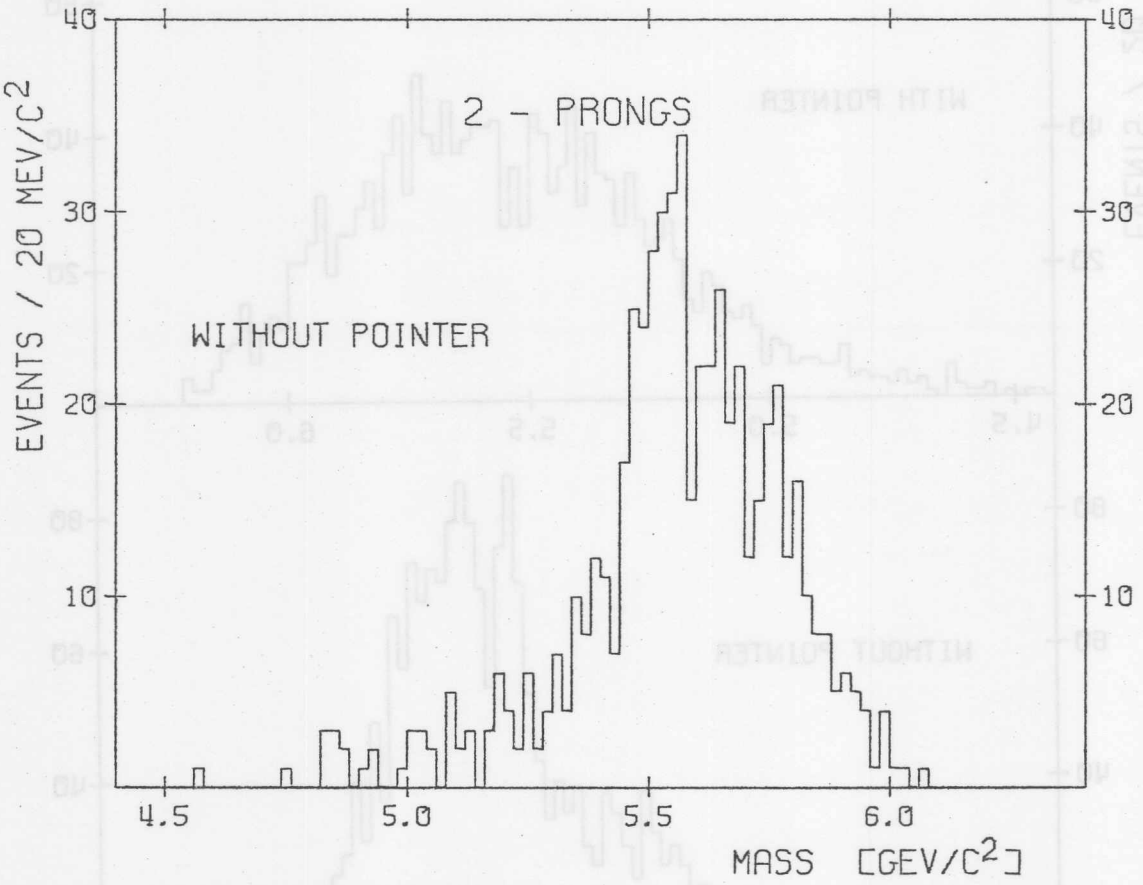

Fig.30 : Mass of the X^- for 2-Prongs without a Pointer

is concluded that the reactions (5-13c) can only be partly responsible for the peaks at 5.55 and 5.65 GeV/c^2, unless the impulse model is strongly violated and these reactions occur favorably at low neutron spectator momenta.

The 2-prong events are expected to show a similar structure from the formation of baryon resonances, except that in addition the $\Delta(1232)$ should be present. If produced by the reactions (5-10c) the Δ- resonance will peak in the m_x- spectrum at 5.48 GeV/c^2. The data in figure 30 were obtained with the same conditions as the corresponding 4-prong data. The signal from the $\Delta(1232)$ resonance is not resolved from the peak at 5.55 GeV/c^2, but the comparison with figure 29 shows the enhancement of events near 5.48 GeV/c^2 clearly.

9.2. ANALYSIS OF THE POINTING TRACK

Although the measurement of the pointing track was designed only as an auxiliary means for a more precise determination of the vertex it seems worthwhile to extract its kinematic variables where ever possible and to analyze these events.

45% of all events have a pointing track that was successfully reconstructed; 2380 of these pointers have a negative charge, 1880 of them are positive. Distributions of some kinematic variables for these tracks, interpreted

as pions, are given in figures 31 to 33. For all these plots the laboratory frame is defined as the rest frame of a neutron moving with the opposite momentum of the spectator proton in the deuteron rest frame. The CM-system is defined as the center-of-mass system of this neutron and the antiproton beam. The Feynman - X variable[37] is calculated assuming interactions without annihilations. The majority of the pointers come from the central region; the definition of the pointer as having an angle greater than 20° with the beam in each camera view causes a cut-off near X = 0. The rapidity distribution in figure 31 as well as the distribution of p^2_{lab} in figure 32 show an increase of the number of negative pointers over the number of positive ones at low momenta. The exponentials drawn into figure 32 are not mathematical fits, yet they do indicate a difference in the slope for pointers of different charge. In figure 33 the distribution of the transverse momenta for the positively charged pointers is averaged over 50 MeV/c intervals and is drawn as a curve into the histogram for the negative tracks. The comparison shows that the excess of pointers with negative charge extends only up to p ≈ 0.5 GeV/c.

The missing mass distributions (Fig.34) for the reaction

$$\bar{p}d \longrightarrow p_s + \text{pointer} + X \qquad (9\text{-}1)$$

with the pointer interpreted as a pion show a difference

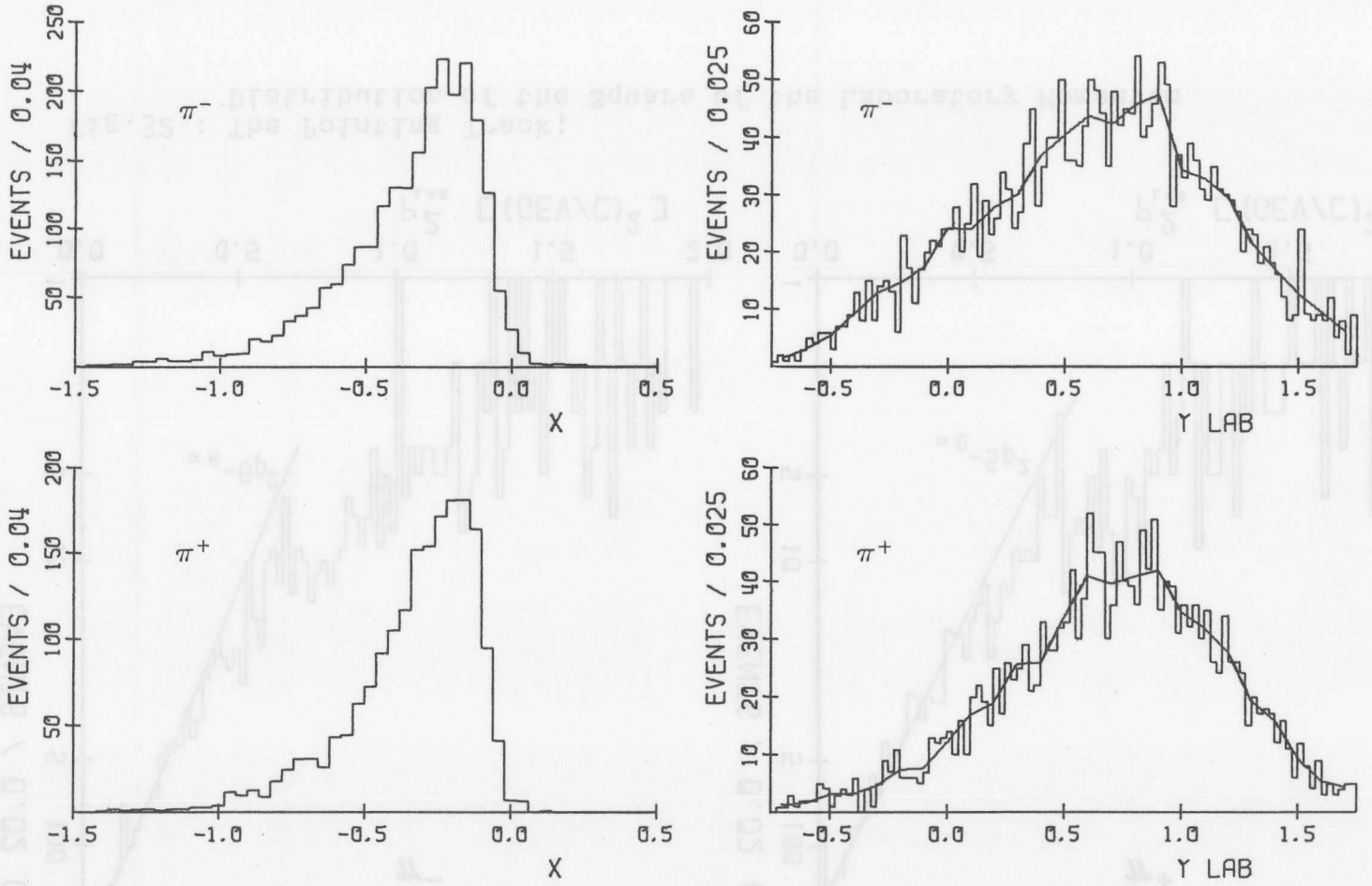

Fig.31 : The Pointing Track;
Plots of the Feynman Variable X and the Rapidity Distribution

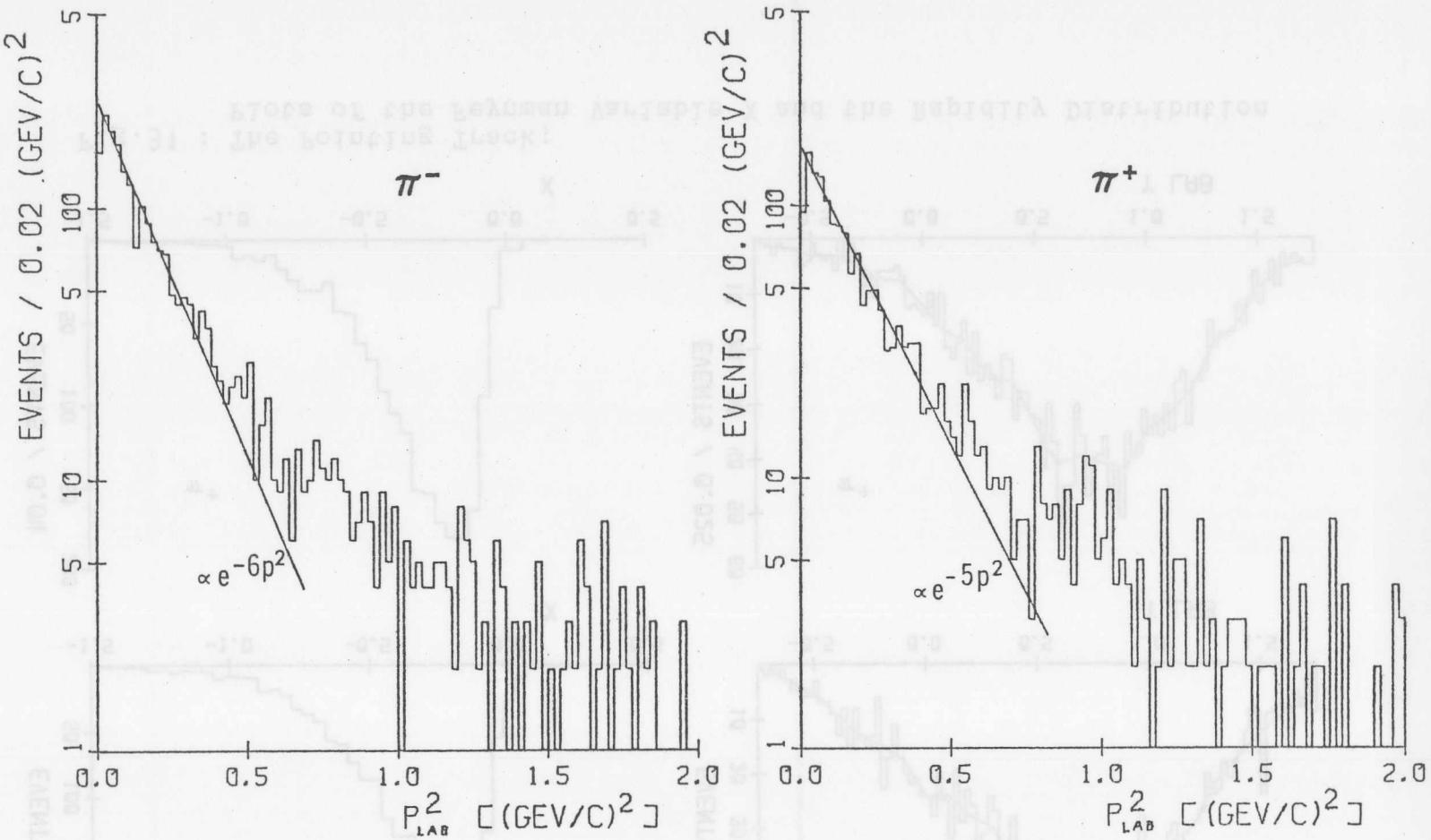

Fig.32 : The Pointing Track;
Distribution of the Square of the Laboratory Momentum

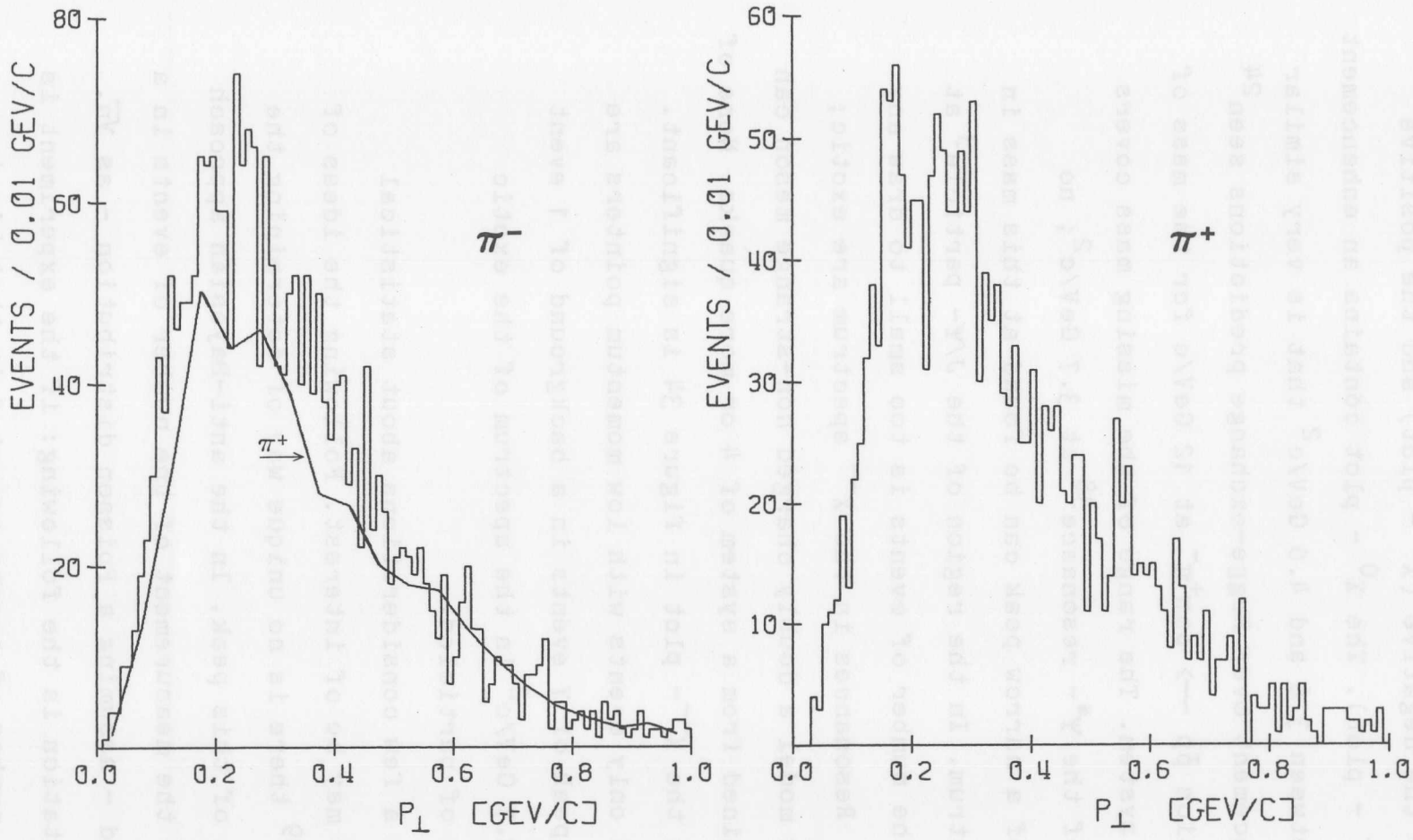

Fig.33 : The Pointing Track;
Distribution of the Transverse Momentum

in shape for the negative (X^0 - plot) and the positive pointer (X^{--} - plot). The X^0 - plot contains an enhancement of events between 3.6 and 4.0 GeV/c^2 that is very similar to the enhancement over Regge-exchange predictions seen[24] in the reaction $\bar{p}p \longrightarrow \bar{p}p\pi^+\pi^-$ at 12 GeV/c for the mass of the $(\bar{p}p\pi^\pm)$- system. The range of the missing mass covers the region of the Ψ^*- resonance[38] at 3.7 GeV/c^2; no indication of a narrow peak can be found at this mass in the X^0- spectrum. In the region of the J/Ψ- particle[3] at 3.1 GeV/c^2 the number of events is too small to draw any conclusions. Resonances in the X^{--} spectrum are exotic; in the quark model a doubly charged non-strange meson can only be obtained from a system of 4 or more quarks. None of the peaks in the X^{--}- plot in figure 34 is significant. In figure 35 only events with low momentum pointers are selected; a peak of 7 events in a background of 1 event appears at 3.7 GeV/c^2 in the spectrum of the exotic combinations of particles.

Here a few considerations about statistical significance may be of interest. Following the ideas of F.T.Solmitz[39] there is no unique way of determining the significance of this peak. In the anti-Bayesian approach the error in the measurement of the number of events in a bin is quoted - assuming a Poisson distribution - as $\sqrt{n}$. The interpretation is the following: if the experiment is repeated the number of events expected in that bin is

n $\pm\sqrt{n}$ with 68% probability. One may now, however, ask for the probability that upon repetition of the experiment the number of events in this bin will be less or equal to the background. For the case of 7 events in a background of 1 event this probability is $1*10^{-5}$, corresponding to 4.4 standard deviations. In this calculation no error has been assigned to the background. When trying to quote the reliability or probability for the estimate of the background one leaves the anti-Bayesian view and different approaches will generally lead to different results. It may be of interest to perform the calculation of the probability for a background of 2 events per bin. In this case the result is $1*10^{-3}$ or 3.2 standard deviations.

Due to the selection criterion for pointers as tracks with a large angle in respect to the beam the sample of pointers is expected to be enriched with K-mesons. The missing mass for the reaction (9-1) with the kaon interpretation for the pointer is displayed in figure 36; events where the measured track length and the curvature of the track are inconsistent with the range-momentum relation ("overstopping") have been omitted. For further enrichment of the sample of pointers by kaons events were selected on the basis of a high transverse momentum for the pointing track. No resonance was found in these data.

The invariant mass of the spectator and the pointer is a quantity with little meaning for neutron interactions

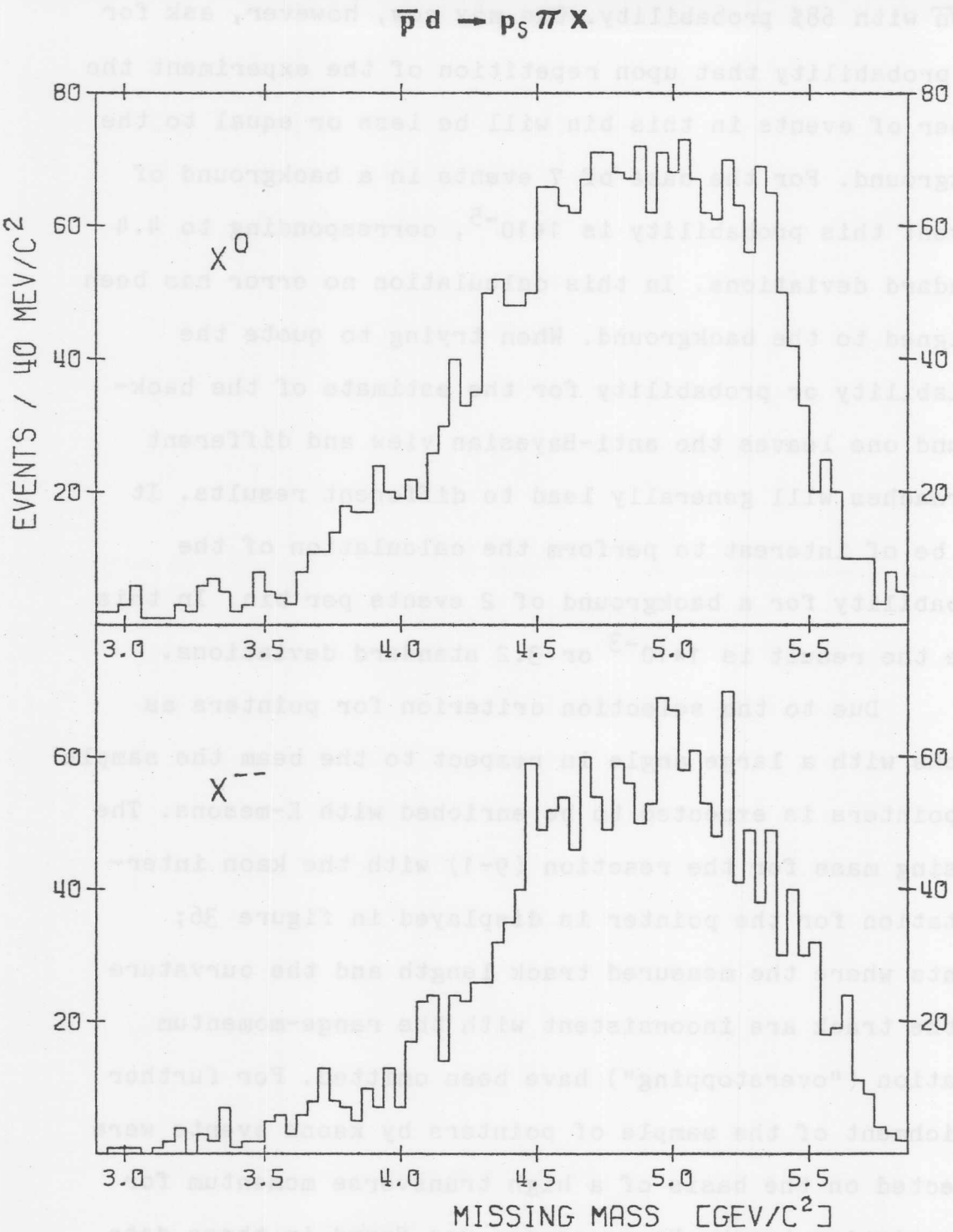

Fig.34 : Missing Mass Recoiling against the Spectator and the Pointer; Pion Interpretation; all Events

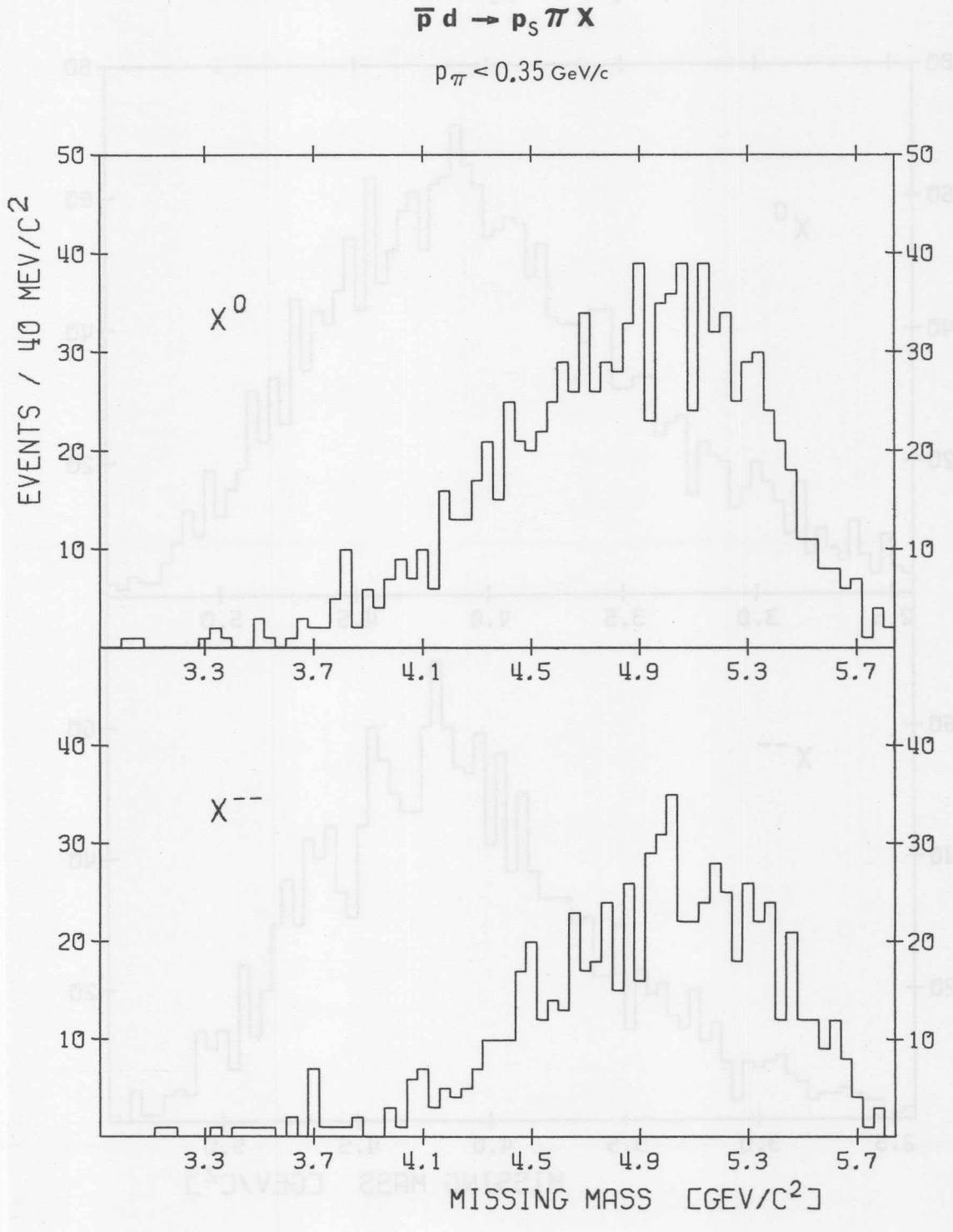

Fig.35 : Missing Mass Recoiling against the Spectator and the Pointer; Pion Interpretation; Events with a Low Momentum Pointer are Selected

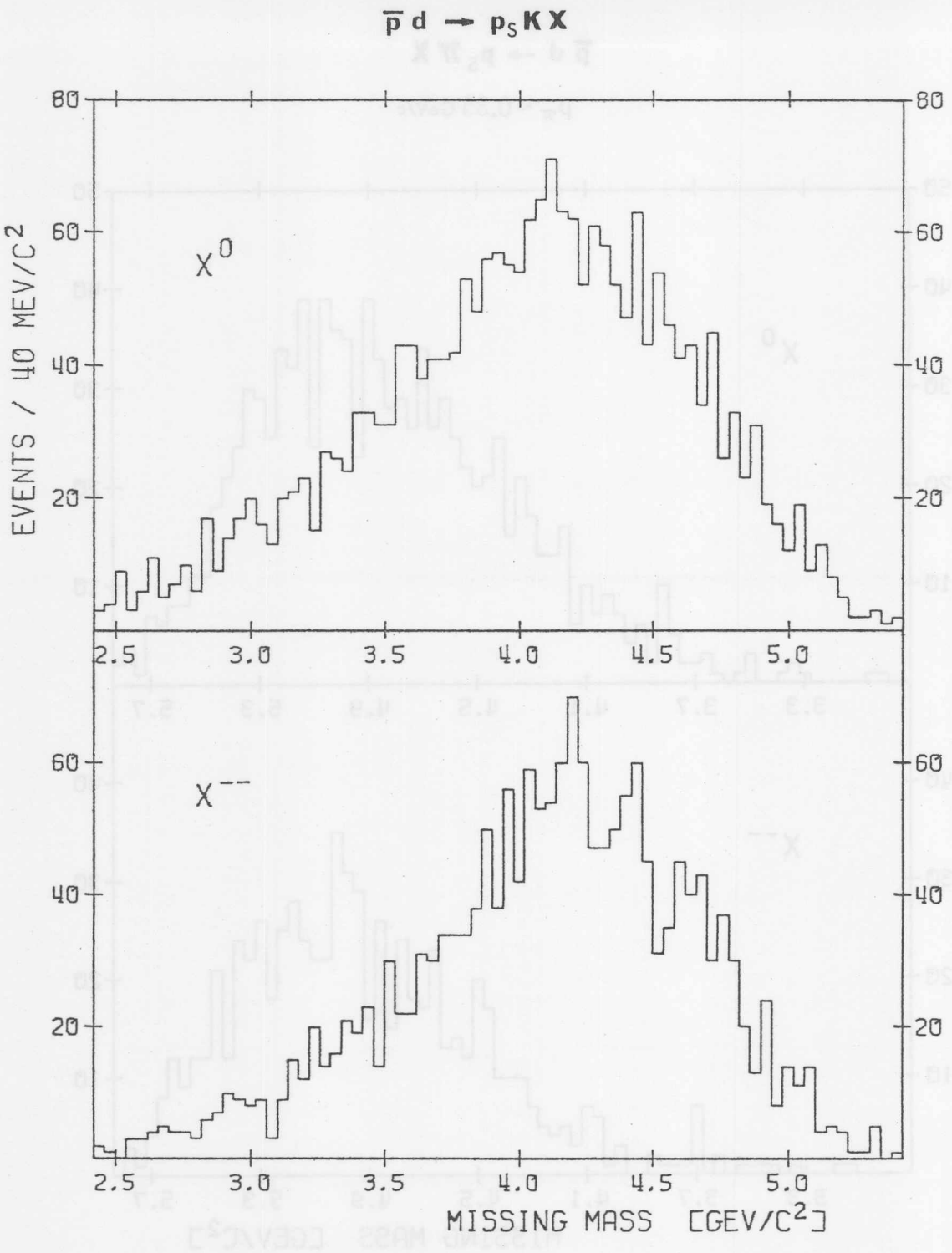

Fig.36 : Missing Mass Recoiling against the Spectator and the Pointer; Kaon Interpretation

by the impulse mechanism. Contaminations by proton interactions are large though, especially in the 2- and 4-prong data. In the $(p\pi^+)$- mass (Fig.37) one expects the presence of the $\Delta^{++}(1232)$ resonance, but as in other experiments[24,39] the Δ- peak cannot be separated visually from the background. The bump near 1.9 GeV/c, usually seen in $\bar{p}\pi^-$ and $p\pi^+$ invariant mass distributions[40], is not found in this experiment.

If the kaon interpretation is used for the pointer the corresponding mass plot shows a narrow peak at 1.85 GeV/c^2 near the mass of the $Z_0(1865)$. The forward-to-backward ratio of the proton direction for the 20 events in this bin is 1, suggesting that the protons in these events are really spectators and that the peak is a reflection of some other process or merely a statistical fluctuation. On the other hand the significance of the forward-to-backward ratio is low and the possibility that Z_0 production is observed cannot be excluded.

Finally in the contaminations from coherent deuteron events one expects to observe d^*- production[41]. The $(d\pi^+)$- mass (Fig.38) shows a peak around 2.18 GeV/c^2 which agrees with the expected mass (2.17 GeV/c^2) for the $(\Delta^{++}n)$- bound state. The $(d\pi^-)$- mass distribution peaks approximately 30 MeV/c^2 below the d^*- mass. It is not clear whether this peak is due to the neutral d-stars $(\Delta^0 n)$ and $(\Delta^- p)$. A similar mass difference between the neutral

and the charged d-stars seems to be indicated in $\pi^+ d$ interactions[42] at 15 GeV/c.

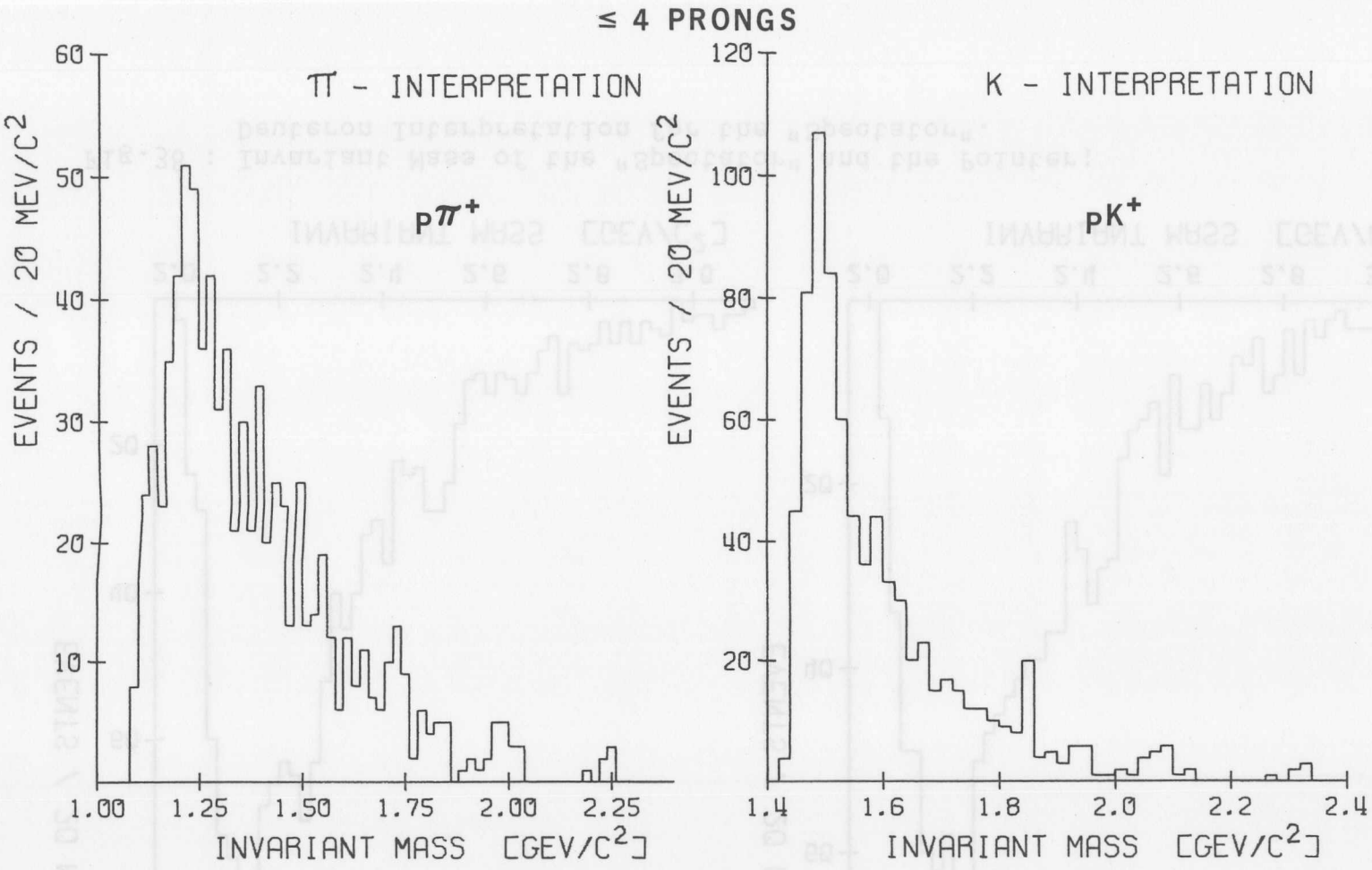

Fig.37 : Invariant Mass of the Spectator and the Pointer
for Events with 4 or fewer Prongs; for Positively Charged Pointers Only

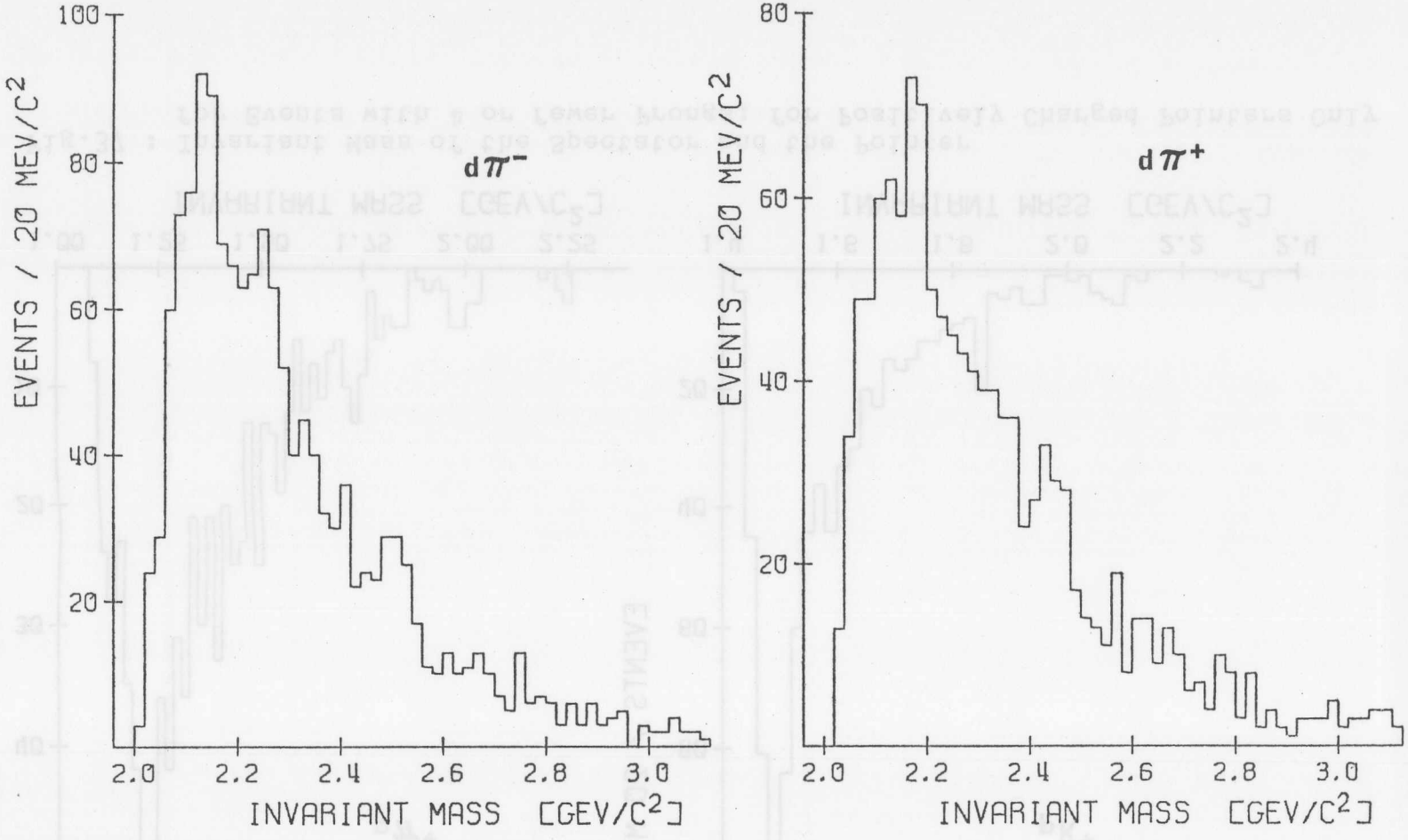

Fig.38 : Invariant Mass of the "Spectator" and the Pointer;
Deuteron Interpretation for the "Spectator".

10. CONCLUSIONS

Approximately 60% of the events with more than 3 prongs in the inclusive experiment

$$\bar{p}d \longrightarrow p_L X^-$$

where p_L is a low momentum particle stopping inside the 80" bubble chamber within a distance of ~50 cm from the vertex, consistent in charge and ionization with being a proton,

are neutron interactions with a spectator proton p_s :

$$\bar{p}d \longrightarrow p_s X^-.$$

Interactions other than single scattering off the neutron occur preferentially with lower multiplicities and at forward angles of the particle p_L in the laboratory frame. 2- and 4-prong events show strong production of excited states of the antiproton.

A resolution of 22 ± 3 MeV/c^2 was achieved for the mass m_x of the X^-. The sensitivity for resolved resonances in the total sample of data is 10 μb per standard deviation of significance near 5.4 GeV/c^2 (for ~200 events / 20 MeV/c^2). No narrow enhancement in the mass spectrum exceeds 2 standard deviations.

In the attempt to convert the topological cross sections for events with a spectator proton to the corresponding neutron cross sections it was found that the corrections due to double scattering and coherent

deuteron interactions amount to ~4 times the Glauber screening correction.

The Feynman - X distribution for the pointing tracks (interpreted as pions) shows that the majority of these particles are produced in the central region. Distributions of the missing mass recoiling against the spectator and the pointer do not show any resonance of appreciable significance.

LIST OF REFERENCES

1. e.g. B.Maglić, MESON RESONANCES, rapporteur's talk at Lund International Conference on Elementary Particles, 1969, p.271
2. For one of the most recent experiments see J.Alspector et al., Phys.Rev.Lett. 30, 511 (1973)
3. J.J.Aubert et al., Phys.Rev.Lett. 33, 1404 (1974)
   J.-E.Augustin et al., Phys.Rev.Lett. 33, 1406 (1974)
   C.Bacci et al., Phys.Rev.Lett. 33, 1408 (1974)
4. W.Galbraith et al., Phys.Rev. 138, B913 (1965)
5. Particle Data Group: J.E.Enstrom et al., NN AND PP INTERACTIONS - A COMPILATION, LBL-58, May 1972
6. R.J.Plano, "NP54", Rutgers BCG Program Library (unpublished)
7. R.J.Plano, "CONGEN", Rutgers BCG Program Library (unpublished)
8. R.I.Louttit, BNL BC-04-3-C, memorandum (1970) and supplementary note (Dec.1971)
9. W.P.Trower, HIGH ENERGY PARTICLE DATA II, UCRL-2426, Vol.II (1966 Rev.)
10. B.B.Culwick, BNL BC-05-2-H, memorandum (1965) and addendum BNL #9984 (1966)
11. H.W.J.Foelsche et al., Rev.Sci.Inst. 38, 879 (1967)
12. H.W.J.Foelsche et al., BNL EP&S 70-6, internal report (1970)
13. H.W.J.Foelsche, private communication
14. R.L.Gluckstern, Nucl.Inst.& Meth. 24, 381 (1963)
15. W.B.Johnson, Rev.Sci.Inst. 38, 1602 (1967)
16. G.F.Chew and H.W.Lewis, Phys.Rev. 84, 779 (1951)
17. R.J.Glauber, Phys.Rev. 100, 242 (1955)
18. V.Franco and R.J.Glauber, Phys.Rev. 142, 1195 (1966)
19. L.Hulthén and M.Sugawara, Handbuch der Physik 39, 1 (1957)

20. e.g.
P.J.Roberts, Nucl.Phys. B1, 114 (1967)
I.J.McGee, Phys.Rev. 151, 772 (1966)
L.Durand,III, Phys.Rev. 123, 1393 (1961)
M.J.Moravcsik, Nucl.Phys. 7, 113 (1958)
V.Bargmann, Rev.Mod.Phys. 21, 488 (1949)

21. e.g.
S.Gartenhaus, Phys.Rev. 100, 900 (1955)
T.Hamada and I.D.Johnston, Nucl.Phys. 34, 382 (1962)

22. C.Møller, Mat.Fys.Medd.Dan.Vid.Selsk. 23, No.1 (1945)

23. Brick et al., Nouvo Cimento 24A, 202 (1974)

24. G.Drews, DESY F1-71/7, internal report (1971)

25. H.Preissner and R.J.Plano,
Bull.Am.Phys.Soc. 17, 490 (1972)

26. E.B.Brucker et al., Phys.Rev. D10, 1373 (1974)

27. e.g. H.Cramér, MATHEMATICAL METHODS OF STATISTICS,
Princeton University Press, Princeton, N.J. (1966)

28. B.Y.Oh et al., Nucl.Phys. B51, 57 (1973)

29. J.Denburg et al., Phys.Rev. D2, 2565 (1970)

30. R.Poster et al., Phys.Rev.Lett. 33, 1625 (1974)

31. D.Birnbaum et al., Phys.Rev.Lett. 23, 663 (1969)

32. F.T.Dao et al., Phys.Lett. 51B, 505 (1974)

33. T.Ferbel et al., Phys.Rev. 173, 1307 (1968)

34. W.Galbraith, Rep.Prog.Phys. 32, 547 (1969)

35. G.Alberi, L.Bertocchi and P.J.R.Soper,
Phys.Lett. 32B, 367 (1970)

36. T.Regge, Nouvo Cimento 18, 947 (1960)

37. For a definition of X,Y see e.g. Particle Data Group:
V.Chaloupka et al., Phys.Lett. 50B, No.1 (1974)

38. G.S.Abrams et al., Phys.Rev.Lett. 33, 1453 (1974)

39. F.T.Solmitz, Ann.Rev.Nucl.Sci. 14, 375 (1964)

40. H.Braun et al., Phys.Rev. D2, 488 (1970);
D.C.Colley, Nucl.Phys. B69, 205 (1974)

41. e.g.
D.Evrard and A.Fridman, Nucl.Phys. 14B, 699 (1969)
M.A.Abolins et al., Phys.Rev.Lett. 15, 125 (1965)
I.Butterworth et al., Phys.Rev.Lett. 15, 500 (1965)

42. C.P.Horne et al., Phys.Rev. D11, 996 (1975)

VITA

Hartmut Preissner

1943	Born March 31, Berlin, Germany.
1946-52	Deportation to the USSR.
1954-63	Attended the Maria-Theresia-Oberrealschule in München (Munich), Germany.
1963	Graduated ("Abitur") from MTO, München.
1963-69	Physics student, University of München.
1969	"Diplom", University of München.
1969-75	Graduate work in Physics, Rutgers University, New Brunswick, N.J., USA.
1969-70	Scholarship from the DAAD, Bonn.
1970-75	Research Assistantship, Department of Physics, Rutgers University.
1975	Ph.D. in Physics, Rutgers University.